LBNL-40334
UC-1600

ERNEST ORLANDO LAWRENCE
BERKELEY NATIONAL LABORATORY

Near-Ground Cooling Efficacies of Trees and High-Albedo Surfaces

Ronnen M. Levinson

Environmental Energy Technologies Division

May 1997
Ph.D. Thesis

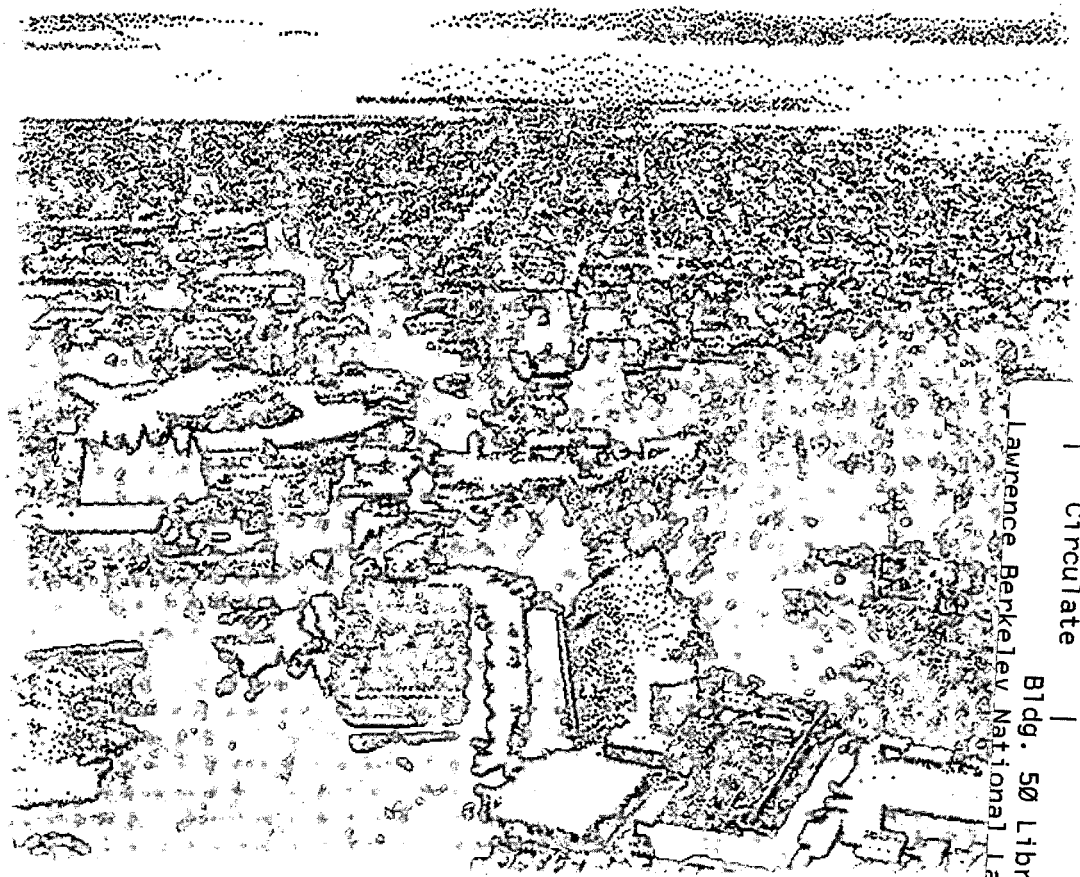

DISCLAIMER

LBNL-40334
UC-1600

NEAR-GROUND COOLING EFFICACIES OF TREES AND HIGH-ALBEDO SURFACES

Ronnen Michael Levinson
Ph.D. Thesis

Department of Mechanical Engineering
University of California

and

Environmental Energy Technologies Division
Lawrence Berkeley National Laboratory
University of California
Berkeley, CA 94720

May, 1997

This work was supported by the Assistant Secretary for Energy Efficiency and Renewable Energy, Office of Building Technology, State and Community Programs of the U.S. Department of Energy, under Contract No. DE-AC03-76SF00098.

Abstract

Near-Ground Cooling Efficacies of Trees and High-Albedo Surfaces

by

Ronnen Michael Levinson

Doctor of Philosophy in Engineering-Mechanical Engineering

University of California, Berkeley

Professor Van P. Carey, Chair

Daytime summer urban heat islands arise when the prevalence of dark-colored surfaces and lack of vegetation make a city warmer than neighboring countryside. Two frequently-proposed summer heat island mitigation measures are to plant trees and to increase the albedo (solar reflectivity) of ground surfaces. This dissertation examines the effects of these measures on the surface temperature of an object near the ground, and on solar heating of air near the ground. Near-ground objects include people, vehicles, and buildings.

The variation of the surface temperature of a near-ground object with ground albedo indicates that a rise in ground albedo will cool a near-ground object only if the object's albedo exceeds a critical value. This critical value of object albedo depends on wind speed, object geometry, and the height of the atmospheric thermal boundary layer. It ranges from 0.15 to 0.37 for a person. If an object has typical albedo of 0.3, increasing the ground albedo by

0.25 perturbs the object's surface temperature by -1 to +2 K.

Comparing a tree's canopy-to-air convection to the reduction in ground-to-air convection induced by tree shading of the ground indicates that the presence of a tree can either increase or decrease solar heating of ground-level air. The tree's net effect depends on the extent to which solar heating of the canopy is dissipated by evaporation, and on the fraction of air heated by the canopy that flows downward and mixes with the ground-level air. A two-month lysimeter (plant-weighing) experiment was conducted to measure instantaneous rates of water loss from a tree under various conditions of weather and soil-moisture. Calculations of canopy-to-air convection and the reduction of ground-to-air convection based on this data indicate that canopy-induced heating would negate shadow-induced cooling if approximately 45% of the canopy-heated air mixed with ground level air. This critical fraction is comparable to typical downward mixing fractions, so the tree's net heating or cooling effect on near-ground air is small.

Table of Contents

List of Figures

List of Tables

List of Symbols

English Symbols

a	coefficient of thermal expansion for an ideal gas, $a = 1/273$
A	area $\left(\mathrm{m}^2\right)$
A_0	total area $\left(\mathrm{m}^2\right)$
c	heat capacity $\left(\mathrm{J\ kg^{-1}\ K^{-1}}\right)$
C	volumetric heat capacity of air at 20°C and 1 atm, $C \equiv \rho c_p$ $\left(\mathrm{J\ m^{-3}\ K^{-1}}\right)$
d	characteristic length (m)
D	damping depth (m)
D	diameter (m)
D_{AB}	molecular diffusivity of water vapor into air $\left(\mathrm{m^2\ s^{-1}}\right)$
E	water-vapor diffusion $\left(\mathrm{kg\ s^{-1}\ m^{-2}}\right)$
$\hat{E}$	area-integrated water-vapor diffusion $\left(\mathrm{kg\ s^{-1}}\right)$
f	area fraction
$f_{\downarrow}$	downward mixing fraction
$f'_{\downarrow}$	critical downward mixing fraction
$F_{A\to B}$	view factor from surface A to surface B
g	acceleration due to gravity, $g = 9.81\ \mathrm{m\ s^{-2}}$
Gr	Grashof number, $\mathrm{Gr} \equiv a g d^3 \Delta T / \nu^2$
h	convection coefficient $\left(\mathrm{W\ m^{-2}\ K^{-1}}\right)$
$\overline{h}$	length-averaged convection coefficient $\left(\mathrm{W\ m^{-2}\ K^{-1}}\right)$
$\overline{h}$	normalized cylinder height, $\overline{h} = H_0/\Delta$
h_r	relative humidity
H	convection loss $\left(\mathrm{W\ m^{-2}}\right)$
$\hat{H}$	area-integrated convection loss (W)
H_0	height of cylinder or cone (m)
I_H	horizontal-surface insolation density $\left(\mathrm{W\ m^{-2}}\right)$
I_N	beam-normal insolation density $\left(\mathrm{W\ m^{-2}}\right)$

k	thermal conductivity $\left(\mathrm{W\ m^{-1}\ K^{-1}}\right)$
K	conduction loss $\left(\mathrm{W\ m^{-2}}\right)$
L	long-wave radiation gain $\left(\mathrm{W\ m^{-2}}\right)$
$\hat{L}$	area-integrated long-wave radiation gain (W)
m	mass (kg)
n_t	upstream-turbulence convection enhancement coefficient
Nu	Nusselt number $Nu \equiv hd/k$
Q	all-wave radiation gain, $Q = L + S$ $\left(\mathrm{W\ m^{-2}}\right)$
$\hat{Q}$	area-integrated all-wave radiation gain, $\hat{Q} = \hat{L} + \hat{S}$ (W)
Q_{dry}	all-wave radiation gain of a dry surface $\left(\mathrm{W\ m^{-2}}\right)$
$\hat{Q}_{\mathrm{dry}}$	area-integrated all-wave radiation gain of a dry surface (W)
r	radius (m)
r_c	conduction resistance $\left(\mathrm{s\ m^{-1}}\right)$
r_e	environmental resistance, $r_e \equiv \left(r_r^{-1} + r_h^{-1}\right)^{-1}$ $\left(\mathrm{s\ m^{-1}}\right)$
r_h	convection resistance $\left(\mathrm{s\ m^{-1}}\right)$
r_{ha}	boundary-layer convection resistance $\left(\mathrm{s\ m^{-1}}\right)$
r_r	(long-wave) radiation resistance $\left(\mathrm{s\ m^{-1}}\right)$
r_v	water-vapor diffusion resistance $\left(\mathrm{s\ m^{-1}}\right)$
r_{va}	boundary-layer water vapor-diffusion resistance $\left(\mathrm{s\ m^{-1}}\right)$
r_{vs}	stomatal water-vapor diffusion resistance $\left(\mathrm{s\ m^{-1}}\right)$
R_0	radius of cylinder or cone (m)
Re	Reynolds number, $\mathrm{Re} \equiv Ud/\nu$
s	slope of saturation vapor density curve, $s \equiv d\rho_v'(T)/dT$ $\left(\mathrm{kg\ m^{-3}\ K^{-1}}\right)$
S	short-wave radiation gain $\left(\mathrm{W\ m^{-2}}\right)$
$\hat{S}$	area-integrated short-wave radiation gain (W)
S_i	incident short-wave radiation $\left(\mathrm{W\ m^{-2}}\right)$
$\hat{S}_i$	area-integrated incident short-wave radiation (W)
$S_\downarrow$	downward short-wave radiation gain $\left(\mathrm{W\ m^{-2}}\right)$
$S_\downarrow^*$	unobstructed downward short-wave radiation gain $\left(\mathrm{W\ m^{-2}}\right)$
t_0	characteristic time (s)

$\bar{T}$	temperature at which the radiative resistance r_r is evaluated (K)
T_0	surface temperature (K)
T_∞	free-stream air temperature (K)
T_a	air temperature (K)
T_c	conductive temperature (K)
T_e	environmental temperature (K)
T_g	ground temperature (K)
T_r	(long-wave) radiative temperature (K)
T_s	sky temperature (K)
u	transient temperature (K)
U	wind speed $\left(\text{m s}^{-1}\right)$
z	height above ground (m)
$\bar{z}$	normalized height above ground, $\bar{z} \equiv z/\Delta$

Greek Symbols

α	cone's angle of elevation
α_0	object albedo
α_0'	temperature-critical object albedo
α_0''	convection-critical object albedo
α_g	ground albedo
β	solar altitude angle
γ	psychrometric constant, $\gamma \equiv C/\lambda$ $\left(\text{kg m}^{-3}\ \text{K}^{-1}\right)$
γ^*	$\gamma^* \equiv \left(r_v/r_h\right)\gamma$
δ	fraction of horizontal-surface insolation that is diffuse in origin
Δ	atmospheric thermal boundary-layer height (m)
ΔH_g	change in ground-to-air convection loss $\left(\text{W m}^{-2}\right)$
$\Delta \hat{H}_g$	area-integrated change in ground-to-air convection loss (W)
ΔT	temperature difference (K)
ε_s	sky emissivity
η	$\eta \equiv r_r/\left(r_r + r_h\right)$
θ	normalized, dimensionless air temperature
$\tilde{\theta}$	height-averaged, normalized, dimensionless air temperature
$\bar{\theta}$	cylinder-averaged, normalized, dimensionless air temperature

κ	thermal diffusivity $\left(\mathrm{m^2\ s^{-1}}\right)$
λ	latent heat of vaporization of water $\left(\mathrm{J\ kg^{-1}}\right)$
ν	kinematic viscosity $\left(\mathrm{m^2\ s^{-1}}\right)$
ρ_{sd}	saturation vapor density deficit of air, $\rho_{sd} \equiv \rho_v'(T_a) - \rho_{va}$ $\left(\mathrm{kg\ m^{-3}}\right)$
ρ_{va}	density of water vapor in air $\left(\mathrm{kg\ m^{-3}}\right)$
ρ_v'	saturation vapor density of water $\left(\mathrm{kg\ m^{-3}}\right)$
σ	shade fraction
σ	surface area $\left(\mathrm{m^2}\right)$
σ_{sb}	Stefan-Boltzmann constant, $\sigma_{sb} = 5.67 \times 10^{-8}\ \mathrm{W\ m^{-2}\ K^{-4}}$

Acknowledgments

I wish to thank my committee members—Professor Van Carey, Professor Kent Udell, and Professor John Harte—for their assistance in this dissertation. I am also grateful for the input of fellow Heat Island Group researchers Dr. Haider Taha and Dr. Melvin Pomerantz. Most of all, I would like to thank my research advisor, Dr. Hashem Akbari, for his guidance over the past three years.

Chapter 1: Introduction

1.1 Motivation

Daytime summer urban heat islands arise when a prevalence of dark-colored surfaces and a lack of vegetation make urban areas warmer than the countryside. The cooling benefits of adding trees to cities and of increasing the solar reflectivity, or albedo†, of urban surfaces have been investigated primarily through finite-difference simulations that predict changes in urban air temperature and building energy demand. While quite thorough, these simulations are numerical in nature, and thus tend to produce non-general results. It would be helpful to have simple physical models with which to explore the effects of vegetation and albedo on the urban environment. Since cooling-energy demand and human comfort depend primarily on the near-ground climate, this study will focus on the reduction of (a) the surface temperature of near-ground objects, and (b) heat convection to air near the ground. Examples of near-ground objects include people, vehicles, and buildings; near-ground air refers to that within the first few meters above the ground.

1.2 Past Studies: Finite-Difference Simulations of Cities and Buildings

1.2.1 Boundary Layer, Urban Canyon, and Building Energy Models

Mesoscale Models. Past investigations of schemes to mitigate urban heat islands begin by altering the descriptions of ground surface albedo and vegetative cover supplied to a "mesoscale" boundary layer model. Mesoscale models have horizontal domains on the order of 100 km, horizontal resolutions on the order of 1 km, and typically march over time domains of several days. The mesoscale simulation predicts the near-ground air temperature change resultant from the changes in vegetative cover and surface albedo.

Microscale Models. In some studies, the change in near-ground air temperature computed by the mesoscale model is piped directly to a "microscale" building energy model. A microscale model has a horizontal domain on the order of 100 m, and typically describes the heat relations of one or more buildings. Also supplied to the microscale model are changes to the building's surface albedo and vegetative cover. The microscale model usually yields a change in a building's demand for cooling energy.

Urban Canyon Models. In other studies, an urban canyon model may be used to link the mesoscale and microscale models. Urban canyon models typically describe the energy exchange over the domain of a city block, and resolve to the scale of one or two buildings. Using the mesoscale model output as a boundary condition, the urban canyon model is run to estimate the air temperature around a building. Urban canyon models can also calculate

†. A surface's "albedo" is the fraction of incident solar energy that it reflects. The solar radiation wavelength spectrum ranges from 0.1 to 4 μm .

the influence of the ground albedo on the amount of solar energy reflected from the ground to building surfaces.

1.2.2 Lack of Generality to Simulation Results

The aforementioned numerical simulations yield case-specific results. That is, given a description of a ground-surface or building, initial conditions, and boundary conditions, each model marches forward in time to solve finite difference equations for hourly values of mesoscale climate, urban-canyon climate, or building energy demand. Other than by regressing the results of an enormous number of computationally-expensive simulations, it is difficult to extract from such models generalized closed-form expressions for the effects of changes to albedo and vegetative cover.

1.3 New Approach: Microscale Physical Models and Measurements

1.3.1 Questions

This paper sets out to answer some fundamental questions about the effects of summer urban heat island mitigation schemes on the near-ground environment:

- Will increasing the albedo of a paved surface warm or cool nearby objects, such as people, vehicles, and buildings?
- By how much will increasing ground albedo or the extent to which an object is shaded change the temperature of the object's surface and the amount of heat convected from the object's surface to the near-ground air?
- Will the introduction of a tree lead to a net cooling or heating of the air near the ground? What is the magnitude of this effect?

1.3.2 Investigations

First, a microscale physical model is constructed to develop formulas for the variations with shading and ground albedo of the surface temperature and convective loss[†] of an object near the ground. near the ground. These variations are then computed for several common near-ground objects—a human, a car, and a small building. Next, a second microscale model is developed to predict the change in ground-level air heating induced by the presence of a tree. This second model is then applied to climate and evapotranspiration[‡] data gathered in a tree lysimeter[§] experiment, and the results used to calculate the change in ground-level air heating induced by the experimental tree.

---

†. When referring to a near-ground object, the terms "convective loss" and "object-to-air convection" will be used interchangeably. The latter is more descriptive, but the former is terser.

‡. "Evapotranspiration" is the evaporation of water from the surfaces of a transpiring plant, primarily leaves.

§. A "lysimeter," or plant-weighing, experiment records the mass of a plant over a period of time to determine its rate of evapotranspiration. Since nearly all changes in plant mass are due to water transport, the plant's rate of total mass loss is very close to its rate of water mass loss.

1.4 PHYSICS

1.4.1 Effects of Ground Albedo and Shading on Near-Ground Objects

Environmental Temperature. The surface temperature of an object near the ground is influenced by convection to the air, and by the exchange of long and short-wave radiations[†] with both ground and sky. These heat flows determine the object's "environmental temperature," or surface temperature attained when no heat is conducted from the object's surface to its core. When surface-to-core conduction is negligible, the study of the variation of an object's surface temperature with radiation and convection reduces to determining the corresponding variations of its environmental temperature.

Convective Heating of Near-Ground Air. Convective heat loss from the surface of a near-ground object warms the air near the ground. Since the magnitude of this flow is proportional to the difference in temperature between the object's surface and the air near the ground, the variation of object-to-air convection can be found from the variations of the difference between the environmental and air temperatures.

Increasing Ground Albedo. Raising the albedo of the ground will increase the amount of solar radiation reflected by the ground. This reduces the amount of solar heat absorbed by the ground, lowering the ground's temperature and thus reducing the magnitudes of convective loss and long-wave radiative loss from the ground. The total decrease in long-wave and convective loss from the ground will equal the increase in solar radiation reflected by the ground. The decrease in ground temperature also lowers the temperature of air near the ground, though the air temperature does not decline as much as the ground temperature.

The effect on the near-ground object of raising the ground albedo is threefold. First, the amount of solar radiation reflected from the ground to the object increases, which tends to raise the object's environmental temperature. Second, the amount of long-wave radiation from the ground to the object decreases, which tends to lower the object's environmental temperature. Third, the temperature of the air around the near-ground object declines, which also tends to lower the object's environmental temperature. The net changes of the object's environmental temperature and convection to the air may be positive or negative.

Increasing Shading. Shading a near-ground object—say, by introducing tree cover—will decrease the amount of short-wave radiation incident on the object, which lowers the object's environmental temperature and its convective loss to the air. The extent of shading can be described by an object's "shade fraction," defined to be the fraction of insolation[‡]

---

†. The spectrum of long-wave (thermal) radiation is typically taken to be $3 - 100\ \mu m$; a 300K black body emits maximum energy per unit wavelength at $9.7\ \mu m$. The spectrum for short-wave radiation is $0.4 - 4\ \mu m$; a 6,000K black body (i.e. the sun) emits maximum energy per unit wavelength at $0.48\ \mu m$.

‡. The terms "solar radiation," "short-wave radiation," "SW radiation," and "insolation" are used interchangeably.

from sky to object that is obstructed by shading. An object with a shade fraction of zero is unshaded, while an object with a shade fraction of one is completely shaded. Increasing the shade fraction will always lower an object's environmental temperature and its convective loss to the air.

1.4.2 Effects of Planting a Tree on the Heating of Near-Ground Air

Planting a tree has two effects on the amount of heat convected into the near-ground air. First, the tree's canopy lowers the temperature of the ground in its shadow, reducing the amount of heat convected from the ground to the air. Second, the tree's canopy convects heat to the canopy-level air. Since some fraction of this heated air will flow to ground level, canopy-level convection will indirectly heat the ground level air. Thus, the introduction of a tree may warm or cool the ground-level air, depending on the relative magnitudes of the ground-to-air convection decrease and the downward-flowing canopy-to-air convection.

Changes in Ground-To-Air Convection. In the absence of a tree, the amount of short-wave radiation striking the ground is simply that incident on any horizontal surface, and the temperature of the surface with which the ground exchanges long-wave radiation[†] is that of the sky. The introduction of a tree canopy reduces the sky-to-ground insolation by the amounts of insolation absorbed or reflected skyward by the canopy. The tree canopy is also warmer than the portion of the sky that it obscures; this increases the amount of long-wave radiation to the ground. The decrease in groundward short-wave radiation generally exceeds the increase in groundward long-wave radiation, so the introduction of a tree decreases the total amount of radiation to the ground. This lowers the temperature of the ground, and thus the amount of heat convected from the ground to the air.

Changes in Canopy-To-Air Convection. Solar heating makes the exterior surface of a tree's canopy warmer than the ambient air. Long-wave radiation loss and latent heat lost by evapotranspiration reduces this temperature elevation, but the average temperature of the leaves in the canopy is generally remains higher than that of the air. Thus, the canopy convects heat to the canopy-level air. Since some fraction of this warmed canopy-level air will flow downward to the ground level to mix with the ground-level air, the introduction of a tree will indirectly heat the ground-level air.

The magnitude of this heat flow from the canopy to the ground-level air depends on (a) the radiative load of the canopy; (b) the rate of latent heat loss from the canopy; and (c) the fraction of canopy-level air that migrates to the ground level. Given the canopy's geometry and climate (e.g. horizontal-surface insolation, air temperature, and so on), the canopy's radiative load may be determined from an energy balance.

It is more difficult to predict the latent heat loss, because a plant's rate of evapotranspiration is strongly controlled by physiological responses to illumination and availability of water. Thus, the rate of latent heat loss must be found from either a complex model of

†. Referred to as the "radiative temperature" to which the ground is exposed.

plant physiology, or from measurements of a plant's rate of evapotranspiration. The latter route was taken in this paper, and is described later in this chapter.

The fraction to canopy-level air that flows down to air level, or "downward mixing fraction," may be determined to varying levels of accuracy. The simplest approach considers only symmetry, which would suggest that half of the canopy-level air will migrate downward. If buoyancy is also taken into account, the downward mixing fraction should be less than one-half, since the warm canopy-level air will tend to rise. A proper evaluation of the downward mixing fraction requires simulation or measurement of the air flow around the canopy of a tree.

1.4.3 Predictors of Signs and Magnitudes of Near-Ground Effects

Near-Ground Object Surface Temperature and Convection. The effects on near-ground objects of changes in shading and ground albedo may be gauged by the derivatives of the object's environmental temperature and convective loss with respect to shade fraction and ground albedo. The expressions for these derivatives contain two critical values of an object's albedo. At the first, the "temperature-critical object albedo," an object's environmental temperature does not vary with ground albedo. At the second, the "convection-critical object albedo," the object's convection loss is insensitive to ground albedo. An object's actual albedo may be compared to these critical albedos to determine if an increase in ground albedo will raise of lower the object's environmental temperature and convection loss.

Tree-Induced Changes in Near-Ground Convection. The net ground-level air heating or cooling induced by the introduction of a tree depends on (a) the change in ground-to-air convection induced by the tree's shadow; (b) the amount of heat convected from the canopy to the canopy-level air; and (c) the downward mixing fraction. There will be some critical value of the downward mixing fraction at which the canopy-induced heating will balance the ground-induced cooling; this fraction is simply the ratio of the ground-level cooling to the canopy-level heating. The expected downward mixing fraction may then be compared to the critical downward mixing fraction to predict whether the net effect of the tree will be to add of remove heat from the ground-level air.

1.5 EXPERIMENT

A tree canopy can dissipate a sizable fraction of its solar heat load by latent heat loss. Since it is difficult to predict a plant's rate of evapotranspiration without detailed knowledge of its physiological responses to climate—particularly with respect to insolation and soil moisture availability—a lysimeter experiment was conducted to measure diurnal profiles of a tree's climate and rate of water loss.

The experimental specimen was a small, potted tree sited on the third-story roof of a building in Berkeley, CA from August to October[†] in 1995. An electronic scale measured the mass of the tree, while an adjacent weather station measured ambient weather conditions, including air temperature, relative humidity, wind speed, and horizontal-surface insola-

tion. This provided the climate and evapotranspiration data needed to calculate the canopy-level and ground-level convections induced by the tree.

1.6 Thesis Overview

1.6.1 The Big Picture

After this introduction and a review of relevant literature, this study pursues two distinct topics: (a) the effects on near-ground objects of ground albedo and shade fraction modifications, and (b) the effects on convection of heat to near-ground air of introducing a tree. The paper's concluding remarks address the results of both investigations, and discuss the merits of the models used within. Multiple appendices detail the theories of heat transfer, mass transfer, and plant physiology employed in the physical models, as well as the experimental and data analysis techniques developed for the lysimeter experiment.

1.6.2 Topic One: Near-Ground Objects

First, a near-ground object energy balance is established to find expressions for (a) the temperature and convection critical object albedos, and (b) the derivatives of environmental temperature and object-to-air convection with respect to ground albedo and shade fraction. Values are then calculated for three typical objects—a human, a car, and a small building—under low and moderate wind conditions, and for short and tall thermal boundary layers, at noon on a summer day.

1.6.3 Topic Two: Tree-Induced Changes in Convection

Second, a coupled mass-energy balance is developed for the canopy of a tree. This yields formulas for the changes in canopy-to-air and ground-to-air convection induced by the presence of a tree. Data from the lysimeter experiment is supplied to the tree model to calculate the experimental tree's heat flows. Diurnal profiles of the convection, long-wave radiation, short-wave radiation, and latent heat flows are explored on four representative days to determine the effect of climate on (a) values of the critical downward mixing fraction, and (b) the role of evapotranspiration in the canopy's energy balance.

1.6.4 Appendices: Background Information

The appendices begin with a treatment of the elements of heat and mass transfer needed to construct energy balances for ground, near-ground-object, and canopy-leaf surfaces. Topics include dry and wet surface energy balances, convective and radiative exchange, and the profile of air temperature in thermal boundary layers. The applicabilities of these idealized energy balances to various real surfaces are then examined. Next, plant physiology is briefly reviewed, with an emphasis on plant water relations. Various experimental and data

---

†. Fog-related weather patterns of the San Francisco Bay Area bring a late summer to Berkeley. Thus, these August through October are among the city's warmest months of the year.

analysis techniques developed for the lysimeter experiment are presented. These including an algorithm for removing wind noise from mass measurements, and a method for measuring the total leaf surface area of a small tree. The appendices conclude with listings of the computer code employed in the near-ground object and tree calculations.

1.7 New Art

1.7.1 Theory

Novel theory introduced in this thesis includes

1. a model of the variation of near-ground object environmental temperature and convective loss with ground albedo and shade fraction;
2. "temperature-critical" and "convection-critical" object albedos;
3. a model of the changes in canopy-to-air and ground-to-air convection induced by a tree;
4. the "critical downward mixing fraction";
5. a useful variant of the expression commonly used to predict the rate of water loss from a leaf (the "Penman-Monteith" formula);
6. a convenient radiation model to close the energy balance of a tree canopy;
7. a technique to filter wind noise from plant-mass measurements, which is helpful in smoothing a mass signal prior to calculating the rate of mass loss; and
8. the view factor† from a vertical, upward-pointing, right-circular cone to the sky.

1.7.2 Experiment

New experimental techniques and data introduced by this study include

1. a technique for measuring the canopy area of a plant using office equipment;
2. two ways to mutually-calibrate outdoor air temperature sensors; and
3. several months of data describing the evapotranspiration rate and climate of a tree in summer.

---

†. The "view factor" (a.k.a. "configuration factor," or "shape factor") from surface A to surface B is the fraction of radiant energy leaving surface A that strikes surface B.

Chapter 2: Literature Review

2.1 Simulations and Measurements of Daytime Summer Urban Heat Islands

While this paper focuses on microscale effects of schemes to cool cities, city-scale numerical simulations and measurements constitute the bulk of prior studies of daytime summer urban heat islands and their mitigation.

2.1.1 Benefits of Increasing Albedo and Vegetative Cover

Simulations. The Heat Island Project of the Lawrence Berkeley National Laboratory in Berkeley, CA has simulated the cooling effects of increasing the surface albedo and vegetative cover of various cities. A recent synopsis by Rosenfeld et al. 1996 of simulations run for the Los Angeles basin finds that (a) increasing the albedo of 1,250 km^2 of roofing by 0.35, (b) increasing the albedo of 1,250 km^2 of concrete pavements by 0.25, and (c) planting 11 million evapotranspiring trees will yield annual air-conditioning energy savings totalling $175 M/yr, and will reduce the 2 PM near-ground air temperature by 3 K in summer. Many other cities have been studied, and significant building energy savings predicted for them (Akbari and Taha 1992).

Measurements. Akbari et al. 1992b report measurements of summer urban heat islands in California, Japan, and China. Akbari et al. 1992a and Akbari et al. 1993 monitored peak power and cooling energy savings due to shade trees and white surfaces in Sacramento, CA, where they found that tree shading of two small houses resulted in seasonal cooling energy savings of 30% and peak cooling energy demand savings of 27 to 42%. They also found that the application of a high-albedo coating to the roof of one of the houses yielded seasonal cooling energy savings of 80%.

2.1.2 Models of Climate and Building Energy

A few references are listed here for those interested in numerical modeling of climate and building energy demand. Models merits will not be examined because numerical climate and building simulations are outside the scope of this paper.

Overviews. A comprehensive discussion of the physical and computational aspects of mesoscale meteorological modeling is presented by Pielke 1984. The nature, limitations and applications of urban climate models are reviewed by Bornstein 1989. Pielke 1989 explores the use of mesoscale meteorological modeling to assess summer urban heat islands, while Martien et al. 1989 and Sailor and Akbari 1992 investigate the use of urban climate models building in energy simulations. Sailor 1993 explores the role of surface characteristics in urban meteorology.

Modern Land-Surface Model. A recent mesoscale land-surface model presented by De Ridder and Schayes 1997 and De Ridder 1997 features sophisticated models of evaporative and radiative exchange between the air and the vegetative canopy.

2.2 Studies of Near-Ground Object Heat Transfer

2.2.1 Human Climate Models

The energy balance developed in this paper for near-ground objects derives from standard models of the climate of humans, such as those presented by Campbell 1977, Monteith 1973, and Threlkeld 1970. This paper extends the human climate model by examining the sensitivity of environmental temperature and object-to-air convection to ground albedo and shade fraction.

2.2.2 Elementary Heat Transfer Relations

The convective resistances and the thermal boundary layer temperature profile required in analysis of near-ground object temperatures are taken from common heat transfer texts, e.g. White 1988 and Kays and Crawford 1993.

Duffie and Beckman 1980 discuss one of the least certain elements of the near-ground object analysis, the determination of a convection coefficient for an outdoor horizontal surface. They find that the most popular empirical formula—originally developed from measurements of heat loss from a small solar collector plate—can not reasonably be extended to larger surfaces. Unfortunately, they do not offer a practical alternative.

2.2.3 Temperatures at and Near the Ground

Sutton 1953, Geiger 1965, Oke 1978, Campbell 1977, and Monteith 1973 describe the variation of air temperature in the first few meters above the ground, and also the variation of soil temperature in the first meter or two below the ground. Their analyses are used here to help estimate the thickness of the thermal boundary layer above the ground, and to estimate the magnitude of heat conduction into the soil.

Oke 1978 and Geiger 1965 examine the effect of ground albedo modification, finding that raising albedo can reduce both ground surface temperatures and upward flows of heat from ground surfaces.

2.3 Studies of Tree Energy Balances and Water Relations

2.3.1 Leaf Evapotranspiration

Penman Model. There is a rather large body of literature that addresses the water relations of plants. Penman 1948, Monteith 1973, and Campbell 1977 each develop the standard "Penman" formulation of latent heat loss from a leaf. This expression for latent heat

loss depends on the magnitude of long-wave radiative exchange, which depends on the leaf temperature, which in turn depends on the amount of latent heat loss. Thus, the standard formula is implicit. This paper derives a variant of the Penman expression in which the latent heat loss is given explicitly.

Stomatal Mechanics. Salisbury and Ross 1985 and Kramer 1983 present elementary treatments of stomatal behavior and plant water loss, elements of which are summarized in this dissertation to explain the diurnal variation of latent heat loss from trees. Readers interested in advanced stomatal physiology are referred to Cowan 1977 and Meidner and Mansfield 1968.

Leaf Convection Enhancement by Upstream Turbulence. Pearman et al. 1971 experimentally determined the factor by which upstream air turbulence increases heat convection and vapor diffusion from leaves. This result is employed in the tree energy model of this dissertation.

2.3.2 Canopy Radiation Models

Transmissive Models. The opaque canopy model of leaf radiation developed in this thesis is less sophisticated than the transmissive canopy radiation models presented by Monteith 1973, Campbell 1977, and Thorpe 1978, in which insolation is allowed to penetrate the canopy. The sole advantage of the model presented herein is its simplicity, which facilitates closed-form solution of the tree's energy balance.

View Factor From Cone To Sky. The opaque canopy model requires the geometric view factor from a cone to the sky—that is, the view factor from a cone to an infinite plane parallel to its base. Surprisingly, a search of the heat transfer literature, including Siegal and Howell 1992, did not turn up an expression for this view factor. However, Kobyshev et al. 1976 calculated the view factor from a cone to a disk concentric with its base. The cone-to-ground and cone-to-sky view factors are computed in this paper as limiting cases of Kobyshev's formula.

2.3.3 Air Flow Around a Tree

Gross 1987 simulates the flow of air around a single tree. His results may be of interest to those who desire an analysis of canopy-level air flow more sophisticated than the hand-waving arguments presented herein.

2.3.4 Water Loss Measurements

Lysimeter (plant-weighing) experiments that measure rates of evapotranspiration are quite common. The sources listed below present evapotranspiration measurements that either (a) involve the species studied in this paper; (b) are plotted diurnally; or (c) compare water intake by various species. The first two types of data may be used to gauge the evapotranspiration measurements obtained in this paper, while the third may be used to extrapolate

the results of the specimen studied in this paper to other species.

Studies Involving *Ligustrum Japonicum* (Japanese Wax-Leaf Privet). Water-use studies involving *Ligustrum Japonicum* (the subject of the lysimeter experiment conducted for this paper) include Steinberg et al. 1991, Heilman and Brittin 1989, Still and Davies 1988, Still and Davies 1993, Beeson 1992, and Lownds and Berghahe 1991.

Diurnal Measurements. Fritschen et al. 1980, Heilman and Brittin 1989, and Thorpe 1978 report diurnal measurements of evapotranspiration from various plants.

Comparisons of Water Intake By Various Species. Kozlowski 1981, Kozlowski 1983, Still and Davies 1993, and Akbari et al. 1992 list annual rates of water consumption by various species. These data may be used to estimate the relative rates of evapotranspiration across species.

Chapter 3: Near-Ground Object Model

3.1 Overview

If a near-ground object conducts no heat from its surface to its core, its surface temperature will equal its environmental temperature (see Appendix A). This chapter explores the dependence of an object's surface temperature and convective heat loss on ground albedo and shading by developing formulas for the derivatives of environmental temperature and object-to-air convection with respect to ground albedo and shade fraction. This analysis leads to the concepts of "temperature-critical" and "convection-critical" object albedos, at which the environmental temperature and convective loss are invariant with ground albedo.

Notation, terminology, and variables used in this section are defined in Appendix A[†].

3.2 Environmental Temperature and Object-To-Air Convection

3.2.1 Heat Flows

Effects of Changing Ground Albedo. A near-ground object's environmental temperature may be modified by either changing the albedo of the ground or shading the object from downward insolation. Raising the ground albedo will (a) increase the amount of insolation reflected from the ground to the object; (b) lower the ground surface temperature; (c) reduce the near-ground-air temperature; and (d) decrease the amount of LW radiation from the ground to the object. The net effect may be either to raise or to lower the environmental temperature and the amount of object-to-air convection. There will even be critical values of the object's albedo at which its environmental temperature and convection loss do not vary at all with ground albedo.

Effects of Increasing Shading. In contrast, increased shading of the object will always reduce the object's solar gain, environmental temperature, and convection loss.

Neglecting Conduction to Ground. The bottom surface of a object resting on the ground may be assumed to have no short-wave, long-wave, or convective heat exchange. It will be further assumed in the following analysis that heat conduction from the bottom surface to the ground may be neglected. This seems reasonable when the object is a human wearing shoes or a vehicle resting on rubber tires, in light of the poor thermal conductivity of shoes and tires and their relatively small areas of contact with the ground. This assumption may or may not work for a building, depending on the degree of thermal contact between the building and the ground.

---

†. The reader may find it helpful to skim the elementary heat transfer theory presented in the appendices before plowing through the near-ground object and tree models.

3.2.2 Magnitudes of Temperature and Convection

Neglecting (a) spatial variations in surface temperature; (b) evaporative cooling (e.g. perspiration); (c) internal heat generation; (d) conduction from body surface to ground; and (e) conduction from body surface to body core, the surface temperature T_0 of a near-ground object equal its environmental temperature, T_e, which in turn depends on SW radiation gain, LW radiation gain, and convection loss. In Section A.4 it is found that

$$T_0 = T_e = C^{-1} r_e S + \eta T_a + (1-\eta) T_r . \tag{3-1}$$

Here C is the volumetric heat capacity of air, r_r and r_h are the resistances to LW radiation and convection, $r_e \equiv \left(r_r^{-1} + r_h^{-1}\right)^{-1}$, $\eta \equiv r_r/(r_r + r_h)$, T_r and T_a are the radiative and air temperatures, and S is the absorbed insolation.

With the same assumptions, the convection loss H from the object to the air is given by Eq. (A-20):

$$H = C r_h^{-1} (T_0 - T_a) = \eta \left[C r_r^{-1} (T_r - T_a) + S \right]. \tag{3-2}$$

3.2.3 Variations With Ground Albedo

An object's insolation, air temperature, and radiative temperature will vary with the ground albedo α_g. Thus, its environmental temperature and convective loss will also vary with ground albedo:

$$\frac{\partial T_0}{\partial \alpha_g} = \frac{\partial T_e}{\partial \alpha_g} = C^{-1} r_e \frac{\partial S}{\partial \alpha_g} + \eta \frac{\partial T_a}{\partial \alpha_g} + (1-\eta) \frac{\partial T_r}{\partial \alpha_g} \tag{3-3}$$

and

$$\frac{\partial H}{\partial \alpha_g} = \eta \left[C r_r^{-1} \left(\frac{\partial T_r}{\partial \alpha_g} - \frac{\partial T_a}{\partial \alpha_g} \right) + \frac{\partial S}{\partial \alpha_g} \right]. \tag{3-4}$$

3.2.4 Variations With Shading

Shade Fraction. The extent to which an object is shielded from downward insolation will be denoted as the "shade fraction," σ. This relates the actual downward insolation $S_\downarrow$ to the unobstructed downward insolation $S_\downarrow^*$ by

$$S_\downarrow = (1-\sigma) S_\downarrow^* . \tag{3-5}$$

The object is unshaded when $\sigma = 0$, and fully shaded when $\sigma = 1$.

Shade Effects. Increased shading of the object will reduce its short-wave radiation gain, environmental temperature, and convective loss. Neglecting shade-induced changes to the air and radiative temperatures†, the variations of the environmental temperature and convection loss with shade fraction are

$$\frac{\partial T_0}{\partial \sigma} = \frac{\partial T_e}{\partial \sigma} = C^{-1} r_e \frac{\partial S}{\partial \sigma} \tag{3-6}$$

and

$$\frac{\partial H}{\partial \sigma} = \eta \left[\frac{\partial S}{\partial \sigma} \right]. \tag{3-7}$$

3.3 Object Geometry

A cylinder is the simplest axially-symmetric geometric form with distinct height and width‡. Thus it is mathematically convenient, though obviously approximate, to represent a near-ground object as a vertical, right-circular cylinder of radius R_0 and height H_0. Usually, the object's height is well-defined, but a suitable cylinder radius must be chosen from considerations of the object's true surface area.

Equivalent Radius. The equivalent cylinder radius R_0 for an object of height H_0 and total surface area A_0 is

$$R_0 = \tfrac{1}{2} \left[\left(H_0^2 + 2 A_0 / \pi \right)^{1/2} - H_0 \right]. \tag{3-8}$$

This gives a cylinder with height H_0 and total surface area equal to A_0.

Typical Human Body Area. The total body area A_0 of a human of mass m and height H_0 may be estimated from the "Dubois" formula (Campbell 1977, p.101),

$$A_0 = 0.2 m^{0.425} H_0^{0.725}. \tag{3-9}$$

Typical human body areas are usually on the order of 2 m^2.

3.4 Area-Averaged Properties

Eqs. (3-1) though (3-7) require values of S, T_a, and T_r that have been averaged over the surface of the near-ground object. The remainder of this chapter evaluates these area-averaged values, then substitutes them into the derivatives of the environmental temperature and convection loss with respect to ground albedo and shade fraction.

---

†. It is assumed here that the area of the shadow that falls over the near-ground object, possibly induced by a tree, is small enough that it does not significantly alter the ambient air and radiative temperatures.

‡. A sphere is simpler, but has only one characteristic dimension.

3.4.1 Area Fractions

An object's insolation, air temperature, and radiative temperature may be calculated as the area-weighted averages of the cylinder-top and cylinder-wall values. That is, denoting the cylinder's lateral wall and top surfaces by the subscripts W and T,

$$S = f_T S_T + f_W S_W, \tag{3-10}$$

$$T_a = f_T T_{a,T} + f_W T_{a,W}, \tag{3-11}$$

and

$$T_r = f_T T_{r,T} + f_W T_{r,W}, \tag{3-12}$$

where f_T and f_W are the top and side surface areas fractions. Since the top and side areas are

$$A_T = \pi R_0^2 \text{ and } A_W = 2\pi R_0 H_0, \tag{3-13}$$

their corresponding area fractions are

$$f_T \equiv \frac{A_T}{A_T + A_W} = \frac{R_0}{R_0 + 2H_0} \tag{3-14}$$

and

$$f_W \equiv \frac{A_W}{A_T + A_W} = 1 - f_T = \frac{2H_0}{R_0 + 2H_0}. \tag{3-15}$$

3.4.2 Properties at Cylinder Top

The average properties at the cylinder top are quite straightforward: the air temperature is that of air at the cylinder height, the radiative temperature is that of the sky, and the incident insolation is the horizontal surface insolation, minus whatever fraction is lost to object shading.

Air Temperature. Air temperature in the atmospheric thermal boundary layer varies from the ground temperature, T_g, at the bottom of the boundary layer $(z = 0)$, to the free-stream air temperature, T_∞, at top of the boundary layer $(z = \Delta)$. Defining the normalized boundary-layer air temperature as

$$\theta(z) \equiv \frac{T_g - T_a(z)}{T_\infty - T_g}, \tag{3-16}$$

the air temperature at some height z may be written

$$T_a(z) = T_\infty + \left[T_g - T_\infty\right]\left[1 - \theta(z)\right]. \tag{3-17}$$

The air temperature at the top of the cylinder is

$$T_{a,T} = T_\infty + \left[T_g - T_\infty\right]\left[1 - \theta(H_0)\right]. \tag{3-18}$$

The functional form of $\theta(z)$ is somewhat arbitrary (see Appendix F), but Eq. (F-1) provides a common profile,

$$\theta(z) = \begin{cases} (z/\Delta)^{1/7} & z < \Delta \\ 1 & z > \Delta \end{cases}. \tag{3-19}$$

LW Radiation. Since the top surface sees only the sky,

$$T_{r,T} = T_s. \tag{3-20}$$

Insolation. The unobstructed insolation incident on this horizontal surface is

$$S^*_{i,T} = I_H. \tag{3-21}$$

Allowing for shading,

$$S_{i,T} = (1-\sigma)S^*_{i,T} = (1-\sigma)I_H. \tag{3-22}$$

The insolation actually absorbed is

$$S_T = (1-\alpha_0)S_{i,T} = (1-\alpha_0)(1-\sigma)I_H. \tag{3-23}$$

3.4.3 Properties at Cylinder Wall

The cylinder wall's average ambient air temperature is the air temperature averaged between ground level and the height of the cylinder. The cylinder sees the sky and ground in equal parts, so its radiative temperature is the average of the sky and ground temperature. Its insolation is the sum of the downward diffuse, downward direct, and upward diffuse short-wave radiations.

Air Temperature. The wall's mean ambient air temperature $T_{a,W}$ is given by Eq. (F-6),

$$T_{a,W} = T_\infty + \left[T_g - T_\infty\right]\left[1 - \tilde{\theta}(H_0)\right], \tag{3-24}$$

where $\tilde{\theta}(H_0)$ is the normalized air temperature averaged between the ground level and height H_0. Eq. (F-5) provides a functional form for $\tilde{\theta}(H_0)$:

$$\tilde{\theta}(H_0) = \begin{cases} \frac{7}{8}\left(\frac{H_0}{\Delta}\right)^{1/7} & H_0 < \Delta \\ 1 - \frac{1}{8(H_0/\Delta)} & H_0 > \Delta \end{cases}. \tag{3-25}$$

Radiative Temperature. Since the side wall sees the ground and sky equally,

$$T_{r,W} = \tfrac{1}{2}\left(T_g + T_s\right). \tag{3-26}$$

The sky temperature is related to the free-stream air temperature T_∞ and relative humidity h_r by Eqs. (D-23), (D-24), and (A-10):

$$T_s = \varepsilon_s^{1/4}\, T_\infty, \qquad \varepsilon_s = 1.56\,\rho_{v\infty}^{1/7}, \qquad \rho_{v\infty} = h_r\,\rho_v'(T_\infty). \tag{3-27}$$

Insolation. From Eq. (D-33), the unobstructed, downward, direct insolation incident on the cylinder wall is

$$S^*_{i,W,\downarrow,\mathrm{dir}} = (1-\delta)\,I_H\left[2\,H_0\,R_0\cot\beta\right]/A_W = \pi^{-1}(1-\delta)\,I_H\cot\beta. \tag{3-28}$$

Combining view factor reciprocity with the fact that the side wall sees the ground and sky equally, the unobstructed, downward, diffuse incident insolation is

$$S^*_{i,W,\downarrow,\mathrm{diff}} = \delta\,I_H\left(A_s\,F_{s\to W}\right)/A_W = \delta\,I_H\left(A_W\,F_{W\to s}\right)/A_W = \tfrac{1}{2}\delta\,I_H. \tag{3-29}$$

Thus the total unobstructed, downward, incident insolation is

$$S^*_{i,W,\downarrow} = \left[\tfrac{1}{\pi}(1-\delta)\cot\beta + \tfrac{1}{2}\delta\right]I_H. \tag{3-30}$$

The upward incident insolation (reflected from ground to wall) is

$$S_{i,W,\uparrow} = \alpha_g\,I_H\left(A_g F_{g\to W}\right)/A_W = \alpha_g\,I_H\left(A_W F_{W\to g}\right)/A_W = \tfrac{1}{2}\alpha_g\,I_H. \tag{3-31}$$

The total isolation absorbed by the side wall is

$$S_W = (1-\alpha_0)\left[(1-\sigma)S^*_{i,W,\downarrow} + S_{i,W,\uparrow}\right]. \tag{3-32}$$

3.4.4 Properties at Ground

The ground temperature in Eqs. (3-18), (3-24), and (3-26) can be determined by applying an adiabatic, dry-surface energy balance to the ground. From Eq. (A-18),

$$T_g = C^{-1} r_{e,g}\,S_g + \eta_g\,T_\infty + \left(1-\eta_g\right)T_{r,g}. \tag{3-33}$$

The subscript g is used to distinguish parameters of the ground energy balance from the unsubscripted object-energy-balance parameters of Eq. (3-1). Explicitly,

$$r_{e,g} = \left(r_{r,g}^{-1} + r_{h,g}^{-1}\right)^{-1} \tag{3-34}$$

and

$$\eta_g = \frac{r_{r,g}}{r_{r,g} + r_{h,g}}, \tag{3-35}$$

where $r_{r,g}$ and $r_{h,g}$ are the radiative and convective resistances associated with the ground, rather than with the object. Since the view factor from the ground to the sky is much

greater than that from the ground to the object,

$$T_{r,g} \approx T_s \tag{3-36}$$

and

$$S_g \approx \left(1-\alpha_g\right) I_H . \tag{3-37}$$

Thus

$$T_g = C^{-1} r_{e,g} \left(1-\alpha_g\right) I_H + \eta_g T_\infty + \left(1-\eta_g\right) T_s . \tag{3-38}$$

3.4.5 Cylinder-Averaged Insolation and Temperatures

Substituting into Eqs. (3-10) through (3-12) (a) the top-surface values of Eqs. (3-18), (3-20), and (3-23), and (b) the wall-surface values of Eqs. (3-24), (3-26), and (3-32), the cylinder-averaged values of insolation, air temperature, and radiative temperature are

$$S = \left(1-\alpha_0\right)\left\{f_T\left[\left(1-\sigma\right)S^*_{i,T}\right] + f_W\left[\left(1-\sigma\right)S^*_{i,W,\downarrow} + S_{i,W,\uparrow}\right]\right\}, \tag{3-39}$$

$$T_a = T_\infty + \left(T_g - T_\infty\right)\left(1-\left[f_T\,\theta\left(H_0\right) + f_W\,\tilde{\theta}\left(H_0\right)\right]\right), \tag{3-40}$$

and

$$T_r = f_T\,T_s + \tfrac{1}{2} f_w \left(T_s + T_g\right). \tag{3-41}$$

The environmental temperature T_e and convection loss H may now be computed by substituting these cylinder-averaged values into Eqs. (3-1) and (3-2). However, the true quantities of interest in this study are the derivatives of T_e and H with respect to ground albedo and shade fraction.

It will prove convenient to define the cylinder-averaged normalized air temperature

$$\bar{\theta} = 1-\left[f_T\,\theta\left(H_0\right) + f_W\,\tilde{\theta}\left(H_0\right)\right], \tag{3-42}$$

so that the cylinder-averaged air temperature may be neatly written as

$$T_a = T_\infty + \left(T_g - T_\infty\right)\bar{\theta} . \tag{3-43}$$

3.4.6 Variation of Environmental Temperature With Ground Albedo

Substituting Eqs. (3-30) through (3-32) into Eq. (3-39), then differentiating with respect to ground albedo, the variation of cylinder-averaged insolation with ground albedo is

$$\frac{\partial S}{\partial \alpha_g} = \left(1-\alpha_0\right) f_W \frac{\partial S_{i,W,\uparrow}}{\partial \alpha_g} = \tfrac{1}{2}\left(1-\alpha_0\right) f_W\, I_H . \tag{3-44}$$

Noting that the ground temperature varies with ground albedo, but that the free-stream air

temperature and normalized air temperature profiles do not, differentiating Eq. (3-40) gives the variation of the cylinder-averaged air temperature with respect to ground albedo as

$$\frac{\partial T_a}{\partial \alpha_g} = \bar{\theta}\,\frac{\partial T_g}{\partial \alpha_g}. \tag{3-45}$$

Since the sky temperature is also invariant with ground albedo, differentiating the cylinder-averaged radiative temperature of Eq. (3-41) with respect to ground albedo yields

$$\frac{\partial T_r}{\partial \alpha_g} = \left(\frac{f_W}{2}\right)\frac{\partial T_g}{\partial \alpha_g}. \tag{3-46}$$

From Eq. (3-38), the derivative of ground temperature with respect to albedo is

$$\frac{\partial T_g}{\partial \alpha_g} = -C^{-1}\, r_{e,g}\, I_H. \tag{3-47}$$

Substituting Eqs. (3-44) through (3-47) into Eq. (3-3), then simplifying, the derivative of the environmental temperature with respect to ground albedo is

$$\frac{\partial T_e}{\partial \alpha_g} = \frac{f_W r_e I_H}{2C}\left\{\alpha_0' - \alpha_0\right\}. \tag{3-48}$$

where

$$\alpha_0' = 1 - \left[(1-\eta) + 2\eta f_W^{-1}\bar{\theta}\right]\frac{r_{e,g}}{r_e} \tag{3-49}$$

is the value of the object's albedo at which its environmental temperature is independent of ground albedo. It will be denoted the "temperature-critical object albedo." Clearly, $\partial T_e/\partial \alpha_g$ will be positive for $\alpha_0 < \alpha_0'$, and negative for $\alpha_0 > \alpha_0'$. Thus, if the object's albedo is sub-critical, an increase in ground albedo will raise its temperature; if its albedo is super-critical, an increase in ground albedo will lower its temperature. This indicates that $\alpha_0 > \alpha_0'$ is required if the surface temperature is to be reduced by raising the ground albedo.

3.4.7 Variation of Convection Loss With Ground Albedo

Substituting Eqs. (3-44) through (3-47) into Eq. (3-4), then simplifying, the derivative of the object's convective loss with respect to ground albedo is

$$\frac{\partial H}{\partial \alpha_g} = \tfrac{1}{2} f_W \eta I_H \left\{\alpha_0'' - \alpha_0\right\}, \tag{3-50}$$

where

$$\alpha_0'' = 1 - \left(1 - 2 f_W^{-1}\bar{\theta}\right)\frac{r_{e,g}}{r_r} \tag{3-51}$$

is the value of the object's albedo at which its convective loss is independent of ground albedo. This will be denoted the "convection-critical object albedo." Clearly, $\partial H/\partial \alpha_g$ will be positive for $\alpha_0 < \alpha_0''$, and negative for $\alpha_0 > \alpha_0''$. Thus, if the object's albedo is sub-critical, an rise in ground albedo will increase its convective loss to the air; if its albedo is super-critical, an rise in ground albedo will decrease its convective loss to the air. This indicates that $\alpha_0 > \alpha_0''$ is required if the convective heating of air by a near-ground object is to be reduced by raising the ground albedo.

3.4.8 Variation of Environmental Temperature With Shade Fraction

Using Eq. (3-39), the derivative of insolation with respect to shade fraction is

$$\frac{\partial S}{\partial \sigma} = -(1-\alpha_0)\left(f_T S_{i,T}^* + f_W S_{i,W,\downarrow}^*\right). \tag{3-52}$$

Substituting Eq. (3-52) into Eq. (3-6),

$$\frac{\partial T_e}{\partial \sigma} = -C^{-1} r_e (1-\alpha_0)\left(f_T S_{i,T}^* + f_W S_{i,W,\downarrow}^*\right). \tag{3-53}$$

It is convenient to introduce the cylinder-averaged, unobstructed, downward, incident insolation,

$$S_{i,\downarrow}^* = \left(f_T S_{i,T}^* + f_W S_{i,W,\downarrow}^*\right). \tag{3-54}$$

Substituting Eqs. (3-21) and (3-30) into Eq. (3-54),

$$S_{i,\downarrow}^* = I_H\left[f_T + f_W\left(\tfrac{1-\delta}{\pi}\cot\beta + \tfrac{\delta}{2}\right)\right]. \tag{3-55}$$

Thus

$$\frac{\partial T_e}{\partial \sigma} = -C^{-1}(1-\alpha_0) r_e S_{i,\downarrow}^*. \tag{3-56}$$

As expected, Eq. (3-56) indicates that the environmental temperature will fall as the shade fraction increases. Note that the magnitude of this variation is independent of ground albedo, because it was assumed above that shading of the object would not influence the ground or air temperatures.

3.4.9 Variation of Object-to-Air Convection With Shade Fraction

Substituting Eqs. (3-52) and (3-54) into Eq. (3-7), the variation of object-to-air convection with the shade fraction is

$$\frac{\partial H}{\partial \sigma} = -(1-\alpha_0)\eta S_{i,\downarrow}^*. \tag{3-57}$$

As expected, the convective loss will decrease when the shade fraction increases.

3.5 ANCILLARY ENERGY BALANCES: GROUND AND ROOF SURFACES

These straightforward cases are included for completeness. The variation of ground-to-air convection with ground albedo is quite relevant, because it may be compared to the corresponding change in object-to-air convection. The discussion of roof heat flows is something of a digression, but is included for the curious.

3.5.1 Variation of Ground-to-Air Convection With Ground Albedo

From Eq. (A-20), the convective loss from the ground to the air is

$$H_g = Q_{\mathrm{dry,g}} = \eta_g \left[C r_{r,g}^{-1} \left(T_{r,g} - T_\infty \right) + S_g \right]. \tag{3-58}$$

Substituting S_g from Eq. (3-37), the variation of ground-to-air convection with ground albedo is

$$\frac{\partial H_g}{\partial \alpha_g} = \eta_g \frac{\partial S_g}{\partial \alpha_g} = -\eta_g I_H . \tag{3-59}$$

It should come as no surprise that an increase in the ground albedo will decrease the ground-to-air convective loss.

3.5.2 Variation of Roof Temperature and Heat Flows With Roof Albedo

Roof Energy Balance. The energy balance for a building roof is particularly simple. In steady state,

$$Q = H + K , \tag{3-60}$$

where

$$H = C r_h^{-1} \left(T_0 - T_a \right) \tag{3-61}$$

is the convection loss to the air, and

$$K = C r_c^{-1} \left(T_0 - T_c \right) \tag{3-62}$$

is the conduction loss to the interior of the building. Here T_c is the interior air temperature and r_c is the conduction resistance.

Neglect of Conduction in Balance. While a typical rooftop convection resistance is usually on the order of $60\ \mathrm{s\ m^{-1}}$, R-3, R-11, and R-19 roofs have equivalent conduction resistances† of $640\ \mathrm{s\ m^{-1}}$, $2430\ \mathrm{s\ m^{-1}}$, and $4050\ \mathrm{s\ m^{-1}}$. Since $r_c \gg r_h$, the magnitude of conduction is much less than that of convection. Thus the no-conduction, dry-surface

†. To convert R-values to conduction resistances, note that $1\ \mathrm{hr\ ft^2\ °F\ BTU^{-1}} = 0.17611\ \mathrm{m^2\ K\ W^{-1}}$, and $C r_c^{-1} = R^{-1}$.

energy balance developed in Section A.4.2 may be used to find the convective loss H and the surface temperature T_0. Applying Eqs. (A-20) and (A-18),

$$H \approx Q_{\text{dry}} = \eta\left[C r_r^{-1}(T_r - T_a) + S\right] \tag{3-63}$$

and

$$T_0 = C^{-1} r_e S + \eta T_a + (1-\eta) T_r. \tag{3-64}$$

Variations of Convection, Surface Temperature, and Conduction. If the roof's albedo is α_0 and the incident horizontal-surface insolation is I_H,

$$S = (1-\alpha_0) I_H. \tag{3-65}$$

The variations of convection, surface temperature, and conduction with albedo are

$$\frac{\partial H}{\partial \alpha_0} = \eta \frac{\partial S}{\partial \alpha_0} = -\eta I_H, \tag{3-66}$$

$$\frac{\partial T_0}{\partial \alpha_0} = C^{-1} r_e \frac{\partial S}{\partial \alpha_0} = -C^{-1} r_e I_H, \tag{3-67}$$

and

$$\frac{\partial K}{\partial \alpha_0} = C r_c^{-1} \frac{\partial T_0}{\partial \alpha_0} = -\frac{r_e}{r_c} I_H. \tag{3-68}$$

Thus increasing the roof's albedo reduces its surface temperature, convection to the air, and conduction into the building.

3.6 Summary of Near-Ground Object Relations

The various near-ground object sensitivities and critical albedos are collected in Table 3-1 for easy reference.

Parameter	Formula
Sensitivity of environmental temperature to ground albedo	$\frac{\partial T_e}{\partial \alpha_g} = \frac{f_W r_e I_H}{2C}(\alpha_0' - \alpha_0)$
Sensitivity of environmental temperature to shade fraction	$\frac{\partial T_e}{\partial \sigma} = -C^{-1}(1-\alpha_0) r_e S_{i,\downarrow}^*$
Sensitivity of object-to-air convection to ground albedo	$\frac{\partial H}{\partial \alpha_g} = \frac{1}{2} f_W \eta I_H (\alpha_0'' - \alpha_0)$
Sensitivity of object-to-air convection to shade fraction	$\frac{\partial H}{\partial \sigma} = -(1-\alpha_0)\eta S_{i,\downarrow}^*$
Temperature-critical object albedo (at which environmental temperature does not vary with ground albedo)	$\alpha_0' = 1 - \left[(1-\eta) + 2\eta f_W^{-1} \bar{\theta}\right] \frac{r_{e,g}}{r_e}$
Convection-critical object albedo (at which object-to-air convection does not vary with ground albedo)	$\alpha_0'' = 1 - \left(1 - 2 f_W^{-1} \bar{\theta}\right) \frac{r_{e,g}}{r_r}$
Unobstructed downward insolation incident on cylindrical object	$S_{i,\downarrow}^* = I_H \left[f_T + f_W \left(\frac{1-\delta}{\pi} \cot\beta + \frac{\delta}{2}\right)\right]$
Object's average ambient normalized air temperature	$\bar{\theta} = 1 - \left[f_T \theta(H_0) + f_W \tilde{\theta}(H_0)\right]$
Normalized air temperature at height of object	$\theta(H_0) = \begin{cases} (H_0/\Delta)^{1/7} & H_0 < \Delta \\ 1 & H_0 > \Delta \end{cases}$
Normalized air temperature averaged between ground-level and height of object	$\tilde{\theta}(H_0) = \begin{cases} \frac{7}{8}\left(\frac{H_0}{\Delta}\right)^{1/7} & H_0 < \Delta \\ 1 - \frac{1}{8(H_0/\Delta)} & H_0 > \Delta \end{cases}$

Table 3-1. Summary of near-ground object sensitivities and critical albedos. Also shown are the insolation and air temperature functions required to evaluate these expressions.

Chapter 4: Near-Ground Object Calculations

4.1 Overview

The sensitivities of a near-ground object's environmental temperature and convection heat loss to ground albedo and shade fraction were computed for three typical near-ground objects: a human, a car, and a small building.

Generally speaking, these sensitivities can be expected to vary strongly with the ambient wind speed, because wind speed controls an object's convection resistance, which in turn strongly influences both surface temperature and convection loss. The variation of environmental temperature with ground albedo will also be strongly affected by the height of the thermal free-stream—that is, the thickness of the atmospheric thermal boundary layer—because the ambient air-temperature change experienced by a near-ground object following an albedo-change induced (or any other) perturbation of the ground temperature is greatest when the thermal free-stream is farthest from the ground (see Appendix F). Therefore, calculations were made for several wind speeds and boundary-layer heights.

4.2 Methodology

4.2.1 Theory

The near-ground object model of Chapter 3 predicts the effects of the changes in shade fraction and ground albedo on the environmental temperature and convection loss of a near ground object.

4.2.2 Cases

Three objects—a human, a compact car, and a bungalow (a small, low building)—were simulated under solar conditions typical of solar noon on July 1 in Berkeley, CA. Calculations were made for low and moderate wind speeds $\left(1 \text{ m s}^{-1} / 5 \text{ m s}^{-1}\right)$, and for "short" and "tall"† heights of the ground's thermal boundary-layer $(5 \text{ m} / 15 \text{ m})$. Thus, there were a total of twelve cases. The assumed values of the 10 independent parameters in these calculations—that is, the object properties and weather—are summarized in Tables 4-1 and 4-2.

4.2.3 Calculations

Values of the following six dependent variables, along with their sensitivities to object

†. These values are just educated guesses for the thermal boundary-layer heights that might be observed for albedo modifications over, say, a parking lot and a neighborhood. The proper estimation of thermal boundary-layer height is a tricky business and lies outside the scope of this study.

albedo α_0, boundary-layer height Δ, and ground convection resistance $r_{h,g}$, are presented case-by-case in Tables 4-9 through 4-20:

1. Temperature-critical object-albedo, α_0'. The object's albedo must exceed this value if its surface temperature is to be lowered by an increase in the ground albedo.
2. Convection-critical object albedo, α_0''. The object's albedo must exceed this value if its convective heating of the air is to reduced by an increase in the ground albedo.
3. Sensitivity of environmental temperature to ground albedo, $\partial T_e/\partial \alpha_g$.
4. Sensitivity of environmental temperature to shade fraction, $\partial T_e/\partial \sigma$.
5. Sensitivity of convection loss to ground albedo, $\partial H/\partial \alpha_g$.
6. Sensitivity of convection loss to shade fraction, $\partial H/\partial \sigma$.

The results-by-property are summarized in Tables 4-3 through 4-8.

4.2.4 Code

These calculations were made with the *Mathematica 3.0* program "Near-Ground Object Temperature Sensitivity Engine," presented in Appendix J.

4.3 RESULTS

4.3.1 Environmental Temperatures Versus Ground Albedo

The temperature-critical object albedo α_0' generally increased with object size and wind speed, and fell with boundary layer height (Table 4-3). The smallest critical albedo, observed for a human in a low wind and a tall boundary layer, was 0.15; this could readily be achieved by wearing light-colored clothing. The highest critical albedo, observed for a bungalow in a moderate wind and a short boundary layer, was 0.70; this would correspond to an unsullied, white-painted surface. The critical albedos may be compared to the typical surface albedos listed in Table D-1.

The sensitivity of environmental temperature to ground albedo, $\partial T_e/\partial \alpha_g$, varied in a complex manner with the object geometry, wind speed, and boundary layer height (Table 4-5). Since the objects were assigned albedo $\alpha_0 = 0.3$ †, their temperature sensitivities was negative—that is, the temperature declined when the ground albedo rose—only when their temperature-critical albedos were less than 0.3. The magnitude of the temperature sensitivity generally was generally greatest for low wind speeds, but the effect was complicated by the dependences of the temperature-critical object albedo on wind speed and boundary layer height (Table 4-3).

Sensitivities fell in the ranges -4.4 to +1.0 K for a human, -0.2 to +3.5 K for a car, and +3.9

†. This is a fairly common value—see Table D-1.

to +9.0 K for a bungalow. A ground albedo increase of $\Delta\alpha_g = 0.25$, such as has been proposed for Los Angeles in a study by Rosenfeld et al. 1996, would yield corresponding environmental temperature changes of -1.1 to +0.3 K, -0.4 to +0.9 K, and +1.0 to +2.3 K.

Obviously, this temperature sensitivity depends strongly on the object's actual albedo. Since $\partial T_e/\partial\alpha_g$ varies linearly with α_0, the value of $\partial T_e/\partial\alpha_g$ for an object with surface albedo other than 0.3 may be calculated from

$$\frac{\partial T_e}{\partial \alpha_g} = \left(\frac{\partial T_e}{\partial \alpha_g}\right)_{\alpha_0=0.3} + \left[\partial_{\alpha_0}\left(\frac{\partial T_e}{\partial \alpha_g}\right)\right](\alpha_0 - 0.3). \qquad (4\text{-}1)$$

Values of the partial derivative $\partial_{\alpha_0}\left(\partial T_e/\partial\alpha_g\right)$ may be found in the case calculations (Tables 4-9 through 4-20).

4.3.2 Environmental Temperature Versus Shade Fraction

Again assuming the near-ground objects have surface albedo $\alpha_0 = 0.3$, the sensitivity of environmental temperature to shade fraction, $\partial T_e/\partial\sigma$, ranged from -8.4 to -32 K in a low wind, and from -4.1 to -16 K in a moderate wind (Table 4-7). The results were independent of boundary-layer height because the shade effect has nothing to do with air temperature changes.

If the introduction of a tree canopy increases an object's shade fraction from 0 to 0.5, such that $\Delta\sigma = 0.5 - 0 = 0.5$, its surface temperature will drop 4.4 to 16 K in a mild wind, or 2.0 to 8.0 K in a strong wind.

4.3.3 Object Convection Versus Ground Albedo

The convection-critical object albedo α_0'' ranged from 0.71 to 1.0, increasing with wind speed and boundary-layer height, and decreasing with object height (Table 4-4). The range was quite small because α_0'' does not depend on an object's convection resistance, only on its height and its wall-area fraction. The convection-critical albedo varied weakly with boundary-layer height, because convection depends on the difference between the surface temperature (the environmental temperature) and the air temperature, and the variations of both with changes in ground temperature are similarly affected by variations in the boundary-layer height. These critical albedos are quite high, indicating that raising the albedo of the ground will increase the ground-level air heating by all but the whitest objects.

Again assuming the near-ground objects have surface albedo $\alpha_0 = 0.3$, the sensitivity of object convection to ground albedo, $\partial H/\partial\alpha_g$, ranged from +45 to +170 W m^{-2} in a low wind, and from +120 to +240 W m^{-2} in a moderate wind (Table 4-6). The sensitivity

increases as the object's convective resistance falls; thus, the effect rose with wind speed, and was stronger for a small-radius, low-resistance human than for the larger-radius, higher-resistance car and bungalow.

The aforementioned ground albedo increase of $\Delta\alpha_g = 0.25$ would raise the convective flux densities by 11 to 43 W m^{-2} in a low wind, and by 30 to 60 W m^{-2} in a moderate wind. As before, these figures depends on the object's actual albedo, and the value of $\partial T_e/\partial\alpha_g$ for an object with surface albedo other than 0.3 may be calculated from

$$\frac{\partial H}{\partial \alpha_g} = \left(\frac{\partial H}{\partial \alpha_g}\right)_{\alpha_0=0.3} + \left[\partial_{\alpha_0}\left(\frac{\partial H}{\partial \alpha_g}\right)\right](\alpha_0 - 0.3). \qquad (4\text{-}2)$$

Values of the partial derivative $\partial_{\alpha_0}\left(\partial H/\partial\alpha_g\right)$ may be found in the case calculations (Tables 4-9 through 4-20).

4.3.4 Object Convection Versus Shade Fraction

With surface albedo $\alpha_0 = 0.3$, the sensitivity of convection to shade fraction, $\partial H/\partial\sigma$, ranged from -81 to -100 W m^{-2} in a mild wind, and from -110 to -220 W m^{-2} in a strong wind (Table 4-8). Increasing the shade fraction by $\Delta\sigma = 0.5$ would decrease the convection flux density by 41 to 50 W m^{-2} in a mild wind, and by 55 to 110 W m^{-2} in a strong wind.

4.4 DISCUSSION

4.4.1 General Observations

Environmental Temperature vs. Ground Albedo. The results of the near-ground object calculations suggest that the albedos of near-ground objects can reasonably be made to exceed the temperature-critical object albedos; that is, it would be possible to lower the surface temperatures of brightly-clothed humans, white cars, and white houses by raising ground albedos. Low wind speeds and tall thermal boundary layers—particularly the latter—promote low temperature-critical object albedos. However, the sensitivity to ground albedo of the environmental temperature of an typical object with albedo $\alpha_0 = 0.3$ is not great: a ground albedo increase of 0.25 will alter the object's environmental and surface temperatures by about -1 to $+2$ K.

Convection Loss vs. Ground Albedo. The convection-critical albedo is much greater than the temperature-critical albedo, and is sufficiently close to unity that convective heating of the near-ground air by near-ground objects will rise with ground albedo for virtually all objects. The convection flux density increase due to a ground-albedo of $\Delta\alpha_g = 0.25$ is

on the order of $50\ \text{W m}^{-2}$. This is not very large. For comparison, note that Eq. (3-69) predicts that the sensitivity of ground-to-air convection to albedo is $\partial H_g/\partial \alpha_g = 770\ \text{W m}^{-2}$ when $r_{h,g} = 60\ \text{s m}^{-1}$ and $I_H = 1000\ \text{W m}^{-2}$. Thus the aforementioned ground albedo rise of $\Delta\alpha_g = 0.25$ will increase the ground-to-air convection flux density by about $200\ \text{W m}^{-2}$.

Environmental Temperature and Convection Loss vs. Shade Fraction. Unsurprisingly, shading yields sizable reductions in the environmental temperature and convection loss of near-ground objects. Increasing the shade fraction by 0.5—that is, half-shading an object that would otherwise be in fully sun—lowers environmental temperatures by about 2 to 16 K, and reduces the convection flux density by an amount on the order of $100\ \text{W m}^{-2}$. The decreases are greatest under low wind conditions, when the object's surface temperature is most sensitive to insolation. At noon, squat objects like a car or bungalow intercept higher solar flux densities than tall objects like a person, and thus exhibit greater shade-induced noontime decreases in environmental temperature and convection loss.

4.4.2 Model Uncertainties

Among the numerous approximations made in the near ground model—e.g. the cylindrical representation of non-cylindrical geometries, an approximate profile of temperature in the ground's thermal boundary layer, the application of long-cylinder convection resistance correlations to finite-length cylinders, and the neglect of free convection—the greatest uncertainties are likely introduced by

1. the arbitrary choice of atmospheric thermal boundary layer height, Δ;
2. the weakly-justified formula for the convection coefficient above a ground surface, Eq. (C-26); and
3. the application of an conductionless surface energy balance to a high-conduction surface like a metal car body.

Boundary Layer Height. The damping effect that the ground-temperature-invariant thermal free-stream has on ground-cooling-induced changes to near-ground air temperatures diminishes as the atmospheric thermal boundary layer grows thicker and the free-stream rises higher above the ground.Thus, the value chosen for the height of the atmospheric thermal boundary layer determines the extent to which changes in the ground temperature perturb the average temperature of air around a near-ground object. Increasing the boundary-layer height from 5 to 15 m reduced calculated values of the temperature-critical object albedo α_0' by about 0.15, which in turn reduced the variation of environmental temperature with ground albedo, $\partial T_e/\partial \alpha_g$, by about 3 K (Table 4-3).

Ground Convection Resistance. The temperature-critical and convection-critical object albedos, and thus the variations with ground albedo of environmental temperature and

convection loss, are sensitive to the ground's convection resistances. Unfortunately, the ground resistance depends on a rather arbitrarily chosen expression for the variation of the ground's convection resistance with wind speed (see Section C.5).

Say the ground convection coefficient is $\bar{h}_g \approx 20 \pm 5$ W m^{-2} K^{-1}, and thus the ground convection resistance is $r_{h,g} \approx 60 \pm 15$ s m^{-1}. The sensitivity of temperature-critical object albedo α_0' to $r_{h,g}$ ranges from about 10^{-3} to 10^{-2} m s^{-1}, so the 15 s m^{-1} uncertainly in $r_{h,g}$ will yield an uncertainly in α_0' of 0.015 to 0.15 (see derivatives in Tables 4-9 through 4-20). Proceeding similarly, the sensitivity of $\partial T_e/\partial \alpha_g$ to $r_{h,g}$ is on the order of 10^{-1} K m s^{-1}, yielding an uncertainty in $\partial T_e/\partial \alpha_g$ of about 1.5 K; the sensitivity of convection-critical object albedo α_0'' to $r_{h,g}$ is about 10^{-3} m s^{-1}, yielding an uncertainty in α_0'' of about 0.015; and the sensitivity of $\partial H/\partial \alpha_g$ to $r_{h,g}$ ranges from about 10^{0} to 10^{-2} W m^{-1} s^{-1}, yielding an uncertainty in $\partial H/\partial \alpha_g$ of 0.15 to 15 W m^{-2}. Thus the uncertainty in the ground convection coefficient has stronger effect on environmental temperature than on convection.

Conductionless Surface Energy Balance. Neglecting conduction of heat from the surface of a car into its metal body greatly overestimates both the surface temperature of the car, and the amount of heat convected from the car to the air. Noting that $L + S = H + K$, or $H - L = S - K$, the conduction loss may be considered equivalent to a reduction in the surface's solar heat gain. The critical object albedos do not vary with insolation, but the sensitivities of environmental temperature and convection to ground albedo and shade fraction are proportional to insolation. Thus, in the case of the car, the predicted critical object albedos are valid, but the predicted temperature and convection sensitivities are too high. It is difficult to quantify this overestimation without constructing a transient energy balance for the car, and the effort involved in that endeavor seems unwarranted.

Object	Description	Height (m)	Radius (m)	Albedo
Human	70 kg, 1.7 m adult	1.7	0.15	0.3
Car	Compact car (e.g. Toyota Corolla)	1.4	1.5	0.3
Bungalow	Small, low building	5	5	0.3

Table 4-1. Near-ground object properties assumed in calculations.

Parameter	Description	Value
U	wind speed	1 m s^{-1} (low) 5 m s^{-1} (moderate)
n_t	turbulence factor	1.5
Δ	ground thermal boundary layer height	5 m (short) 15 m (tall)
I_N	beam-normal insolation flux density	800 W m^{-2}
β	solar elevation	77°
δ	diffuse fraction of horizontal insolation	0.2
$\overline{T}$	temperature used to calculate radiative resistances of ground and object	300 K

Table 4-2. Weather conditions assumed for solar noon on July 1 in Berkeley, CA.

α_0'	Human	Car	Bungalow
Short Boundary Layer			
Low Wind	0.29	0.41	0.56
Moderate Wind	0.37	0.45	0.70
Tall Boundary Layer			
Low Wind	0.15	0.32	0.42
Moderate Wind	0.18	0.29	0.53

Table 4-3. Temperature-critical object albedo, α_0', in low and moderate winds, and short and tall ground thermal boundary layers, for human, car, and bungalow.

α_0''	Human	Car	Bungalow
Short Boundary Layer			
Low Wind	0.81	0.89	0.71
Moderate Wind	0.90	0.94	0.85
Tall Boundary Layer			
Low Wind	0.90	1.0	0.86
Moderate Wind	0.95	1.0	0.93

Table 4-4. Convection-critical object albedo, α_0'', in low and moderate winds, and short and tall ground thermal boundary layers, for human, car, and bungalow.

$\partial T_e/\partial \alpha_g$	Human	Car	Bungalow
Short Boundary Layer			
Low Wind	-0.19	3.5	9.0
Moderate Wind	1.0	2.3	6.8
Tall Boundary Layer			
Low Wind	-4.4	0.67	6.1
Moderate Wind	-1.8	-0.17	3.9

Table 4-5. Variation of environmental temperature with ground albedo, $\partial T_e/\partial \alpha_g$, in low and moderate winds, and short and tall ground thermal boundary layers, for human, car, and bungalow. Units are K, and object albedo α_0 is assumed to be 0.3.

$\partial H/\partial \alpha_g$	Human	Car	Bungalow
Short Boundary Layer			
Low Wind	140	76	45
Moderate Wind	230	140	120
Tall Boundary Layer			
Low Wind	170	94	63
Moderate Wind	240	160	140

Table 4-6. Variation of object-to-air convection with ground albedo, $\partial H/\partial \alpha_g$, in low and moderate winds, and short and tall ground thermal boundary layers, for human, car, and bungalow. Units are W m^{-2}, and object albedo α_0 is assumed to be 0.3.

$\partial T_e/\partial\sigma$	Human	Car	Bungalow
Short Boundary Layer			
Low Wind	-8.4	-30	-32
Moderate Wind	-4.1	-15	-16
Tall Boundary Layer			
Low Wind	-8.4	-30	-32
Moderate Wind	-4.1	-15	-16

Table 4-7. Variation of environmental temperature with shade fraction, $\partial T_e/\partial\sigma$, in low and moderate winds, and short and tall ground thermal boundary layers, for human, car, and bungalow. Units are K, and object albedo α_0 is assumed to be 0.3.

$\partial H/\partial\sigma$	Human	Car	Bungalow
Short Boundary Layer			
Low Wind	-210	-130	-100
Moderate Wind	-110	-220	-200
Tall Boundary Layer			
Low Wind	-210	-130	-100
Moderate Wind	-110	-220	-200

Table 4-8. Variation of object-to-air convection with shade fraction, $\partial H/\partial\sigma$, in low and moderate winds, and short and tall ground thermal boundary layers, for human, car, and bungalow. Units are W m^{-2}, and object albedo α_0 is assumed to be 0.3.

Case: Human, low wind, short boundary layer, noon, July 1.

(H_0=1.7, R_0=0.15, U=1, n_t=1.5, Δ=5, I_N=800, α_0=0.3, β=77, δ=0.2, $\overline{T}$=300)

	α_0'	α_0''	$\frac{\partial T_e}{\partial \alpha_g}$	$\frac{\partial T_e}{\partial \sigma}$	$\frac{\partial H}{\partial \alpha_g}$	$\frac{\partial H}{\partial \sigma}$
value	2.9×10^{-1}	8.1×10^{-1}	-1.9×10^{-1}	-8.4	1.4×10^{2}	-8.1×10^{1}
∂_{α_0}	0.0	0.0	-3.0×10^{1}	1.2×10^{1}	-2.8×10^{2}	1.2×10^{2}
∂_{Δ}	-2.8×10^{-2}	1.8×10^{-2}	-8.2×10^{-1}	0.0	5.0	0.0
$\partial_{r_{h,g}}$	-3.4×10^{-3}	-9.1×10^{-4}	-1.0×10^{-1}	0.0	-2.6×10^{-1}	0.0

Table 4-9. Human in a low wind and a short thermal boundary layer: calculations of the temperature-critical and convection-critical object albedos α_0' and α_0'', and the sensitivities of environmental temperature T_e and convection loss H to ground albedo α_g and shade fraction σ. Also, the partial derivatives of these properties with respect to the object albedo α_0, boundary-layer height Δ, and ground convection resistance $r_{h,g}$.

Case: Human, moderate wind, short boundary layer, noon, July 1.

(H_0=1.7, R_0=0.15, U=5, n_t=1.5, Δ=5, I_N=800, α_0=0.3, β=77, δ=0.2, $\overline{T}$=300)

	α_0'	α_0''	$\frac{\partial T_e}{\partial \alpha_g}$	$\frac{\partial T_e}{\partial \sigma}$	$\frac{\partial H}{\partial \alpha_g}$	$\frac{\partial H}{\partial \sigma}$
value	3.7×10^{-1}	9.0×10^{-1}	1.0	-4.1	2.3×10^{2}	-1.1×10^{2}
∂_{α_0}	0.0	0.0	-1.5×10^{1}	5.9	-3.8×10^{2}	1.5×10^{2}
∂_{Δ}	-3.8×10^{-2}	8.9×10^{-3}	-5.5×10^{-1}	0.0	3.4	0.0
$\partial_{r_{h,g}}$	-1.0×10^{-2}	-1.6×10^{-3}	-1.5×10^{-1}	0.0	-6.0×10^{-1}	0.0

Table 4-10. Human in a moderate wind and a short thermal boundary layer: calculations of the temperature-critical and convection-critical object albedos α_0' and α_0'', and the sensitivities of environmental temperature T_e and convection loss H to ground albedo α_g and shade fraction σ. Also, the partial derivatives of these properties with respect to the object albedo α_0, boundary-layer height Δ, and ground convection resistance $r_{h,g}$

Case: Human, low wind, tall boundary layer, noon, July 1.

(H_0=1.7, R_0=0.15, U=1, n_t=1.5, Δ=15, I_N=800, α_0=0.3, β=77, δ=0.2, $\bar{T}$=300)

	α_0'	α_0''	$\frac{\partial T_e}{\partial \alpha_g}$	$\frac{\partial T_e}{\partial \sigma}$	$\frac{\partial H}{\partial \alpha_g}$	$\frac{\partial H}{\partial \sigma}$
value	1.5×10^{-1}	9.0×10^{-1}	-4.4	-8.4	1.7×10^{2}	-8.1×10^{1}
∂_{α_0}	0.0	0.0	-3.0×10^{1}	1.2×10^{1}	-2.8×10^{2}	1.2×10^{2}
∂_{Δ}	-7.9×10^{-3}	5.0×10^{-3}	-2.3×10^{-1}	0.0	1.4	0.0
$\partial_{r_{h,g}}$	-4.0×10^{-3}	-4.8×10^{-4}	-1.2×10^{-1}	0.0	-1.4×10^{-1}	0.0

Table 4-11. Human in a low wind and a tall thermal boundary layer: calculations of the temperature-critical and convection-critical object albedos α_0' and α_0'', and the sensitivities of environmental temperature T_e and convection loss H to ground albedo α_g and shade fraction σ. Also, the partial derivatives of these properties with respect to the object albedo α_0, boundary-layer height Δ, and ground convection resistance $r_{h,g}$.

Case: Human, moderate wind, tall boundary layer, noon, July 1.

(H_0=1.7, R_0=0.15, U=5, n_t=1.5, Δ=15, I_N=800, α_0=0.3, β=77, δ=0.2, $\bar{T}$=300)

	α_0'	α_0''	$\frac{\partial T_e}{\partial \alpha_g}$	$\frac{\partial T_e}{\partial \sigma}$	$\frac{\partial H}{\partial \alpha_g}$	$\frac{\partial H}{\partial \sigma}$
value	1.8×10^{-1}	9.5×10^{-1}	-1.8	-4.1	2.4×10^{2}	-1.1×10^{2}
∂_{α_0}	0.0	0.0	-1.5×10^{1}	5.9	-3.8×10^{2}	1.5×10^{2}
∂_{Δ}	-1.1×10^{-2}	2.5×10^{-3}	-1.6×10^{-1}	0.0	9.6×10^{-1}	0.0
$\partial_{r_{h,g}}$	-1.3×10^{-2}	-8.4×10^{-4}	-2.0×10^{-1}	0.0	-3.2×10^{-1}	0.0

Table 4-12. Human in a moderate wind and a tall thermal boundary layer: calculations of the temperature-critical and convection-critical object albedos α_0' and α_0'', and the sensitivities of environmental temperature T_e and convection loss H to ground albedo α_g and shade fraction σ. Also, the partial derivatives of these properties with respect to the object albedo α_0, boundary-layer height Δ, and ground convection resistance $r_{h,g}$.

Case: Car, low wind, short boundary layer, noon, July 1.

(H_0=1.4, R_0=1.5, U=1, n_t=1.5, Δ=5, I_N=800, α_0=0.3, β=77, δ=0.2, $\overline{T}$=300)

	α_0'	α_0''	$\frac{\partial T_e}{\partial \alpha_g}$	$\frac{\partial T_e}{\partial \sigma}$	$\frac{\partial H}{\partial \alpha_g}$	$\frac{\partial H}{\partial \sigma}$
value	4.1×10^{-1}	8.9×10^{-1}	3.5	-3.0×10^{1}	7.6×10^{1}	-1.3×10^{2}
∂_{α_0}	0.0	0.0	-3.1×10^{1}	4.3×10^{1}	-1.3×10^{2}	1.8×10^{2}
∂_{Δ}	-1.8×10^{-2}	2.6×10^{-2}	-5.6×10^{-1}	0.0	3.4	0.0
$\partial_{r_{h,g}}$	-2.8×10^{-3}	-5.3×10^{-4}	-8.6×10^{-2}	0.0	-6.8×10^{-2}	0.0

Table 4-13. Car in a low wind and a short thermal boundary layer: calculations of the temperature-critical and convection-critical object albedos α_0' and α_0'', and the sensitivities of environmental temperature T_e and convection loss H to ground albedo α_g and shade fraction σ. Also, the partial derivatives of these properties with respect to the object albedo α_0, boundary-layer height Δ, and ground convection resistance $r_{h,g}$.

Case: Car, moderate wind, short boundary layer, noon, July 1.

(H_0=1.4, R_0=1.5, U=5, n_t=1.5, Δ=5, I_N=800, α_0=0.3, β=77, δ=0.2, $\overline{T}$=300)

	α_0'	α_0''	$\frac{\partial T_e}{\partial \alpha_g}$	$\frac{\partial T_e}{\partial \sigma}$	$\frac{\partial H}{\partial \alpha_g}$	$\frac{\partial H}{\partial \sigma}$
value	4.5×10^{-1}	9.4×10^{-1}	2.3	-1.5×10^{1}	1.4×10^{2}	-2.2×10^{2}
∂_{α_0}	0.0	0.0	-1.5×10^{1}	2.1×10^{1}	-2.2×10^{2}	3.1×10^{2}
∂_{Δ}	-3.2×10^{-2}	1.3×10^{-2}	-4.9×10^{-1}	0.0	3.0	0.0
$\partial_{r_{h,g}}$	-8.9×10^{-3}	-9.1×10^{-4}	-1.3×10^{-1}	0.0	-2.1×10^{-1}	0.0

Table 4-14. Car in a moderate wind and a short thermal boundary layer: calculations of the temperature-critical and convection-critical object albedos α_0' and α_0'', and the sensitivities of environmental temperature T_e and convection loss H to ground albedo α_g and shade fraction σ. Also, the partial derivatives of these properties with respect to the object albedo α_0, boundary-layer height Δ, and ground convection resistance $r_{h,g}$.

Case: Car, low wind, tall boundary layer, noon, July 1.

(H_0=1.4, R_0=1.5, U=1, n_t=1.5, Δ=15, I_N=800, α_0=0.3, β=77, δ=0.2, $\overline{T}$=300)

	α_0'	α_0''	$\frac{\partial T_e}{\partial \alpha_g}$	$\frac{\partial T_e}{\partial \sigma}$	$\frac{\partial H}{\partial \alpha_g}$	$\frac{\partial H}{\partial \sigma}$
value	3.2×10^{-1}	1.0	6.7×10^{-1}	-3.0×10^{1}	9.4×10^{1}	-1.3×10^{2}
∂_{α_0}	0.0	0.0	-3.1×10^{1}	4.3×10^{1}	-1.3×10^{2}	1.8×10^{2}
∂_{Δ}	-5.2×10^{-3}	7.5×10^{-3}	-1.6×10^{-1}	0.0	9.7×10^{-1}	0.0
$\partial_{r_{h,g}}$	-3.2×10^{-3}	1.1×10^{-4}	-9.9×10^{-2}	0.0	1.5×10^{-2}	0.0

Table 4-15. Car in a low wind and a tall thermal boundary layer: calculations of the temperature-critical and convection-critical object albedos α_0' and α_0'', and the sensitivities of environmental temperature T_e and convection loss H to ground albedo α_g and shade fraction σ. Also, the partial derivatives of these properties with respect to the object albedo α_0, boundary-layer height Δ, and ground convection resistance $r_{h,g}$.

Case: Car, moderate wind, tall boundary layer, noon, July 1.

(H_0=1.4, R_0=1.5, U=5, n_t=1.5, Δ=15, I_N=800, α_0=0.3, β=77, δ=0.2, $\overline{T}$=300)

	α_0'	α_0''	$\frac{\partial T_e}{\partial \alpha_g}$	$\frac{\partial T_e}{\partial \sigma}$	$\frac{\partial H}{\partial \alpha_g}$	$\frac{\partial H}{\partial \sigma}$
value	2.9×10^{-1}	1.0	-1.7×10^{-1}	-1.5×10^{1}	1.6×10^{2}	-2.2×10^{2}
∂_{α_0}	0.0	0.0	-1.5×10^{1}	2.1×10^{1}	-2.2×10^{2}	3.1×10^{2}
∂_{Δ}	-9.3×10^{-3}	3.8×10^{-3}	-1.4×10^{-1}	0.0	8.6×10^{-1}	0.0
$\partial_{r_{h,g}}$	-1.2×10^{-2}	2.0×10^{-4}	-1.8×10^{-1}	0.0	4.4×10^{-2}	0.0

Table 4-16. Car in a moderate wind and a tall thermal boundary layer: calculations of the temperature-critical and convection-critical object albedos α_0' and α_0'', and the sensitivities of environmental temperature T_e and convection loss H to ground albedo α_g and shade fraction σ. Also, the partial derivatives of these properties with respect to the object albedo α_0, boundary-layer height Δ, and ground convection resistance $r_{h,g}$.

Case: Bungalow, low wind, short boundary layer,noon, July 1.

(H_0=5, R_0=5, U=1, n_t=1.5, Δ=5, I_N=800, α_0=0.3, β=77, δ=0.2, $\bar{T}$=300)

	α_0'	α_0''	$\frac{\partial T_e}{\partial \alpha_g}$	$\frac{\partial T_e}{\partial \sigma}$	$\frac{\partial H}{\partial \alpha_g}$	$\frac{\partial H}{\partial \sigma}$
value	5.6×10^{-1}	7.1×10^{-1}	9.0	-3.2×10^{1}	4.5×10^{1}	-1.0×10^{2}
∂_{α_0}	0.0	0.0	-3.5×10^{1}	4.6×10^{1}	-1.1×10^{2}	1.5×10^{2}
∂_{Δ}	-1.6×10^{-2}	3.1×10^{-2}	-5.6×10^{-1}	0.0	3.4	0.0
$\partial_{r_{h,g}}$	-2.1×10^{-3}	-1.4×10^{-3}	-7.4×10^{-2}	0.0	-1.6×10^{-1}	0.0

Table 4-17. Bungalow in a low wind and a short thermal boundary layer: calculations of the temperature-critical and convection-critical object albedos α_0' and α_0'', and the sensitivities of environmental temperature T_e and convection loss H to ground albedo α_g and shade fraction σ. Also, the partial derivatives of these properties with respect to the object albedo α_0, boundary-layer height Δ, and ground convection resistance $r_{h,g}$.

Case: Bungalow, moderate wind, short boundary layer, noon, July 1.

(H_0=5, R_0=5, U=5, n_t=1.5, Δ=5, I_N=800, α_0=0.3, β=77, δ=0.2, $\bar{T}$=300)

	α_0'	α_0''	$\frac{\partial T_e}{\partial \alpha_g}$	$\frac{\partial T_e}{\partial \sigma}$	$\frac{\partial H}{\partial \alpha_g}$	$\frac{\partial H}{\partial \sigma}$
value	7.0×10^{-1}	8.5×10^{-1}	6.8	-1.6×10^{1}	1.2×10^{2}	-2.0×10^{2}
∂_{α_0}	0.0	0.0	-1.7×10^{1}	2.3×10^{1}	-2.2×10^{2}	2.9×10^{2}
∂_{Δ}	-3.3×10^{-2}	1.6×10^{-2}	-5.6×10^{-1}	0.0	3.4	0.0
$\partial_{r_{h,g}}$	-5.0×10^{-3}	-2.4×10^{-3}	-8.5×10^{-2}	0.0	-5.4×10^{-1}	0.0

Table 4-18. Bungalow in a moderate wind and a short thermal boundary layer: calculatio ns of the temperature-critical and convection-critical object albedos α_0' and α_0'', and the sensitivities of environmental temperature T_e and convection loss H to ground albedo α_g and shade fraction σ. Also, the partial derivatives of these properties with respect to the object albedo α_0, boundary-layer height Δ, and ground convection resistance $r_{h,g}$.

Case: Bungalow, low wind, tall boundary layer, noon, July 1.

(H_0=5, R_0=5, U=1, n_t=1.5, Δ=15, I_N=800, α_0=0.3, β=77, δ=0.2, $\overline{T}$=300)

	α_0'	α_0''	$\frac{\partial T_e}{\partial \alpha_g}$	$\frac{\partial T_e}{\partial \sigma}$	$\frac{\partial H}{\partial \alpha_g}$	$\frac{\partial H}{\partial \sigma}$
value	4.8×10^{-1}	8.6×10^{-1}	6.1	-3.2×10^{1}	6.3×10^{1}	-1.0×10^{2}
∂_{α_0}	0.0	0.0	-3.5×10^{1}	4.6×10^{1}	-1.1×10^{2}	1.5×10^{2}
∂_{Δ}	-4.6×10^{-3}	8.8×10^{-3}	-1.6×10^{-1}	0.0	9.8×10^{-1}	0.0
$\partial_{r_{h,g}}$	-2.5×10^{-3}	-6.6×10^{-4}	-8.7×10^{-2}	0.0	-7.3×10^{-2}	0.0

Table 4-19. Bungalow in a low wind and a tall thermal boundary layer: calculations of the temperature-critical and convection-critical object albedos α_0' and α_0'', and the sensitivities of environmental temperature T_e and convection loss H to ground albedo α_g and shade fraction σ. Also, the partial derivatives of these properties with respect to the object albedo α_0, boundary-layer height Δ, and ground convection resistance $r_{h,g}$.

Case: Bungalow, moderate wind, tall boundary layer, noon, July 1.

(H_0=5, R_0=5, U=5, n_t=1.5, Δ=15, I_N=800, α_0=0.3, β=77, δ=0.2, $\overline{T}$=300)

	α_0'	α_0''	$\frac{\partial T_e}{\partial \alpha_g}$	$\frac{\partial T_e}{\partial \sigma}$	$\frac{\partial H}{\partial \alpha_g}$	$\frac{\partial H}{\partial \sigma}$
value	5.3×10^{-1}	9.3×10^{-1}	3.9	-1.6×10^{1}	1.4×10^{2}	-2.0×10^{2}
∂_{α_0}	0.0	0.0	-1.7×10^{1}	2.3×10^{1}	-2.2×10^{2}	2.9×10^{2}
∂_{Δ}	-9.4×10^{-3}	4.4×10^{-3}	-1.6×10^{-1}	0.0	9.8×10^{-1}	0.0
$\partial_{r_{h,g}}$	-7.7×10^{-3}	-1.1×10^{-3}	-1.3×10^{-1}	0.0	-2.5×10^{-1}	0.0

Table 4-20. Bungalow in a moderate wind and a tall thermal boundary layer: calculations of the temperature-critical and convection-critical object albedos α_0' and α_0'', and the sensitivities of environmental temperature T_e and convection loss H to ground albedo α_g and shade fraction σ. Also, the partial derivatives of these properties with respect to the object albedo α_0, boundary-layer height Δ, and ground convection resistance $r_{h,g}$.

Chapter 5: Tree Model

5.1 Overview

The rates of latent and sensible heat loss from a tree leaf can be found from coupled balances of vapor and heat flow (see Section A.5). To determine the corresponding rates for the entire canopy of a tree, a model of the spatial variation of insolation, radiative temperature, air temperature, and air humidity within the canopy is required. This section introduces an "opaque-cone" canopy model that partition a densely-foliated, conically-shaped tree canopy into three regions: the cone's lateral wall, the cone's base, and the cone's interior. The wall receives insolation from and exchanges LW radiation with the sky and ground; the base receives reflected insolation from and exchanges LW radiation with the ground; the interior is assumed to gain neither insolation nor LW radiation. The air temperature and humidity are assumed uniform throughout the canopy.

The opaque-cone model is used to derive expressions for (a) the convection and latent heat losses from the canopy; (b) the canopy-averaged stomatal resistance; (c) the decrease in ground-to-air convection induced by the tree's shadow; and (d) the critical downward mixing fraction. The last item compares the tree's ground-level cooling effect to its canopy-level heating effect.

5.2 Areal (Area-Integrated) Heat Flows

5.2.1 Latent Heat Loss

Evaluating the vapor density slope at air temperature, the latent heat loss per unit area of a leaf given by Eq. (A-49) is

$$\lambda E = \frac{C r_h^{-1} \rho_{sd} + s_a Q_{\text{dry}}}{\gamma^* + \eta s_a}. \tag{5-1}$$

Recall that

$$\gamma^* \equiv \frac{r_v}{r_h}\gamma \text{ and } \eta \equiv \frac{r_r}{r_r + r_h}. \tag{5-2}$$

If the convective resistance r_h, radiative resistance r_r, diffusive resistance r_v, saturation deficit ρ_{sd}, and air temperature T_a are uniform over some area A, Eq. (5-1) may be integrated to find the areal latent heat loss,

$$\lambda \hat{E} = \iint_A dA\, \lambda E = \iint_A dA\, \frac{C r_h^{-1} \rho_{sd} + s_a Q_{\text{dry}}}{\gamma^* + \eta s_a} = \frac{A C r_h^{-1} \rho_{sd} + s_a \hat{Q}_{\text{dry}}}{\gamma^* + \eta s_a}. \tag{5-3}$$

5.2.2 Dry-Surface All-Wave Radiative Gain

Integrating Eq. (A-20), the areal dry AW radiative gain $\hat{Q}_{\text{dry}}$ is

$$\hat{Q}_{\text{dry}} = \iint_A dA\, Q_{\text{dry}} = \iint_A dA\, \eta\left[C r_r^{-1}(T_r - T_a) + S\right]. \tag{5-4}$$

If the long-wave radiative temperature T_r is constant over the area of integration,

$$\hat{Q}_{\text{dry}} = \eta\left[A C r_r^{-1}(T_r - T_a) + \hat{S}\right], \tag{5-5}$$

where

$$\hat{S} = \iint_A dA\, S. \tag{5-6}$$

5.2.3 Convective Loss and Long-Wave Radiative Gain

The areal convective loss $\hat{H}$ and areal LW radiative gain $\hat{L}$ may be calculated by integrating Eqs. (A-50) and (A-51), yielding

$$\hat{H} = \hat{Q}_{\text{dry}} - \eta\, \lambda\hat{E} \tag{5-7}$$

and

$$\hat{L} = \hat{Q}_{\text{dry}} + (1-\eta)\lambda\hat{E} - \hat{S}. \tag{5-8}$$

5.2.4 Surface Temperature

If T is the surface temperature, multiplying Eq. (A-2) by A gives the areal convective loss

$$\hat{H} = A C r_h^{-1}(T - T_a). \tag{5-9}$$

Solving Eqs. (5-7) and (5-9) for the surface temperature yields

$$T = T_a + (A C)^{-1} r_h\left(\hat{Q}_{\text{dry}} - \eta\lambda\hat{E}\right). \tag{5-10}$$

5.3 Back-Calculating the Diffusive Resistances

It is frequently desired in plant studies to determine the stomatal diffusive resistance r_{vs} from measured values of the latent heat loss $\lambda\hat{E}$. The total diffusive resistance of leaves that transpire on only one side is

$$r_v = r_{vs} + r_{va}, \tag{5-11}$$

where r_{va} is the boundary-layer diffusive resistance. Eqs. (5-2) and (5-3) may be rearranged to find the total diffusive resistance

$$r_v = \frac{r_h}{\gamma}\gamma^* = \frac{r_h}{\gamma}\left[\frac{AC r_h^{-1}\rho_{sd} + s_a\hat{Q}_{\text{dry}}}{\lambda\hat{E}} - \eta s_a\right]. \tag{5-12}$$

If the leaf is modeled as a flat plate with a turbulent upstream, the boundary layer resistance r_{va} may be computed from Eqs. (C-7) and (C-18). Then the stomatal resistance may be calculated from Eqs. (5-11) and (5-12) as

$$r_{vs} = r_v - r_{va} = \frac{r_h}{\gamma}\left[\frac{AC r_h^{-1}\rho_{sd} + s_a\hat{Q}_{\text{dry}}}{\lambda\hat{E}} - \eta s_a\right] - r_{va}. \tag{5-13}$$

5.4 PARTITIONING THE CANOPY

5.4.1 Need For Uniform Radiative Temperatures

The stomatal resistance expression given by Eq. (5-13) can not be applied unless $\lambda\hat{E}$ and $\hat{Q}_{\text{dry}}$ are known over the same area. This presents a small problem: while lysimeter (plant-weighting) experiments measure the whole-canopy latent heat loss $\lambda\hat{E}_0$, the convenient expression in Eq. (5-5) for the dry AW gain $\hat{Q}_{\text{dry}}$ applies only to a collection of leaves exposed to the same LW radiative temperature T_r.

5.4.2 Regions

Let the tree's whole-canopy area A_0 be partitioned into N non-overlapping regions $n = 1 \ldots N$ such that

$$A_0 = \sum_{n=1}^{N} A_n. \tag{5-14}$$

If each region sees radiative temperature $T_{r,n}$ and has SW gain $\hat{S}_n$, Eq. (5-5) yields

$$\hat{Q}_{\text{dry},n} = \eta\left[A_n C r_r^{-1}\left(T_{r,n} - T_a\right) + \hat{S}_n\right]. \tag{5-15}$$

The whole-canopy dry AW gain is

$$\hat{Q}_{\text{dry},0} = \iint_{A_0} dA\, Q_{\text{dry}} = \sum_{n=1}^{N} \hat{Q}_{\text{dry},n}. \tag{5-16}$$

5.4.3 Regional Latent Heat Losses

Applying Eq. (5-3) to $\hat{Q}_{\text{dry},n}$ and to $\hat{Q}_{\text{dry},0}$,

$$\lambda\hat{E}_n = \frac{A_n C r_h^{-1} \rho_{sd} + s_a \hat{Q}_{\text{dry},n}}{\gamma^* + \eta s_a} \tag{5-17}$$

and

$$\lambda\hat{E}_0 = \frac{A_0 C r_h^{-1} \rho_{sd} + s_a \hat{Q}_{\text{dry},0}}{\gamma^* + \eta s_a}. \tag{5-18}$$

Dividing Eq. (5-17) by Eq. (5-18), the ratio ω_n of the latent heat loss from a single region n to that from the whole canopy is

$$\omega_n \equiv \frac{\lambda\hat{E}_n}{\lambda\hat{E}_0} = \frac{A_n C r_h^{-1} \rho_{sd} + s_a \hat{Q}_{\text{dry},n}}{A_0 C r_h^{-1} \rho_{sd} + s_a \hat{Q}_{\text{dry},0}}. \tag{5-19}$$

Thus if the whole-canopy latent heat loss $\lambda\hat{E}_0$ is known, the latent heat loss from a single region n may be calculated from

$$\lambda\hat{E}_n = \omega_n \lambda\hat{E}_0. \tag{5-20}$$

5.5 Opaque-Cone Canopy Model

5.5.1 Assumptions

If a canopy is sufficiently dense that most incident sunlight is stopped by a shallow layer of leaves on the outside of the canopy, it is logical to partition the canopy into a dark inner canopy and a sunlit outer canopy. The following model is proposed for a densely-foliated, conical tree (Figure 5-1).

1. The canopy is represented by an upward-pointing right-circular cone of radius R_0 and height H_0.
2. The outer canopy consists of the cone's curved lateral wall, denoted W, and the cone's base, denoted B. The inner canopy, denoted I, is the interior of the cone.
3. The outer canopy is idealized as an unbroken surface, one-leaf-thick. Each leaf has an outward-facing side that sees the sky and/or ground and an inward-facing side that sees the inner canopy.
4. The inner canopy sees only itself. It is assumed thick enough that edge effects may be neglected; that is, the fact that the outermost leaves of the inner canopy will see the outer canopy is ignored.
5. The inner canopy receives enough sunlight to open the stomata of its leaves, but little enough that heat gain by insolation may be neglected. This is reasonable given that stomata typically open when exposed to as little as 1/30 to 1/1000 of full sunlight (Salis-

bury and Ross 1985, p.61).

6. Each region—outer canopy side, outer canopy base, and inner canopy—is assumed isothermal.

5.6 RADIATIVE TEMPERATURES

5.6.1 Inner Canopy

If the inner canopy is isothermal, sees only itself, and receives no insolation, then $L_I = S_I = 0$. Thus

$$Q_I = L_I + S_I = 0. \tag{5-21}$$

Since

$$Q_I = H_I + \lambda E_I = C r_h^{-1}\left(T_I - T_a\right) + \lambda E_I = 0, \tag{5-22}$$

latent heat loss will depress the leaf temperature below air temperature:

$$T_a - T_I = C^{-1} r_h \lambda E_I. \tag{5-23}$$

However, this difference may be quite small. In the lysimeter experiment detailed in Chapter 6, $r_h \approx 20$ s m^{-1} and $\lambda E_I < 50$ W m^{-2}, which yields a maximum expected temperature depression of less than 1 K. Thus it will be assumed that

$$T_{r,I} = T_I = T_a. \tag{5-24}$$

5.6.2 Outer-Canopy Side Wall

The inner surface of the side wall sees only the inner canopy, so it sees a radiative temperature of

$$T_{r,W,1} = T_I \approx T_a. \tag{5-25}$$

The wall's outer surface sees both sky and ground. Using view factors from Eqs. (D-18) and (D-20),

$$F_{W\to s} = \tfrac{1}{2}(1 + \cos\alpha) \tag{5-26}$$

and

$$F_{W\to g} = 1 - F_{W\to s}. \tag{5-27}$$

As usual, $\alpha = \arctan\left(H_0/R_0\right)$ is the cone's angle of elevation. The outer surface sees

$$T_{r,W,2} = F_{W\to s} T_s + F_{W\to g} T_g = F_{W\to s} T_s + \left(1 - F_{W\to s}\right) T_g. \tag{5-28}$$

Substituting Eq. (D-23) for the sky temperature,

$$T_{r,W,2} = F_{W\to s}\, \varepsilon_s^{1/4}\, T_a + \left(1 - F_{W\to s}\right) T_g \tag{5-29}$$

Thus the wall sees the average radiative temperature

$$T_{r,W} = \tfrac{1}{2}\left(T_{r,W,1} + T_{r,W,2}\right) = \tfrac{1}{2}\left[\left(1+\varepsilon_s^{1/4} F_{W\to s}\right)T_a + \left(1 - F_{W\to s}\right)T_g\right]. \tag{5-30}$$

Since the side wall exchanges radiation on two sides, its radiative resistance is given by Eq. (D-13):

$$C r_r^{-1} = 8\sigma \overline{T}^3, \quad \overline{T} \approx T_a. \tag{5-31}$$

5.6.3 Outer-Canopy Base

The upper surface of the base sees the inner canopy, while the outer surface sees the ground, so the base sees an average radiative temperature

$$T_{r,B} = \tfrac{1}{2}\left(T_a + T_g\right). \tag{5-32}$$

Its radiative resistance is the same as the wall's.

5.6.4 Ground Temperature

The ground temperature in Eqs. (5-30) and (5-32) may be found from Eq. (3-38).

5.7 SHORT-WAVE RADIATION

5.7.1 Inner Canopy

By assumption,

$$\hat{S}_I = 0. \tag{5-33}$$

5.7.2 Outer-Canopy Side Wall

Eq. (D-29) gives the direct insolation incident on the side wall:

$$\hat{S}_{i,W,\mathrm{dir}} = \begin{cases} (1-\delta) I_H A_B & \beta > \alpha \\ (1-\delta) I_H A_B \pi^{-1}\left[(\pi - \phi_0) + \tan\phi_0\right] & \beta < \alpha \end{cases}, \tag{5-34}$$

where $A_B = \pi R_0^2$ is the area of the cone base. The solar altitude β and illumination angle ϕ_0 are defined by Eqs. (D-27) and (D-30), respectively. The side wall also receives diffuse insolation descended from the sky and reflected up from the ground:

$$\hat{S}_{i,W,\mathrm{diff}} = \delta I_H A_W F_{W\to s} + \alpha_g I_H A_W F_{W\to g} = A_W I_H\left[\delta F_{W\to s} + \alpha_g\left(1 - F_{W\to s}\right)\right], \tag{5-35}$$

where α_g is the ground albedo and $A_W = A_B\left(1+\tan^2\alpha\right)^{1/2}$ is the wall area. Thus the total

insolation incident on the wall is

$$\hat{S}_{i,W} = \hat{S}_{i,W,\text{dir}} + \hat{S}_{i,W,\text{diff}}$$
$$= \begin{cases} A_B I_H \left[\begin{array}{l} (1-\delta) + \\ \left(1+\tan^2\alpha\right)^{1/2} \left(\delta F_{W\to s} + \alpha_g \left[1 - F_{W\to s}\right]\right) \end{array} \right] & \beta > \alpha \\ A_B I_H \left[\begin{array}{l} (1-\delta)\pi^{-1}\left(\left[\pi - \phi_0\right] + \tan\phi_0\right) + \\ \left(1+\tan^2\alpha\right)^{1/2} \left(\delta F_{W\to s} + \alpha_g \left[1 - F_{W\to s}\right]\right) \end{array} \right] & \beta < \alpha \end{cases} . \quad (5\text{-}36)$$

The total insolation *absorbed* is

$$\hat{S}_W = \begin{cases} (1-\alpha_0) A_B I_H \left[\begin{array}{l} (1-\delta) + \\ \left(1+\tan^2\alpha\right)^{1/2} \left(\delta F_{W\to s} + \alpha_g \left[1 - F_{W\to s}\right]\right) \end{array} \right] & \beta > \alpha \\ (1-\alpha_0) A_B I_H \left[\begin{array}{l} (1-\delta)\pi^{-1}\left(\left[\pi - \phi_0\right] + \tan\phi_0\right) + \\ \left(1+\tan^2\alpha\right)^{1/2} \left(\delta F_{W\to s} + \alpha_g \left[1 - F_{W\to s}\right]\right) \end{array} \right] & \beta < \alpha \end{cases} , \quad (5\text{-}37)$$

where α_0 is the leaf albedo.

5.7.3 Outer-Canopy Base

The only insolation received by the base of the cone is that reflected off the ground:

$$\hat{S}_{i,B,\text{diff}} = \alpha_g I_H A_B F_{B\to g} , \quad (5\text{-}38)$$

where $F_{B\to g} = 1$ is the view factor from the base to the ground. Thus the incident insolation is

$$\hat{S}_{i,B} = \hat{S}_{i,B,\text{diff}} = \alpha_g I_H A_B , \quad (5\text{-}39)$$

and the insolation absorbed is

$$\hat{S}_B = (1-\alpha_0)\hat{S}_{i,B} = (1-\alpha_0) A_B \alpha_g I_H . \quad (5\text{-}40)$$

5.8 Regional Fluxes and Whole-Canopy Fluxes

5.8.1 Dry-Surface All-Wave Radiative Gains

Collecting Eqs. (5-24), (5-30), (5-32), (5-33), (5-37), and (5-40) for easy reference, the regions' radiative temperatures are

$$T_{r,I} = T_a , \quad (5\text{-}41)$$

$$T_{r,W} = \tfrac{1}{2}\left(T_{r,W,1} + T_{r,W,2}\right) = \tfrac{1}{2}\left[\left(1+\varepsilon_s^{1/4} F_{W\to s}\right)T_a + \left(1 - F_{W\to s}\right)T_g\right], \tag{5-42}$$

$$T_{r,B} = \tfrac{1}{2}\left(T_a + T_g\right), \tag{5-43}$$

while their short-wave areal fluxes are

$$\hat{S}_I = 0, \tag{5-44}$$

$$\hat{S}_W = \begin{cases} \left(1-\alpha_0\right) A_B I_H \left[\begin{array}{l}(1-\delta)+ \\ \left(1+\tan^2\alpha\right)^{1/2}\left(\delta F_{W\to s} + \alpha_g\left[1 - F_{W\to s}\right]\right)\end{array}\right] & \beta > \alpha \\ \left(1-\alpha_0\right) A_B I_H \left[\begin{array}{l}(1-\delta)\pi^{-1}\left(\left[\pi - \phi_0\right] + \tan\phi_0\right)+ \\ \left(1+\tan^2\alpha\right)^{1/2}\left(\delta F_{W\to s} + \alpha_g\left[1 - F_{W\to s}\right]\right)\end{array}\right] & \beta < \alpha \end{cases}, \tag{5-45}$$

$$\hat{S}_B = \left(1-\alpha_0\right) A_B \alpha_g I_H . \tag{5-46}$$

These temperatures and fluxes may be substituted into Eqs. (5-15) and (5-16) to calculate the regional dry-AW gains $\hat{Q}_{\text{dry},n}$, $n = I, W, B$ and the whole-canopy dry-AW gain $\hat{Q}_{\text{dry},0}$.

5.8.2 Latent Heat Losses

Letting $n = I, W, B$, Eq. (5-19) may be applied to each $\hat{Q}_{\text{dry},n}$ to find the latent heat loss fraction ω_n. If the whole-canopy latent heat loss $\lambda\hat{E}_0$ is known, the regional latent heat losses $\lambda\hat{E}_n$ may be computed from Eq. (5-20).

5.8.3 Convective Losses and Surface Temperatures

$\hat{Q}_{\text{dry},n}$ and $\lambda\hat{E}_n$ may be substituted into Eqs. (5-7) and (5-10) to calculate the regional latent heat losses $\hat{H}_n$ and the regional surface temperatures T_n. The whole-canopy convective loss may be found by summing the regional losses:

$$\hat{H}_0 = \sum_{n=I,W,B} \hat{H}_n . \tag{5-47}$$

H_0 is particularly important because it measures how much heat the canopy convects into the air. Note from Eqs. (5-7), (5-22), and (5-20) that

$$\hat{H}_I = -\lambda\hat{E}_I = -\omega_I \lambda\hat{E}_o , \tag{5-48}$$

and

$$\begin{aligned}\hat{H}_W + \hat{H}_B &= \left(\hat{Q}_{\text{dry,W}} - \eta\lambda\hat{E}_W\right) + \left(\hat{Q}_{\text{dry,B}} - \eta\lambda\hat{E}_B\right) \\ &= \hat{Q}_{\text{dry,W}} + \hat{Q}_{\text{dry,B}} - \eta(1-\omega_I)\lambda\hat{E}_0\end{aligned} \tag{5-49}$$

Thus the whole-canopy convective loss may be written as

$$\hat{H}_0 = \hat{H}_W + \hat{H}_B + \hat{H}_I = \hat{Q}_{\text{dry,W}} + \hat{Q}_{\text{dry,B}} - \left[\eta(1-\omega_I) + \omega_I\right]\lambda\hat{E}_0 . \tag{5-50}$$

Substituting $\hat{Q}_{\text{dry},n}$ from Eq. (5-15),

$$\begin{aligned}\hat{H}_0 = \eta\left\{C r_r^{-1}\left[A_W\left(T_{r,W} - T_a\right) + A_B\left(T_{r,B} - T_a\right)\right] + \hat{S}_W + \hat{S}_B\right\} - \\ \left[\eta(1-\omega_I) + \omega_I\right]\lambda\hat{E}_0\end{aligned} \tag{5-51}$$

5.8.4 Long-Wave Radiative Gains

Eq. (5-8) may be employed to calculate the regional and whole-canopy values of the LW radiative gains:

$$\hat{L}_n = \hat{Q}_{\text{dry,n}} + (1-\eta)\lambda\hat{E}_n - \hat{S}_n, \qquad n = I, W, B \tag{5-52}$$

and

$$\hat{L}_0 = \sum_{n=I,W,B} \hat{L}_n . \tag{5-53}$$

5.9 Calculating Stomatal Resistance

Assuming that preconditions for Eq. (5-3)—uniform air temperature, saturation deficit, et cetera—hold over the whole canopy, Eq. (5-13) may be now be used to calculate the stomatal resistance from $\hat{Q}_{\text{dry},0}$ and $\lambda\hat{E}_0$:

$$r_{vs} = \frac{r_h}{\gamma}\left[\frac{A_0 C r_h^{-1}\rho_{sd} + s_a\hat{Q}_{\text{dry},0}}{\lambda\hat{E}_0} - \eta s_a\right] - r_{va} . \tag{5-54}$$

5.10 Ground-Level Convective Heating of the Air

5.10.1 Change in Convective Heat Loss

The steady-state energy balance on a dry ground surface is

$$H_g = Q_g , \tag{5-55}$$

where Eq. (A-20) gives

$$Q_g = Q_{\text{dry},g} = \eta_g \left[C r_{r,g}^{-1} \left(T_{r,g} - T_\infty \right) + S_g \right]. \tag{5-56}$$

Thus the areal convective loss from the ground to the air is

$$\hat{H}_g = A_g H_g = A_g Q_g = \eta_g \left[A_g C r_{r,g}^{-1} \left(T_{r,g} - T_\infty \right) + \hat{S}_g \right], \tag{5-57}$$

where $\hat{S}_g = A_g S_g$. If $T_{r,g}$ is increased by $\Delta T_{r,g}$ and $\hat{S}_g$ is increased by ΔS_g, $\hat{H}_g$ will increase by

$$\Delta \hat{H}_g = \eta_g \left[C r_{r,g}^{-1} A_g \Delta T_{r,g} + \Delta \hat{S}_g \right]. \tag{5-58}$$

5.10.2 Changes Induced by a Tree

In the absence of a tree, the ground sees only the sky, so

$$T_{r,g} = T_s. \tag{5-59}$$

Adding a opaque-cone tree to the system, the ground sees the sky, cone base, and cone wall. The new radiative temperature is

$$T'_{r,g} = F_{g \to s} T_s + F_{g \to B} T_B + F_{g \to W} T_W. \tag{5-60}$$

Since

$$F_{g \to s} + F_{g \to B} + F_{g \to W} = 1, \tag{5-61}$$

Eq. (5-59) may be rewritten

$$T_{r,g} = \left(F_{g \to s} + F_{g \to B} + F_{g \to W} \right) T_s = F_{g \to s} T_s + F_{g \to B} T_s + F_{g \to W} T_s. \tag{5-62}$$

Subtracting Eq. (5-62) from Eq. (5-60),

$$\Delta T_{r,g} = T'_{r,g} - T_{r,g} = F_{g \to B} \left(T_B - T_s \right) + F_{g \to W} \left(T_W - T_s \right). \tag{5-63}$$

Multiplying Eq. (5-63) by the ground area and applying view factor reciprocity,

$$A_g \Delta T_{r,g} = A_B F_{B \to g} \left(T_B - T_s \right) + A_W F_{W \to g} \left(T_W - T_s \right). \tag{5-64}$$

Substituting $F_{B \to g} = 1$,

$$A_g \Delta T_{r,g} = A_B \left(T_B - T_s \right) + A_W F_{W \to g} \left(T_W - T_s \right). \tag{5-65}$$

The wall and base temperatures may be found from Eq. (5-10), while the view factor from the wall to the ground is given by Eqs. (5-26) and (5-27).

If the outer canopy is opaque, the only portion of the wall-incident sunlight $\hat{S}_{i,W}$ that will

reach the ground is the groundward-reflected component, $F_{W\to g}\,\alpha_0\,\hat{S}_{i,W}$. Thus

$$\Delta\hat{S}_g = (1-\alpha_g)\left(F_{W\to g}\alpha_0\,\hat{S}_{i,W} - \hat{S}_{i,W}\right) = -(1-\alpha_g)(1-F_{W\to g}\,\alpha_0)\hat{S}_{i,W}, \tag{5-66}$$

where the incident solar flux $\hat{S}_{i,W}$ is given by Eq. (5-36).

Substituting Eqs. (5-64) and (5-66) into Eq. (5-58),

$$\Delta\hat{H}_g = \eta_g \left\{ \begin{matrix} C\,r_{r,g}^{-1}\left[A_B(T_B - T_s) + A_W\,F_{W\to s}(T_W - T_s)\right] - \\ (1-\alpha_g)(1-F_{W\to g}\,\alpha_0)\hat{S}_{i,W} \end{matrix} \right\}. \tag{5-67}$$

This is the amount of heat (expected to be negative) that the presence of the tree adds to the ground-level air by lowering the ground temperature.

5.11 Canopy-Level Convective Heating of the Air

The convective loss from the whole canopy to the air, $\hat{H}_0$, is given by Eq. (5-47). Given the high vapor-diffusion stomatal resistances typical of tree leaves, $\hat{H}_0 = \hat{Q}_0 - \lambda\hat{E}_0$ is expected to be positive; that is, the AW radiative gain is expected to exceed the latent heat loss. The amount of heat that the introduction of a tree adds to the canopy-level air is

$$\Delta\hat{H}_0 = \hat{H}_0 - 0 = \hat{H}_0. \tag{5-68}$$

Assume that some fraction $f_\downarrow$ of the canopy-level air travels downward to mix with the ground-level air. Then the amount of heat that the canopy adds indirectly to the ground-level air is

$$\Delta\hat{H}_{\text{ind}} = f_\downarrow\,\Delta\hat{H}_0 = f_\downarrow\,\hat{H}_0. \tag{5-69}$$

The actual value of $f_\downarrow$ depends on the free and forced flow patterns around the tree, but a reasonable guess (based on symmetry alone) would be $f_\downarrow \sim \frac{1}{2}$. Strong buoyancy would tend to reduce $f_\downarrow$.

5.12 Total Convective Heating of the Air

5.12.1 Term bxy Term

The total ground-level air heating induced by the presence of the tree is

$$\Delta\hat{H} = f_\downarrow\,\hat{H}_0 + \Delta\hat{H}_g. \tag{5-70}$$

Substituting from Eqs. (5-51) and (5-69),

$$\Delta\hat{H} = f_{\downarrow}\begin{Bmatrix}\eta\left(Cr_r^{-1}\left[A_W\left(T_{r,W}-T_a\right)+A_B\left(T_{r,B}-T_a\right)\right]+\hat{S}_W+\hat{S}_B\right)\\ -\left[\eta\left(1-\omega_I\right)+\omega_I\right]\lambda\hat{E}_0\end{Bmatrix} \\ +\eta_g\begin{Bmatrix}Cr_{r,g}^{-1}\left[A_B\left(T_B-T_s\right)+A_W F_{W\to s}\left(T_W-T_s\right)\right]\\ -\left(1-\alpha_g\right)\left(1-\alpha_0 F_{W\to g}\right)\hat{S}_{i,W}\end{Bmatrix} \tag{5-71}$$

Writing $\hat{S}_n = \left(1-\alpha_0\right)\hat{S}_{i,n}$ and rearranging,

$$\begin{aligned}\Delta\hat{H} = {} & \eta\left(1-\alpha_0\right)f_{\downarrow}\,\hat{S}_{i,B} \\ & +\left[\eta\left(1-\alpha_0\right)f_{\downarrow}-\eta_g\left(1-\alpha_g\right)\left(1-\alpha_0 F_{W\to g}\right)\right]\hat{S}_{i,W} \\ & -f_{\downarrow}\left[\eta\left(1-\omega_I\right)+\omega_I\right]\lambda\hat{E}_0 \\ & +f_{\downarrow}\left\{\eta\left(Cr_r^{-1}\left[A_B\left(T_{r,B}-T_a\right)+A_W\left(T_{r,W}-T_a\right)\right]\right)\right\} \\ & +\eta_g\left\{Cr_{r,g}^{-1}\left[A_B\left(T_B-T_s\right)+A_W F_{W\to s}\left(T_W-T_s\right)\right]\right\}\end{aligned} \tag{5-72}$$

There are five additive terms in this expression for near-ground air heating. The first will always be positive; the third, always negative; and the fifth, always positive. The signs of the second and fourth terms depend in a complex fashion of the values of the variables therein. Thus, the introduction of a tree may induce either net heating or net cooling of the ground-level air.

5.12.2 Critical Downward Mixing Fraction

The critical downward-mixing fraction $f_{\downarrow}'$ at which canopy-level heating negates ground-level cooling may be obtained by setting Eq. (5-70) to zero:

$$f_{\downarrow}' = -\frac{\Delta\hat{H}_g}{\hat{H}_0}. \tag{5-73}$$

Eq. (5-70) may be rewritten in the form

$$\Delta\hat{\mathrm{H}} = f_{\downarrow}\,\hat{\mathrm{H}}_0 + \Delta\hat{\mathrm{H}}_{\mathrm{g}} = \left(f_{\downarrow}-f_{\downarrow}'\right)\hat{\mathrm{H}}_0. \tag{5-74}$$

Thus a low critical value suggests that canopy-level heating is likely to overwhelm ground-level cooling.

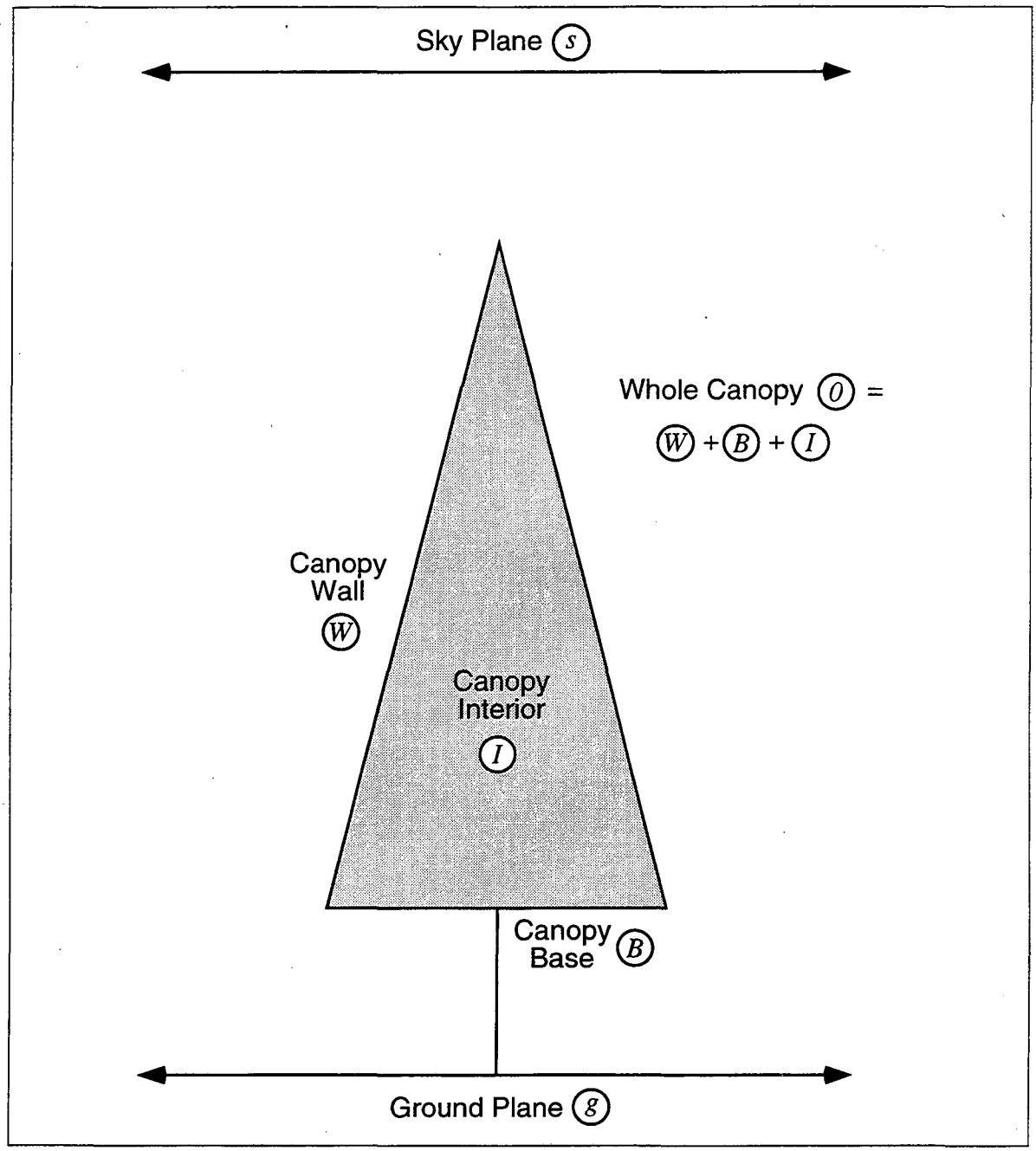

Figure 5-1. Regions and surfaces of the opaque canopy radiation model.

Chapter 6: Tree Experiment

6.1 Overview

The simplest way to measure the rate of evapotranspiration from a plant is to grow the plant in a pot and weigh the pot at intervals. This arrangement of weighing a containerized plant is termed a "weighing lysimeter" and has been used for nearly three centuries (Kramer 1983, p.331).

A lysimeter experiment was conducted for this study of near-ground cooling to measure the daily profiles of evapotranspiration and climate of a tree. Once the tree's rates of SW radiative gain, LW radiative gain, and latent heat loss had been calculated from measurements of plant mass, horizontal surface insolation, air temperature, relative humidity, and wind speed, the tree and ground energy balances could be solved for the convection from canopy-to-air and the change in ground-to-air convection induced by the presence of the tree.

The evapotranspiration and weather data may also be used to compute the canopy-averaged leaf stomatal resistance. Since the stomatal resistance strongly regulates the rate of evapotranspiration (see Appendix H), general trends observed in diurnal profiles of the stomatal resistance can be used to predict rates of latent heat loss on days for which evapotranspiration data is not available.That is, diurnal profiles of stomatal resistance can reveal the daily onsets of such physiological water-regulation mechanisms as late-morning wilting and mid-afternoon turgor recovery.

In this study, a small potted tree was set on a building roof in Berkeley, CA, where its mass, temperature, and ambient environmental conditions were recorded continuously from August through October of 1995. The tree was run through several watering cycles to vary evapotranspiration with soil moisture as well as weather. At the end of the experiment, the canopy was destructively sampled to determine the total area of its leaves.

6.2 Site

The tree and weather tower were stationed on the northwest corner of the third-floor roof of a four-story building at the Lawrence Berkeley National Laboratory in Berkeley, CA[†] (Figure 6-1). The tree was 4 m from the north edge and 8 m from the west edge of the roof; the weather tower was 3 m west of the tree. The building's fourth floor shaded the experimental site each morning until approximately 8 AM.

†. Latitude 37°52' N, longitude 122°20' W.

6.3 APPARATUS

6.3.1 Tree

Specimen. A small Japanese wax-leaf privet tree†, two meters high and one meter wide, was purchased from a nursery for this experiment. The thickly-foliated, conically-shaped evergreen was potted in a 15-gallon (57 liter) black plastic container with bottom drainage holes. A blanket of dead leaves covering the soil, impeding evaporation from the soil surface. No nutrients were added to the plant once it left the nursery.

The canopy was destructively sampled at the end of the experiment to determine that the total (single-sided) leaf area was approximately 6.9 m^2. Further leaf statistics and details of the sampling method are given in Section I.3.

Species. Wax-leaf privet (*Ligustrum Japonicum*) is a popular evergreen shrub or tree that grows up to 3 meters high. It is native to Japan and Korea but is planted in the U.S. as far north as Washington, D.C. Privets are hardy, grow well in ordinary soils, tolerate but do not prefer some shade, and are commonly used as hedge plants or containerized plants (Everett 1981-82, p.2005). All varieties of privet have stomatal pores only on the underside of their leaves (Bold et al. 1987, p.629).

Ligustrum Japonicum was selected for this experiment based on its reputation for heavy water consumption (Still and Davies 1993). It is also a popular subject for water-use experiments (Steinberg, Zajicek, and McFarland 1991; Heilman and Brittin 1989; Still and Davies 1993; Still and Davies 1988; Beeson 1992; Lownds and Berghahe 1991).

Plant System. The term "plant system" will be used to refer to everything that was weighed on the scale, i.e. the tree, soil pot, and the sensors attached to the tree. Since soil evaporation was negligible, and the tree lost few leaves over the course of the experiment, slow declines in the plant system mass could generally be attributed to evapotranspiration. (By contrast, drainage after watering yielded large, sudden changes in the plant system mass).

6.3.2 Instrumentation

Tree Sensors. A load cell (Ishida MT-300; still-air accuracy ±10 g, repeatability ±50 g in 2 m s^{-1} wind) beneath the potted tree measured the mass of the plant system, while a thermistor probe (Campbell Scientific 107B; accuracy ±0.4 K) measured the soil temperature. Teflon-insulated, five-mil, type-T thermocouples (Omega 5SC-TT-T-36-36:G1; accuracy ±0.3 K) were attached to (a) the underside of a sunny leaf at the top of the canopy and (b) the underside of a shaded leaf in the center of the canopy (Figure 6-2).

---

†. This specimen of wax-leaf privet had multiple stems and was therefore technically a shrub. However, it had the shape of a tree (see Figure 6-2), and will be referred to as such in this paper.

An aspirated, radiation-shielded air temperature sensor (Figure 6-4) was constructed by suspending an Omega thermocouple in the center of a 30-cm-long, 2-cm-wide PVC pipe. The pipe was surrounded by 1.5 cm of foam insulation that was in turn wrapped in white plastic tape to reduce solar heating. A small electric fan drew air through the top of the pipe to aspirate the thermocouple. The sensor unit was mounted vertically in the center of the canopy to measure the inner-canopy air temperature.

Weather Station. The rooftop weather station's six-foot tripod (Campbell Scientific CM6) held a horizontal semiconductor pyranometer (LI-COR LI200S; accuracy ±3%), a three-cup anemometer (Campbell Scientific 014A Met One; accuracy $\pm 0.1 \text{ m s}^{-1}$), a wind direction vane (Campbell Scientific 024A Met One; accuracy ±5°), and an air temperature and humidity sensor (Campbell Scientific RH207; accuracies ±0.4 K and ±5% RH) housed in a 12-plate passive radiation shield (Gill 41004-5; radiation error ±0.7 K @ 1080 W m^{-2} & 2 m s^{-1}) (Figure 6-3).

Air Temperature Sensor Array. Figure 6-2 shows an array of three more aspirated, shielded temperature sensors set in line with the air-temperature sensor in the center of the tree's canopy. These were intended to detect warming of the air as it passed over the canopy, but the idea proved impractical for such a small tree. Consider: the cross-section of the privet tree is approximately $A = 1 \text{ m}^2$. If the canopy absorbs 1000 W of insolation and convects $\hat{H} = 500 \text{ W}$ to air passing through with velocity $U = 2 \text{ m s}^{-1}$, the corresponding rise in air temperature ΔT is given by

$$U A C \Delta T = \hat{H} \tag{6-1}$$

or

$$\Delta T = \frac{\hat{H}}{CUA} = \frac{(500 \text{ W})}{\left(1210 \text{ J m}^{-3} \text{ K}^{-1}\right) \times \left(2 \text{ m s}^{-1}\right) \times \left(1 \text{ m}^2\right)} = 0.2 \text{ K}. \tag{6-2}$$

Under ideal conditions (i.e. no solar heating), standard thermocouples can measure air temperatures to accuracies of about ±0.3 K. Housing them in the aspirated radiation shields described above and placing them outdoors introduced a radiation error of ±0.5 to 1.5 K (see Section I.4). Thus this portion of the experiment was abandoned as ill-conceived.

Datalogger and Computers. A 386-class PC was used to communicate with the datalogger (Campbell Scientific 21X) that controlled all sensors. Data recorded on the PC was later uploaded to a Unix workstation for storage.

Electronic Water Timer. A programmable electronic water timer (Nelson 5450) controlled the delivery of water to the soil. Water flowed from a rooftop standpipe, through the timer, though a 90 m length of quarter-inch irrigation tubing, and then into the soil.

6.4 Watering Cycles

The tree was subjected to various watering cycles (Table 6-1) to explore the effect of soil moisture on the rate of evapotranspiration.

Automatic Nightly Watering. An electronic timer watered the tree for 30 minutes each morning at 2 am. After unabsorbed water leaked out of the pot's drainage holes, the soil retained about 4 kg of water, which was approximately equal to the water mass that evapotranspired daily. Nightly watering thus kept the amount of water in the soil at the start of day roughly constant.

Saturation and Dryout. To saturate the soil, water was added repeatedly over the course of a day until the soil gained little net mass from additional watering. The daily water timer was then turned off and the soil allowed to dry out for a week. This saturation and dryout process was repeated three times.

6.5 Data

6.5.1 Measurements

The datalogger executed all measurements once-a-second, 24-hours-a-day from August 9 to October 19, 1995. Data collection was continuous and uneventful except for those incidents listed in Table 6-2. Datalogger measurements were immediately uploaded to the PC and written to the PC disk every 30 seconds. Approximately 9 megabytes of data were uploaded daily from the PC to the workstation for long-term storage.

6.5.2 Calculations

Data Reduction. All measurements were taken and recorded at a frequency of 1 Hertz. This very large data set—approximately 500 MB—was averaged over periods of 1 minute and 30 minutes to provide smaller, smoother data sets from which to calculate the rate of evapotranspiration and to calculate the energy flows associated with the tree.

Evapotranspiration. One-minute averages of the plant system mass were further smoothed with an iterative linear filter before the rate of mass loss (water loss) was calculated as a finite difference derivative of the mass signal. Details of the smoothing are given in Section I.2.

6.5.3 Results

Tree Mass, Mass Loss Rate, and Weather. Time series of the plant system mass, mass loss rate, pyranometer insolation, air and soil temperatures, sunny and shaded leaf temperatures, saturation deficit, and wind speed are plotted in Figures 6-5 through 6-8. These data are explored in the energy balance calculations of Chapter 7.

Soil Watering Regimes	
1. Days 220-257	Soil watered automatically every night around 2 am.
2. Days 257-261	Soil watered automatically every other night around 2 am.
3. Days 261-271	Soil watered manually, then allowed to dry out for 10 days.
4. Days 279-285	Soil watered manually, then allowed to dry out for 7 days.
5. Days 287-292	Soil watered manually, then allowed to dry out for 6 days.

Table 6-1. Watering regimes.

Exceptional Events	
1. Days 227.8-228.6	Data interrupted: measurements could not be stored due to loss of electrical power to computer.
2. Days 229.6-229.7	Measurement changed (temporarily): tree canopy enveloped in plastic to capture evapotranspired water.
3. Days 230.6-233.6	Measurement changed (temporarily): tree removed from load cell and replaced by bucket of water for three days.
4. Days 235.5-241.7	Data interrupted: measurements could not be stored due to the failure on a hard disk on the data-recording computer.
5. Days 252.3-252.7	Data interrupted: measurements could not be stored due to loss of electrical power to computer.
6. Day 255.7	Sensor added: thermocouple attached to underside of sunny leaf at top of the canopy.
7. Day 256.7	Sensor added: thermocouple attached to underside of shaded leaf in center of canopy.

Table 6-2. Exceptional events.

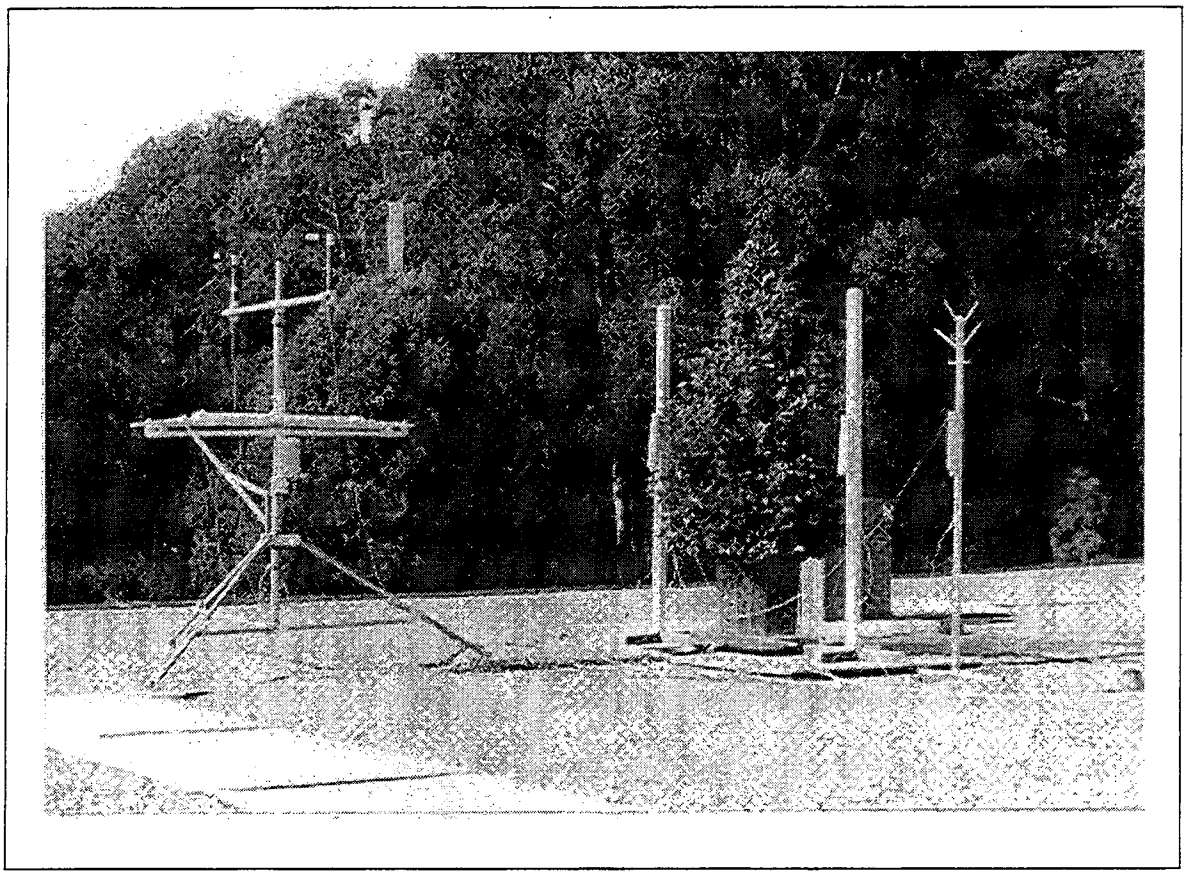

Figure 6-1. Weather station and potted tree on third-story building roof in Berkeley, CA. A linear array of air temperature sensors surrounds the tree. A shaded assembly of PVC piping, used to join the air temperature sensors to a common air source for mutual calibration, is mounted halfway up the weather tower.

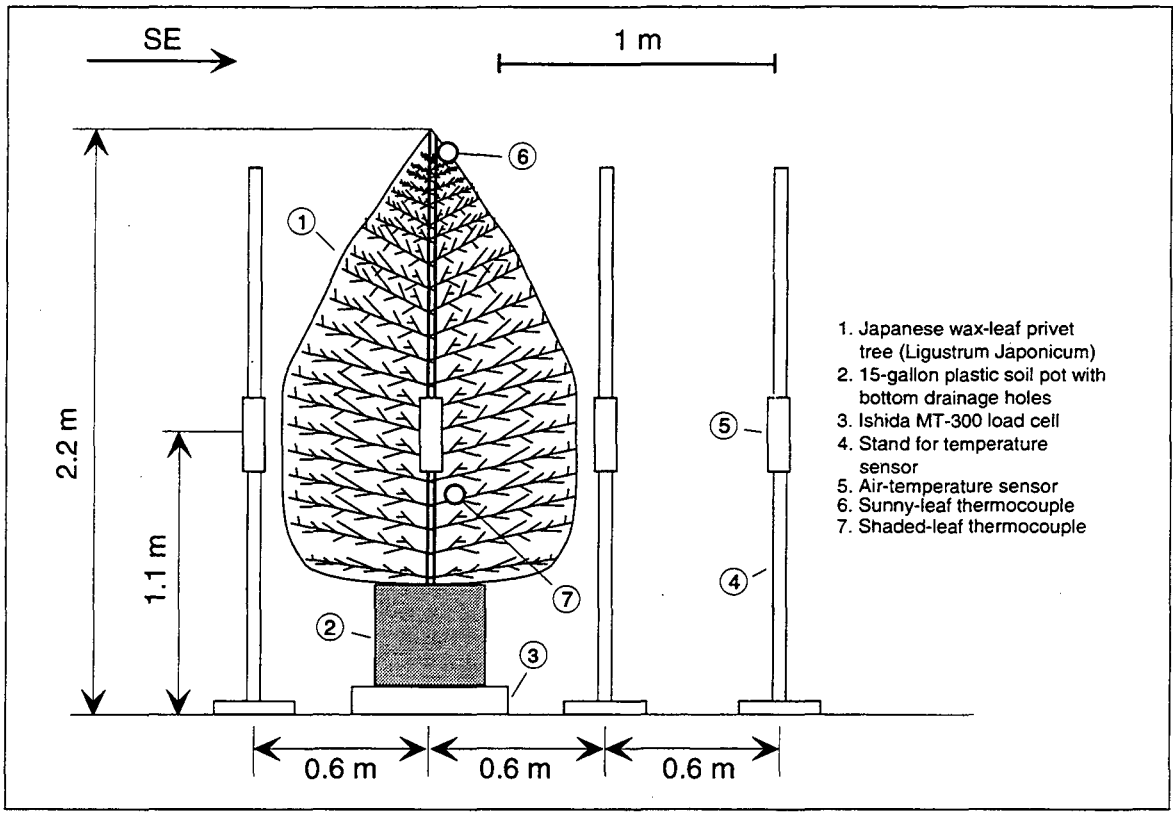

Figure 6-2. Tree, load cell, and sensors, drawn to scale.

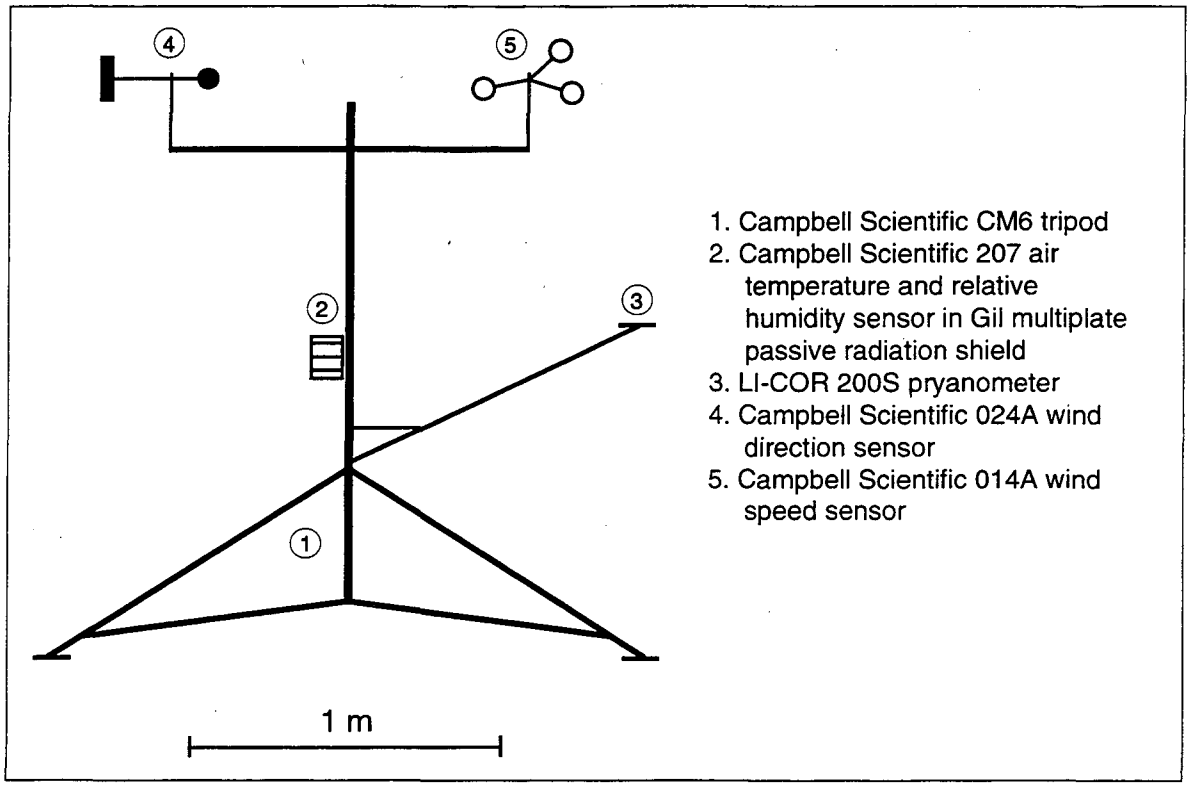

Figure 6-3. Rooftop weather station set 3 m west of the tree, drawn to scale.

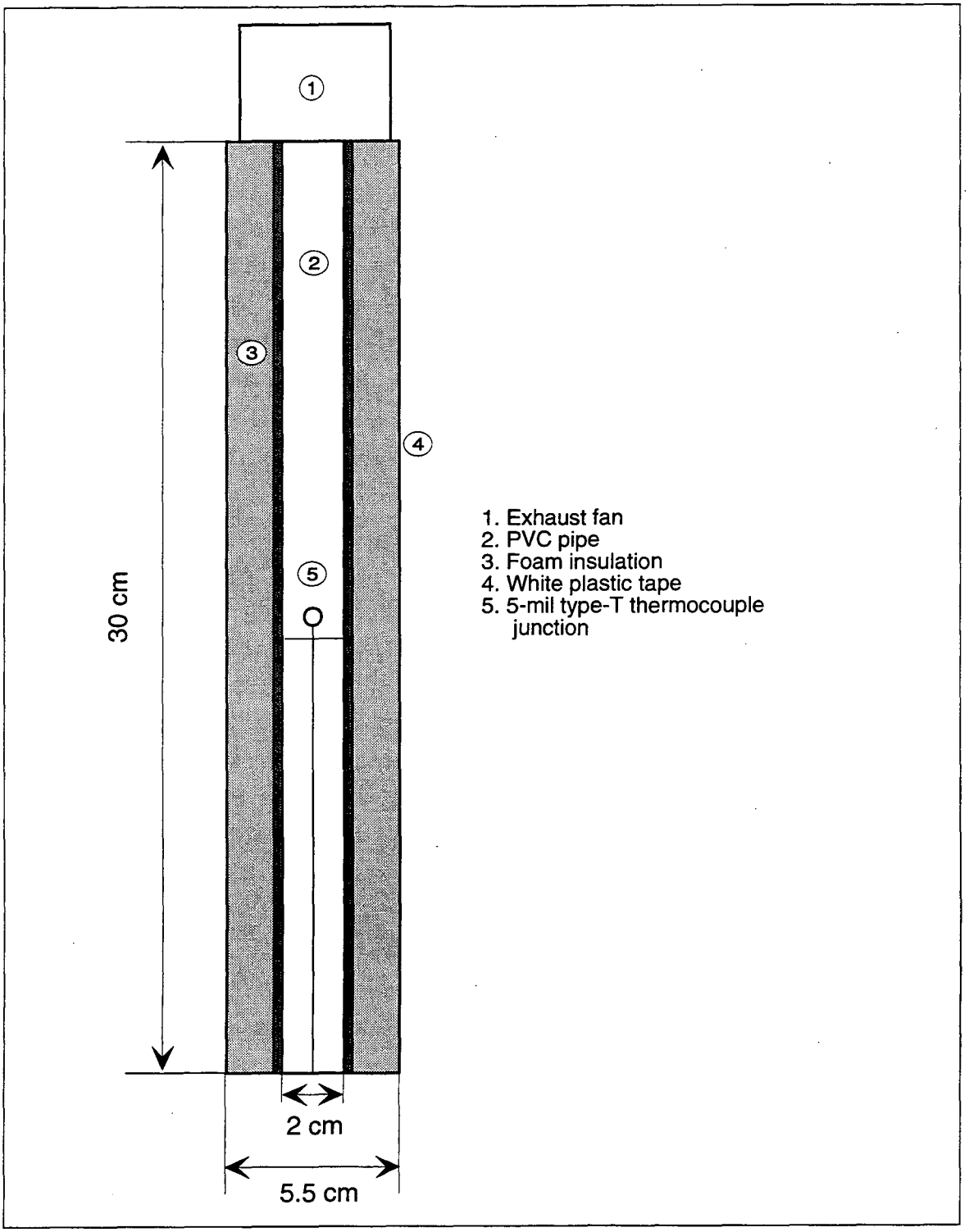

Figure 6-4. Aspirated, radiation-shielded thermocouple air temperature sensor, drawn to scale.

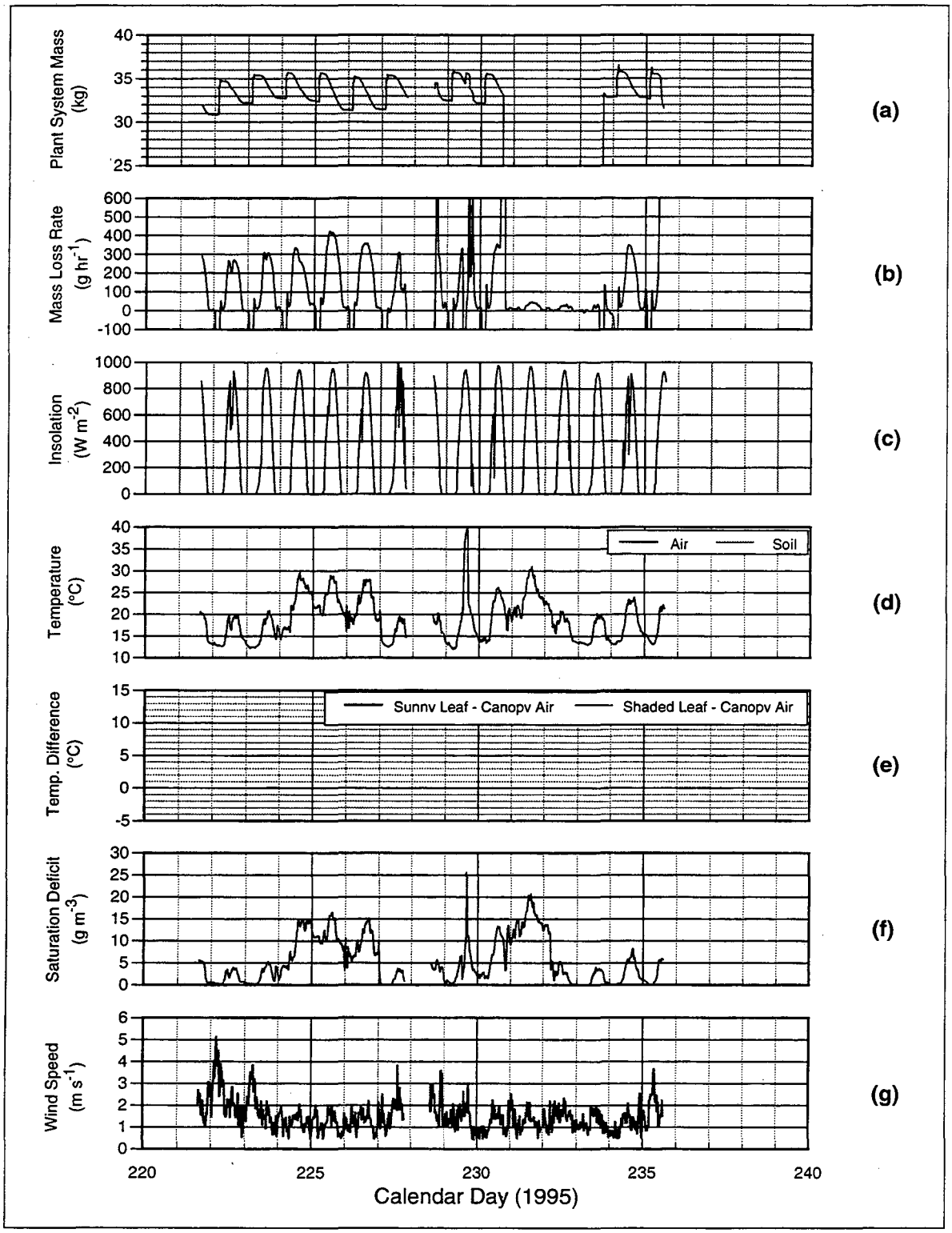

Figure 6-5. Measurements on calendar days 221-239 (August 9-27, 1995) of (a) tree system mass, (b) tree system mass loss rate, (c) horizontal pyranometer insolation, (d) air and soil temperature (soil temperature not available), (e) sunny and shaded leaf temperature elevations (not available), (f) saturation deficit, and (g) wind speed.

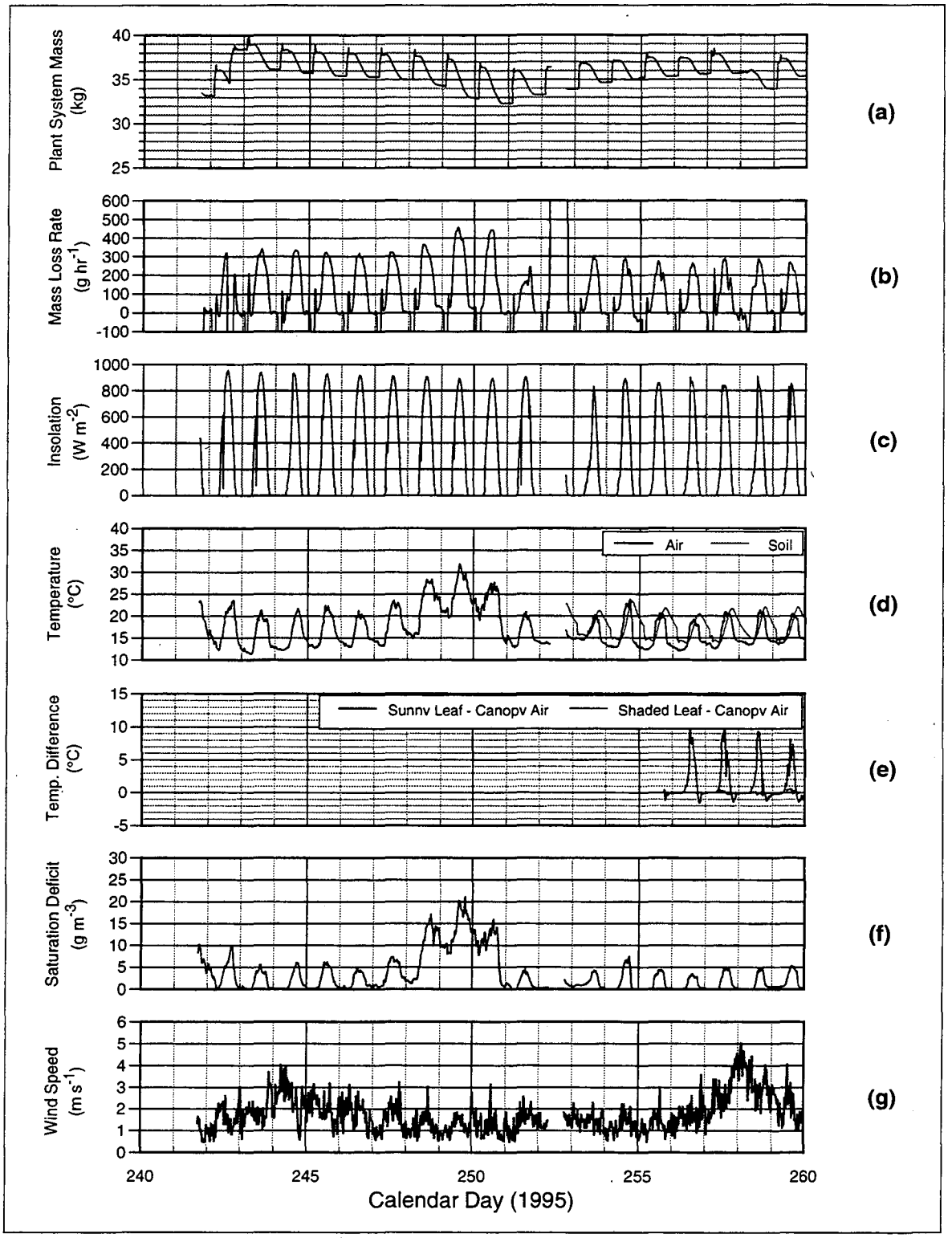

Figure 6-6. Measurements on calendar days 240-259 (August 28-September 16, 1995) of (a) tree system mass, (b) tree system mass loss rate, (c) horizontal pyranometer insolation, (d) air and soil temperature, (e) sunny and shaded leaf temperature elevations, (f) saturation deficit, and (g) wind speed.

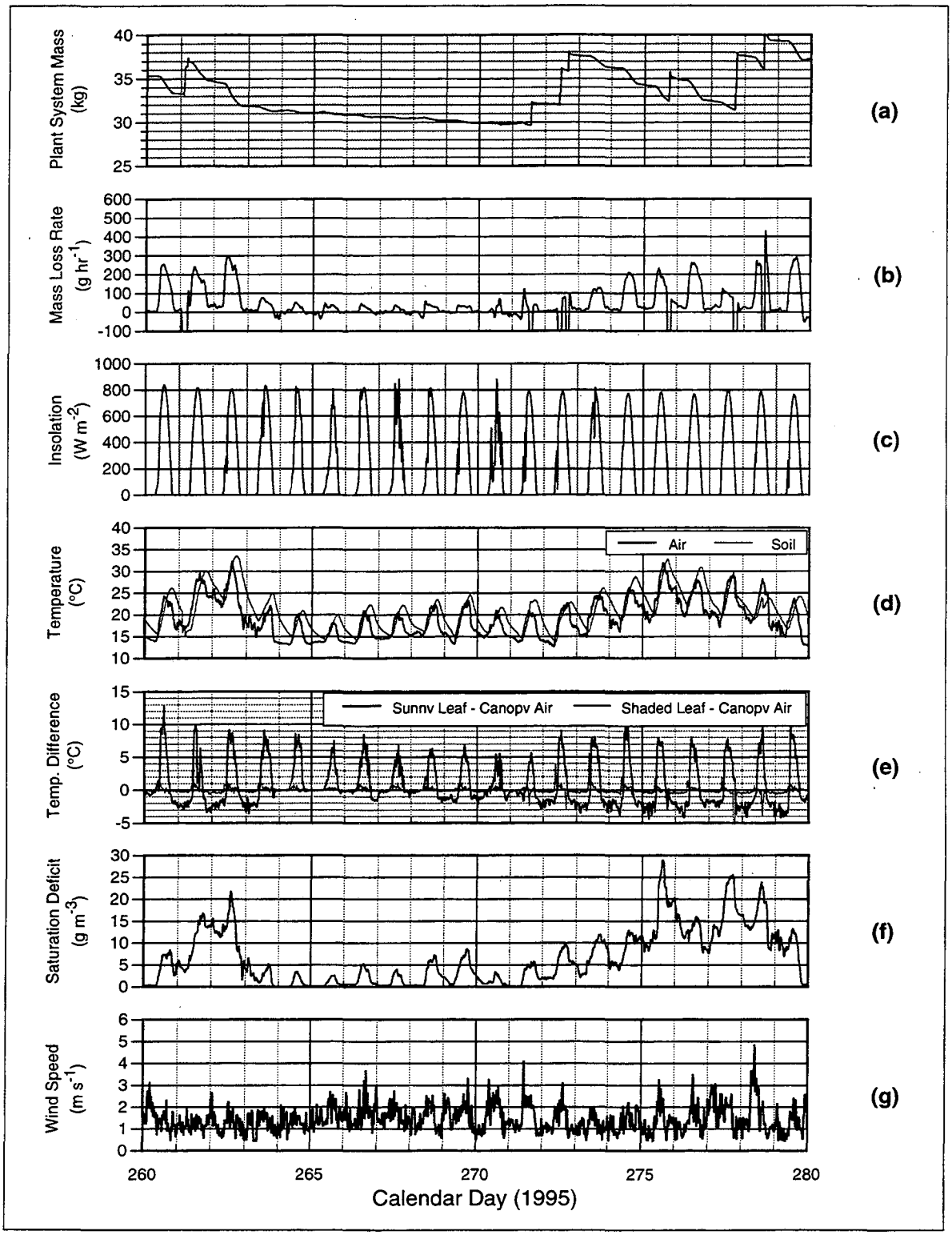

Figure 6-7. Measurements on calendar days 260-279 (September 17-October 6, 1995) of (a) tree system mass, (b) tree system mass loss rate, (c) horizontal pyranometer insolation, (d) air and soil temperature, (e) sunny and shaded leaf temperature elevations, (f) saturation deficit, and (g) wind speed.

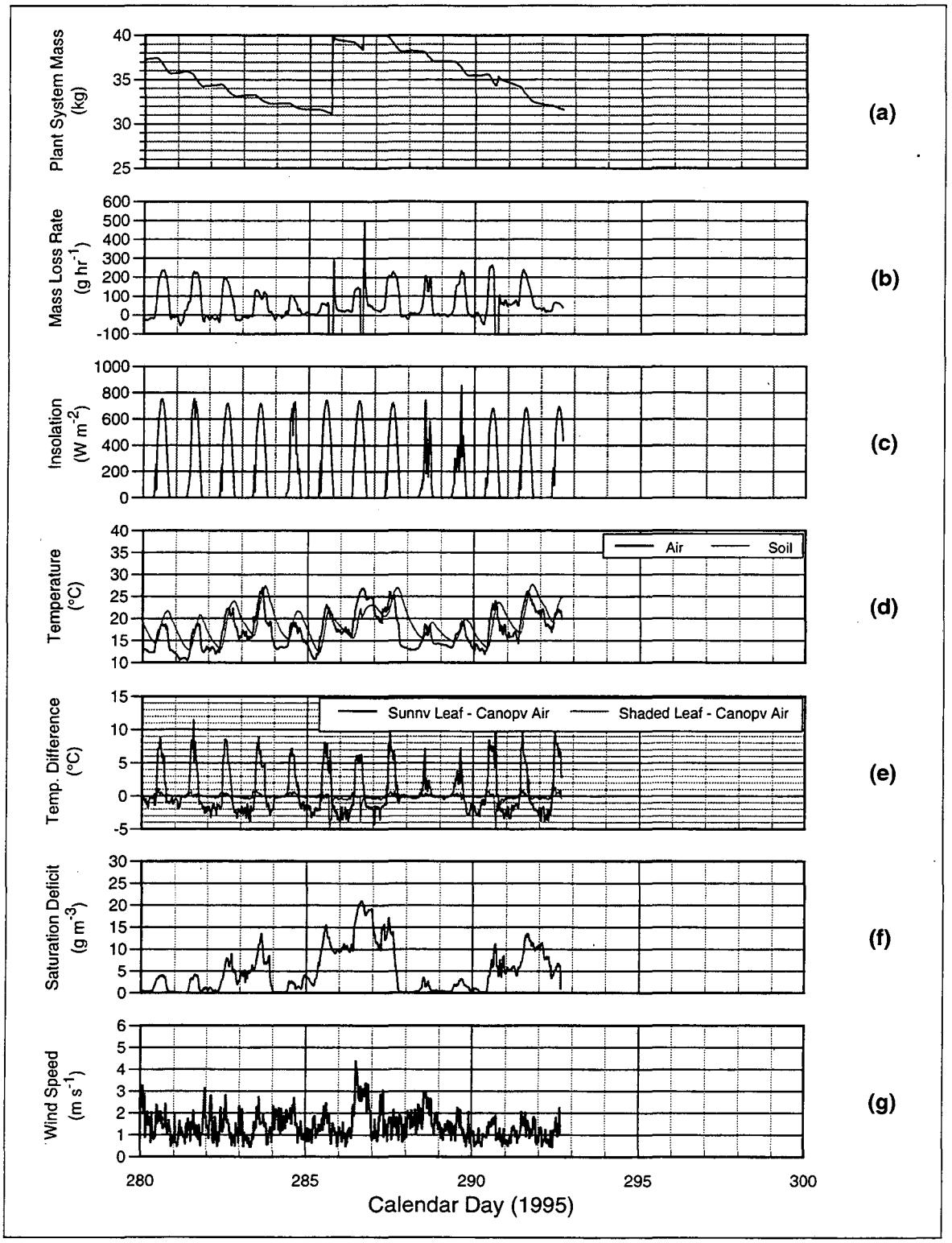

Figure 6-8. Measurements on calendar days 280-292 (October 7-19, 1995) of (a) tree system mass, (b) tree system mass loss rate, (c) horizontal pyranometer insolation, (d) air and soil temperature, (e) sunny and shaded leaf temperature elevations, (f) saturation deficit, and (g) wind speed.

Chapter 7: Tree Calculations

7.1 Overview

The tree energy model was applied to the evapotranspiration and climate data gathered in the lysimeter experiment to calculate the canopy heat flows, the tree-induced changes to ground-to-air convection, and the tree's resistance to water loss under various weather and soil moisture conditions. Four days were selected from the experimental data: one "normal," one cloudy, one arid, and one on which the plant was wilted. One each day, the magnitudes of the various forms of canopy heat transfer—short-wave radiation, long-wave radiation, convection, and latent heat loss—were compared to determine which modes dominated the canopy's energy balance. Next, the amount of canopy-to-air convection was compared to the tree-induced reduction in ground-to-air convection to determine the net effect of the presence of the tree on the amount of heat convected to the air. Finally, the canopy-averaged stomatal resistance was computed to gauge the plant's physiological response to its climate.

7.2 Methodology

7.2.1 Cases

Four days of data—a "normal" day, a "cloudy" day, an "arid" day, and a "wilted" day—were selected to represent important variations in the plant's environment.† The base-case, normal day (CD 246) was sunny, moderately dry, and had well-wetted soil. The cloudy day (CD 253) was similar to the normal day, but had morning clouds; the arid day (CD 249) was similar to the normal day, but had very dry air; and the wilted day (CD 269) was similar to the normal day, but had dry soil. The insolation, air temperature, relative humidity, saturation deficit, plant system mass, and wind speed on these four days are compared in Figures 7-9 through 7-14. Other parameters are listed in Table 7-1.

7.2.2 Calculations

The following diurnal calculations were performed for each of the four representative days.

1. Single-day profiles of the whole-canopy flow densities of all-wave radiation Q_0, short-wave radiation S_0, convection H_0, latent heat loss λE_0, and long-wave radiation L_0 (Figures 7-1 through 7-4). The relative magnitudes of these flows gauge the importance of each mode of heat transfer to the canopy's energy balance.
2. Single-day profiles of the convective loss $\hat{H}_n$ from each region of the canopy, and the

†. A purely "windy" day was also desired, but the few strongly windy days in this experiment were also cloudy.

change in ground-level convection, $\Delta\hat{H}_g$, induced by the presence of the tree (Figures 7-5 through 7-8). These indicate how much heat each region of the tree adds to or removes from the air, as well as the amount of ground-level cooling causes by the shadow of the tree.

3. Multi-day comparisons of the stomatal resistance r_{vs}, indicating the physiological response of the plant to its environment (Figures 7-15 and 7-16).
4. Multi-day comparisons of the canopy latent heat loss $\lambda\hat{E}_0$ (Figure 7-17), convection loss $\hat{H}_0$ (Figure 7-18), and Bowen ratio $\mathrm{Bo} = H_0/\lambda E_0$ (Figures 7-19 and 7-20).
5. Multi-day comparisons of the change in ground-level convection, $\Delta\hat{H}_g$, induced by the presence of the tree (Figure 7-21).
6. Multi-day comparisons of the critical downward mixing fraction $f'_{\downarrow}$ (Figure 7-22). If the fraction of heated canopy-level air that flows to ground level exceeds this value, the tree will have a net heating effect on the ground-level air.

7.2.3 Code

These calculations were made with the *Mathematica 3.0* program "Tree Heat-Mass Balance Calculation Engine," presented in Appendix J.

7.3 RESULTS

7.3.1 Modes of Heat Flow in the Canopy

The canopy gained heat primarily from insolation, and lost heat primarily via convection (Figures 7-1 through 7-4). Though the direction of the LW radiative exchange changed over the course of the day—the canopy gained heat from LW radiation from 9 AM to 3 PM, when the ground surface was warmest, and lost heat otherwise— its magnitude rarely exceeded 20% of that of the SW radiation.

The amount of heat dissipated by evaporation was also fairly small. On the normal day, the ratio of convective loss to latent heat loss (Bowen ratio) was approximately 5; on the arid day, when the high saturation deficit promoted evapotranspiration, it was 3; and on the cloudy morning, when there was when there little solar heating of the leaves, the ratio fell to about 1 (Figure 7-19). The Bowen ratio skyrocketed when the plant was wilted because evapotranspiration was negligible on that day (Figure 7-20).

7.3.2 Diurnal Variations of Evapotranspiration and Stomatal Resistance

On the normal and arid days, the tree evapotranspired more rapidly in the mornings than in the afternoon (Figure 7-17), despite the fact that the air was warmer and drier in the afternoons (Figures 7-10 through 7-12). This indicates a gradual leaf wilting and resultant stomatal closure. The computed stomatal resistance rose throughout the normal and arid

days, reaching twice their 9 AM values by 3 PM (Figure 7-15).

On the cloudy morning, the evapotranspiration rate rose linearly from 6 AM to noon (Figure 7-17). For some unknown reason, the stomatal resistance fell by a factor of three from 6 AM to 9 AM (Figure 7-15). The resistance remained constant for the rest of the morning, probably because the rate of evapotranspiration was low enough to prevent a wilting before noon. The stomatal resistance doubled by 3 PM, presumably due to an afternoon-onset wilting and stomatal closure.

Evapotranspiration was small but measurable on the wilted day; the calculated stomatal resistance was very high (Figure 7-16).

7.3.3 Canopy-Level and Ground-Level Convective Flows

The warm outer regions of the canopy (the side wall and base) convected more heat into the air than the cool interior region removed from air. On the normal day, the ratio of canopy-level heating to canopy-level cooling was about 20; on the arid day, about 9; on the cloudy morning, about 3; and on the wilted day, essentially infinite, because the canopy interior drew a negligible amount of heat from the air (Figures 7-5 through 7-8).

Under a clear sky at noon, the canopy convected about 850 to 1050 W into the air, while its shadow reduced the amount of heat convection from ground to air by 400 to 450 W. On all four days, the magnitude of canopy-level convective heating of the air was about twice that of the ground-level cooling of the air induced by the tree's shadow. Thus, the critical downward mixing fraction was about 0.45 (Figure 7-22).

7.4 DISCUSSION

7.4.1 Significance of Latent Heat Loss in the Canopy Energy Balance

The canopy's latent heat loss was generally small compared to its solar gain, suggesting that evapotranspirative cooling played a fairly minor role in the energy balance of the tree. The notable exception was on the arid day, when the high saturation deficit significantly increased the rate of latent heat loss to the point where the canopy's convective and latent heat losses were comparable.

7.4.2 Net Heating of Air Induced By Presence of Tree

In this experiment, the canopy itself was at ground level, so all heat dissipated by the canopy was added directly to the ground level air. Thus, the presence of the tree added about 500 W of heat to the near-ground air. However, since the critical downward mixing fraction was about 0.5, and since buoyancy can generally be expected to make the downward mixing fraction less than one-half, this tree would likely have had a net cooling effect on the near-ground air had its canopy been high.

7.4.3 Net Air Heating Per Unit Area

There is some ambiguity in choice of tree area when attempting to generalize the heat flows obtained for one tree to another tree of arbitrary size. That is, the areal flows may be expressed per unit canopy area of the tree, or per unit canopy base area. Canopy heat flows are dominated by the incident insolation $\hat{S}_{i,0}$, which can greatly exceed $A_B I_H$ when the canopy is tall (Figure 7-23). The incident diffuse insolation is proportional to the area of the canopy wall, while the incident direct insolation is proportional to the area of the canopy base (at least when the sun is high enough to illuminate the entire canopy). Unfortunately, the direct and diffuse flows are comparable in magnitude. Thus, if base area is to be used as a gauge of canopy size, all trees being compared should have roughly the same ratio of wall area to base area. That is, they should be of the same shape.

Expressed per unit base area, the noontime canopy air heating was $1080-1330$ W m^{-2}, and ground air cooling was $510-570$ W m^{-2}. Since the canopy was at ground level, the net ground-level air heating was about 660 W m^{-2}. However, a more general expression for the net ground-level air heating, derived from Eq. (5-74), would be

$$\Delta H = \left(f_{\downarrow} - f_{\downarrow}'\right) H_0 = \left(f_{\downarrow} - 0.45\right) \times \left(1200 \text{ W m}^{-2}\right). \tag{7-1}$$

7.4.4 Stomatal Control of Evapotranspiration

Late-morning wilting without mid-afternoon recovery was observed on the normal, cloudy, and arid days. This suggests that even after the late-morning stomatal closure reduced the rate of water loss, the tree could not transport water from soil to leaves fast enough to restore leaf turgor, and thus reopen the stomatal pores, before nightfall.

The noontime stomatal resistances of 500, 250, and 1200 s m^{-1} calculated on the normal, cloudy, and arid days agree in order of magnitude with the noontime resistances of 200 to 1000 s m^{-1} reported for *Ligustrum Japonicum* by Steinberg et al. 1991.

7.4.5 Validity of Opaque Canopy Radiation Model

While the opaque canopy radiation model introduced in this paper yielded stomatal resistances of the right order of magnitude, the calculated diurnal profiles of the stomatal resistance are not entirely satisfactory. Particularly suspect are (a) the sharp decline of computed stomatal resistance from 6 AM to 9 AM on the cloudy morning, and (b) the fact that the computed stomatal resistance was much higher on the arid day than on the normal and cloudy days. However, there may be a physiological explanation for the latter: the arid day followed a warm and dry night during which the leaves may have failed to recover their full turgor.

As stated earlier, the only particular strength of this radiation model over its more sophisti-

cated counterparts in the literature is the ease with which it can be used to explicitly close the canopy's energy balance.

Parameter	Description	Value
H_0	canopy height	1.7 m
R_0	canopy radius	0.5 m
A_0	total canopy leaf area	6.9 m^2
α_0	canopy albedo	0.2
α_g	ground albedo	0.2
n_t	turbulence factor	1.5
δ	diffuse fraction of horizontal insolation	0.2

Table 7-1. Parameters of tree and ground energy balance calculations.

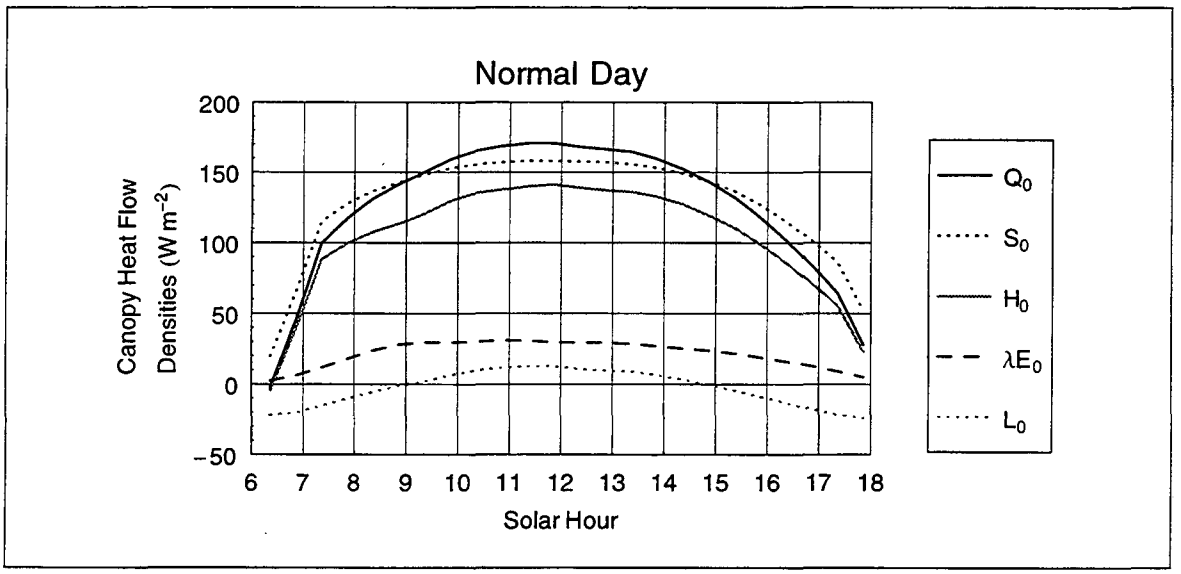

Figure 7-1. Normal-day, whole-canopy heat flow densities of all-wave radiation Q_0, short-wave radiation S_0, convection H_0, latent heat λE_0, and long-wave radiation L_0.

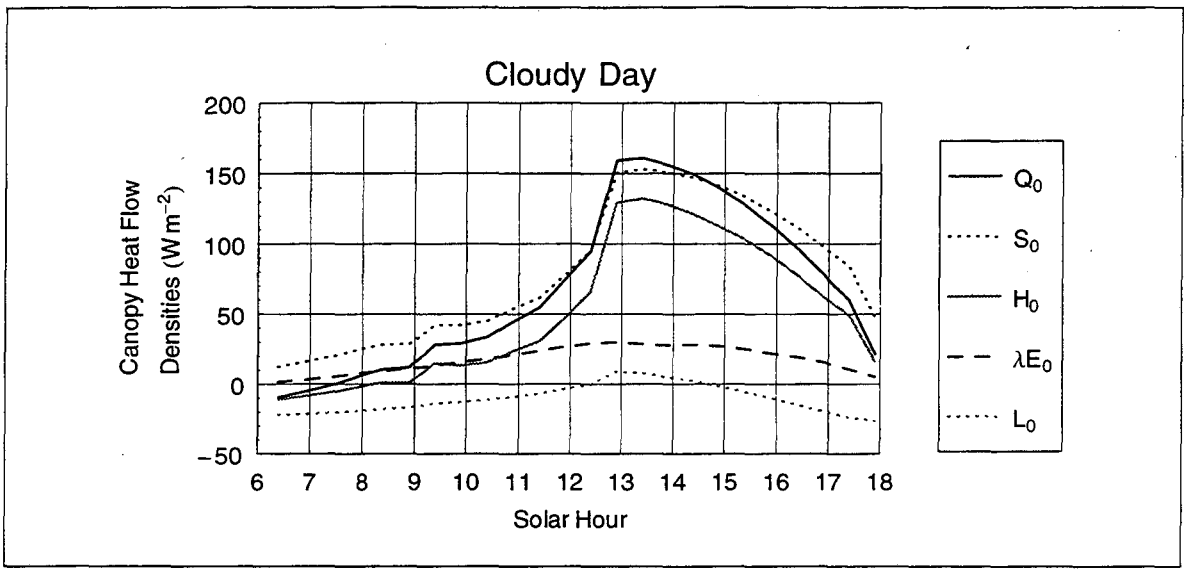

Figure 7-2. Cloudy-day, whole-canopy heat flow densities of all-wave radiation Q_0, short-wave radiation S_0, convection H_0, latent heat λE_0, and long-wave radiation.

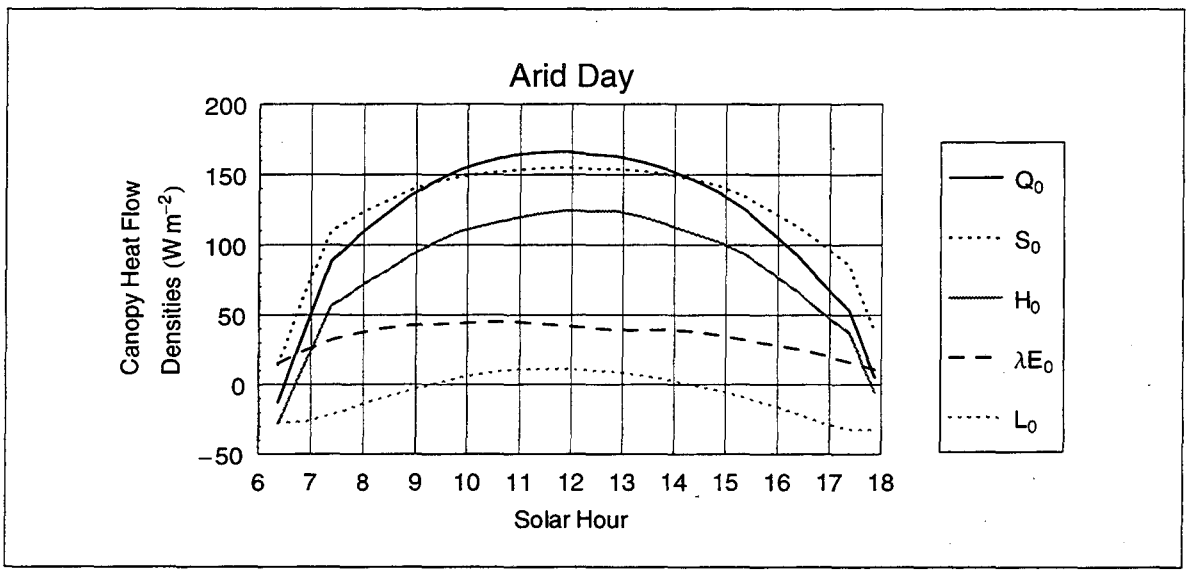

Figure 7-3. Arid-day, whole-canopy heat flow densities of all-wave radiation Q_0, short-wave radiation S_0, convection H_0, latent heat λE_0, and long-wave radiation L_0.

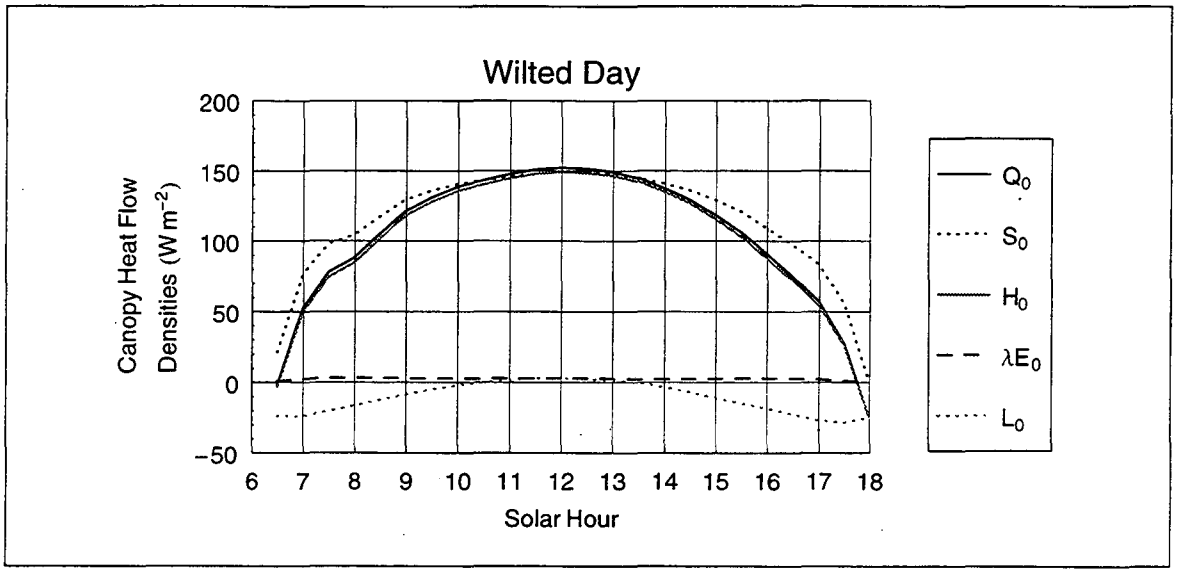

Figure 7-4. Wilted-day, whole-canopy heat flow densities of all-wave radiation Q_0, short-wave radiation S_0, convection H_0, latent heat λE_0, and long-wave radiation L_0.

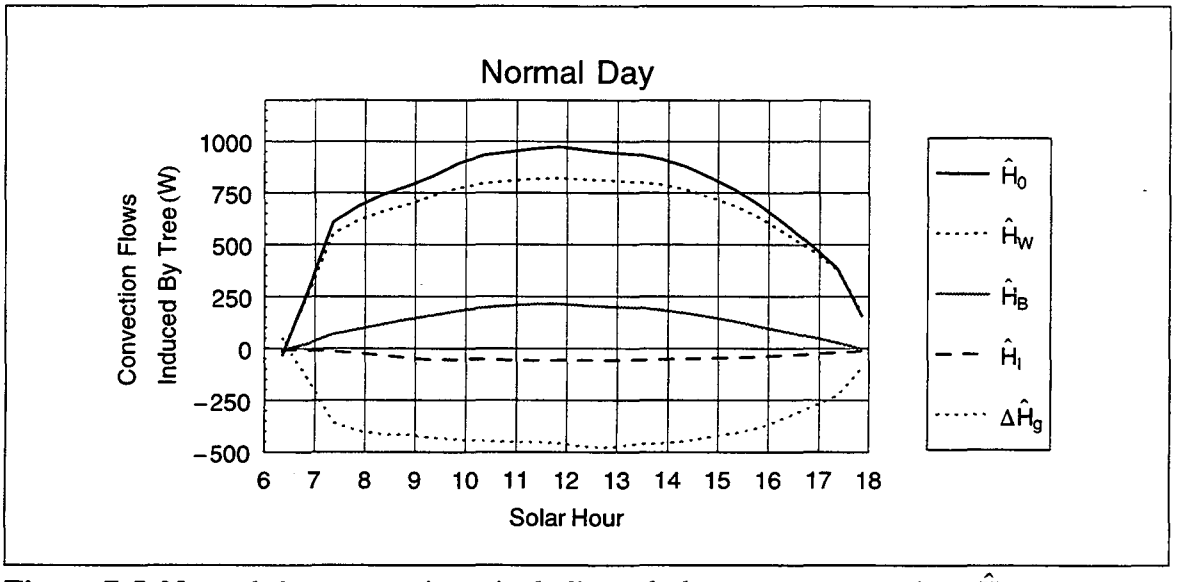

Figure 7-5. Normal-day convections, including whole-canopy convection $\hat{H}_0$, canopy-wall convection $\hat{H}_W$, canopy-base convection $\hat{H}_B$, canopy-interior convection $\hat{H}_I$, and ground-level convection change $\Delta\hat{H}_g$ induced by the presence of the tree.

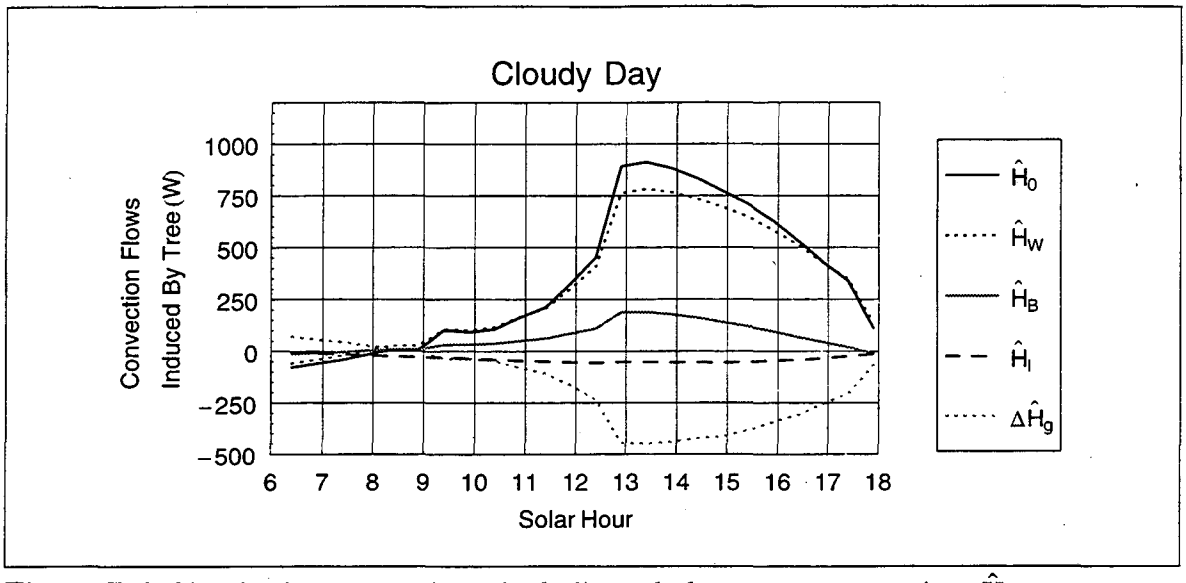

Figure 7-6. Cloudy-day convections, including whole-canopy convection $\hat{H}_0$, canopy-wall convection $\hat{H}_W$, canopy-base convection $\hat{H}_B$, canopy-interior convection $\hat{H}_I$, and ground-level convection change $\Delta\hat{H}_g$ induced by the presence of the tree.

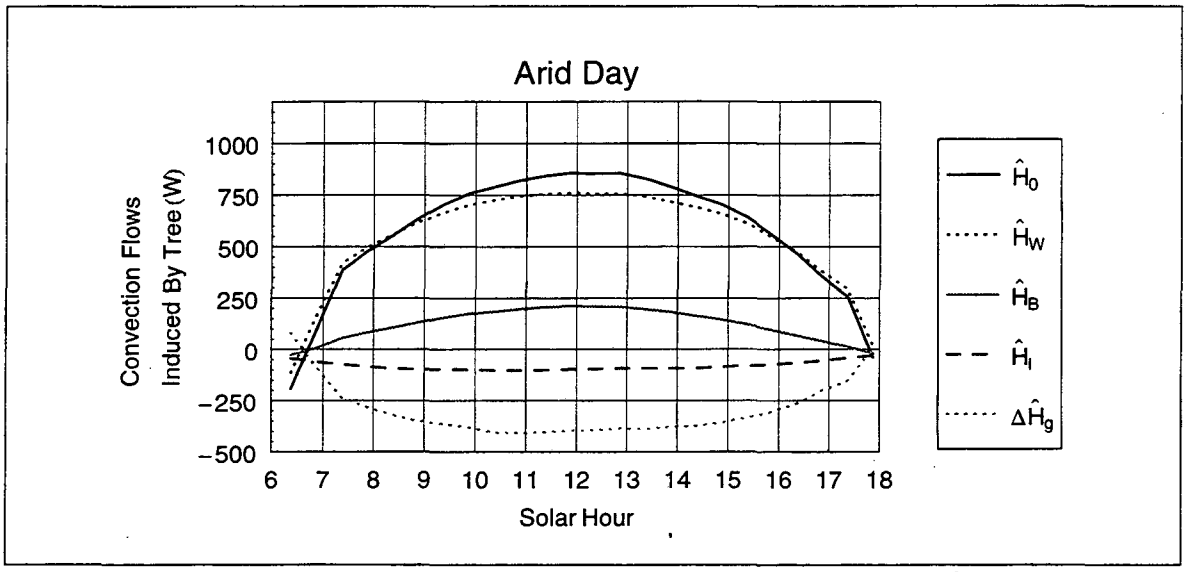

Figure 7-7. Arid-day convections, including whole-canopy convection $\hat{H}_0$, canopy-wall convection $\hat{H}_W$, canopy-base convection $\hat{H}_B$, canopy-interior convection $\hat{H}_I$, and ground-level convection change $\Delta\hat{H}_g$ induced by the presence of the tree.

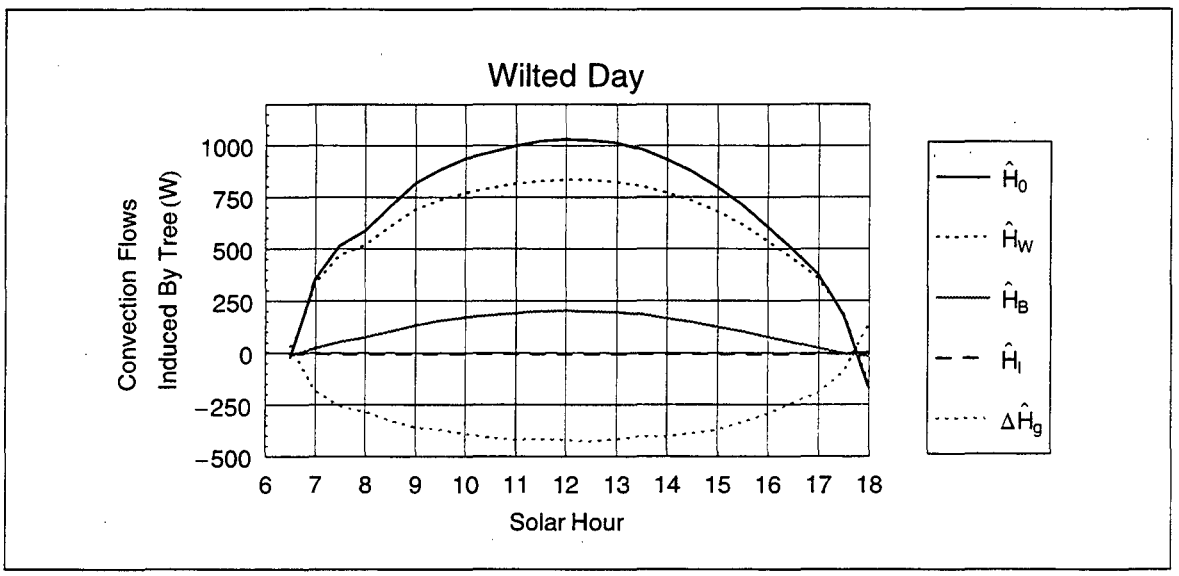

Figure 7-8. Wilted-day convections, including whole-canopy convection $\hat{H}_0$, canopy-wall convection $\hat{H}_W$, canopy-base convection $\hat{H}_B$, canopy-interior convection $\hat{H}_I$, and ground-level convection change $\Delta\hat{H}_g$ induced by the presence of the tree.

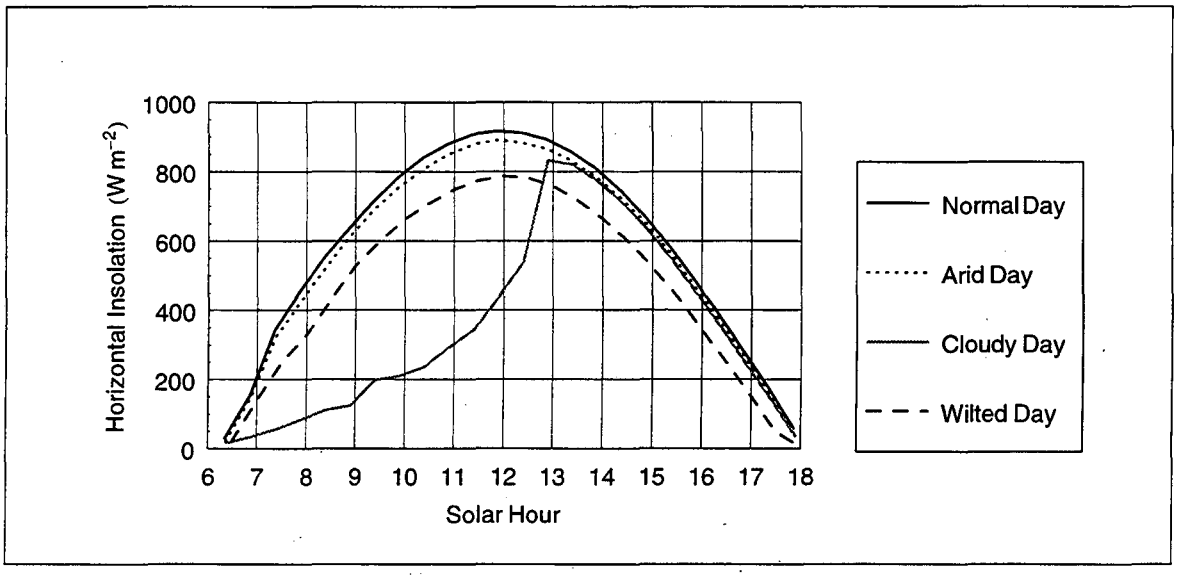

Figure 7-9. Horizontal-plane insolation I_H on four representative days.

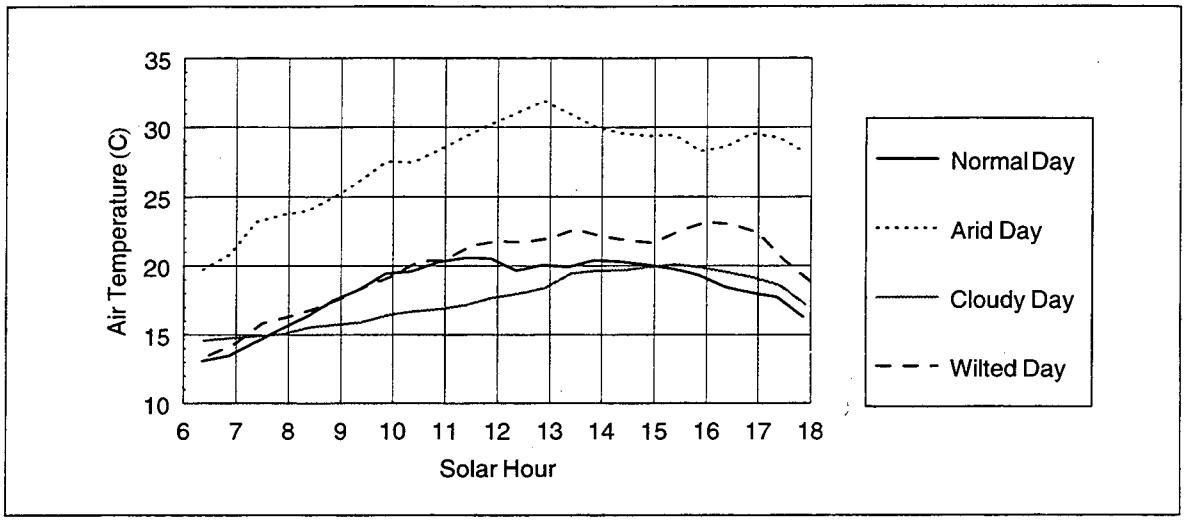

Figure 7-10. Air temperature T_a on four representative days.

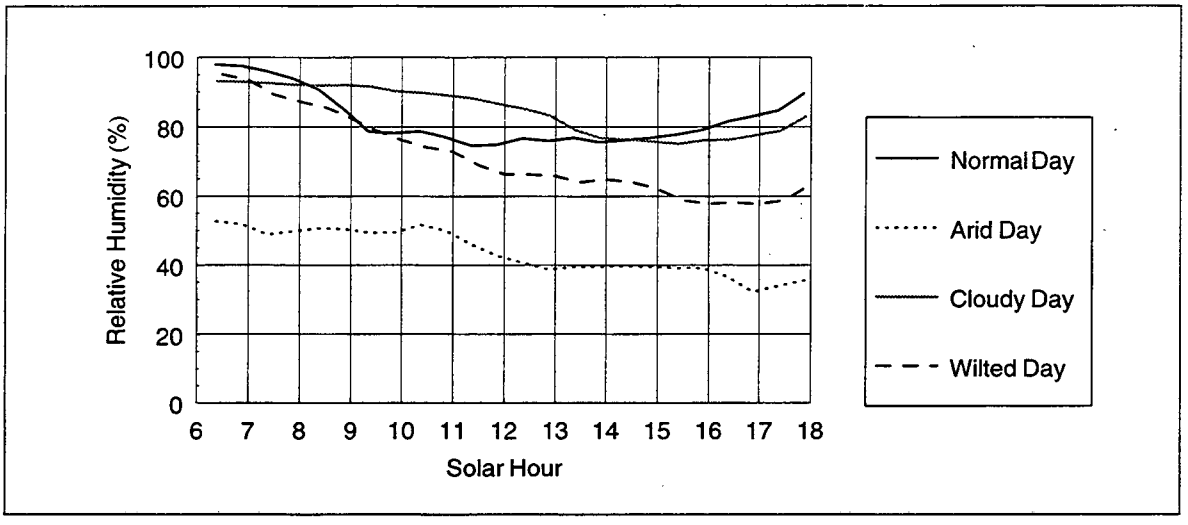

Figure 7-11. Relative humidity h_r on four representative days.

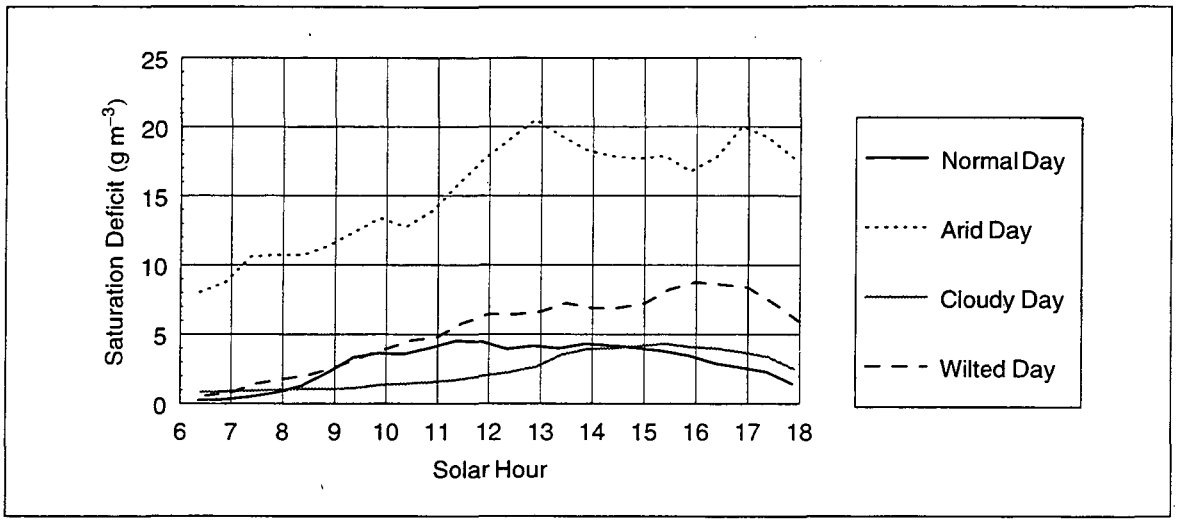

Figure 7-12. Water-vapor-density saturation deficit ρ_{sd} on four representative days.

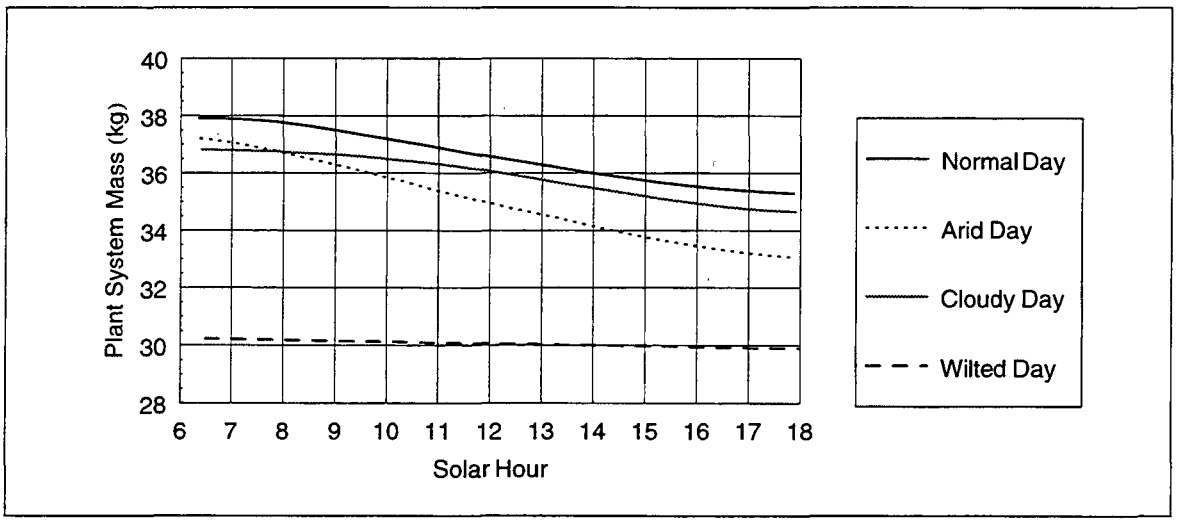

Figure 7-13. Plant system mass on four representative days.

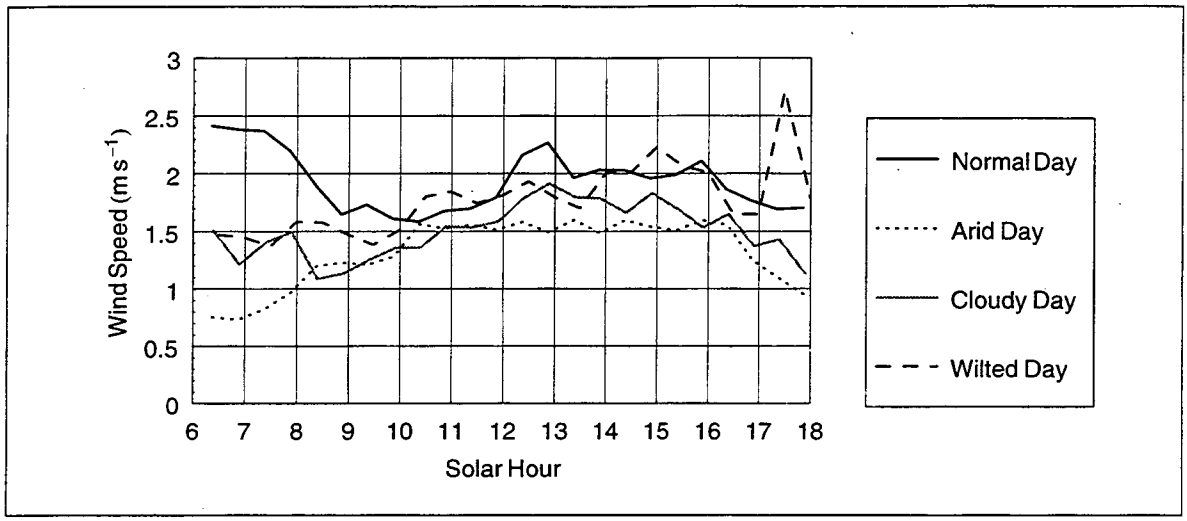

Figure 7-14. Wind speed U on four representative days.

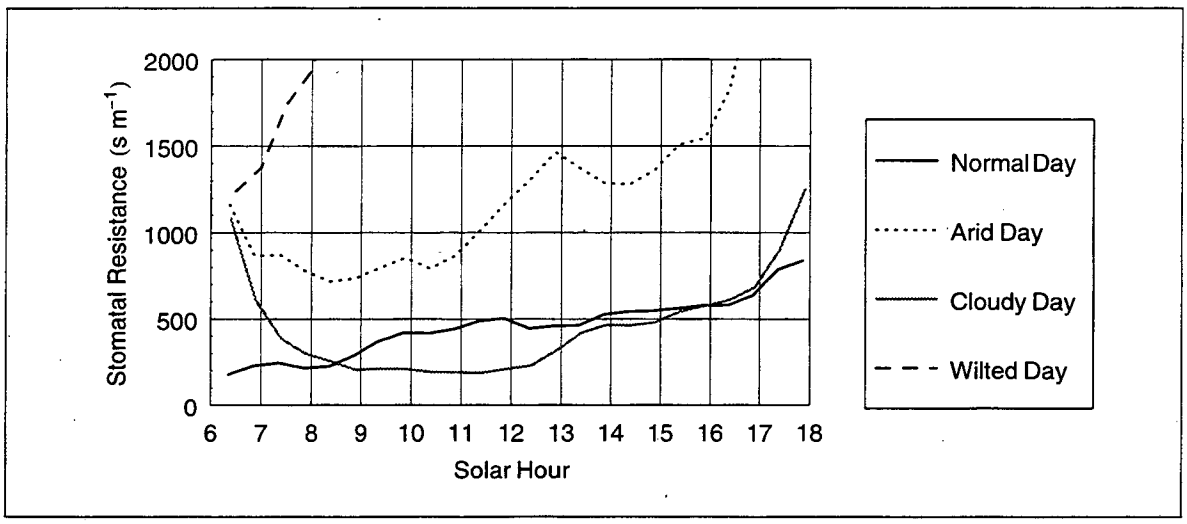

Figure 7-15. Stomatal resistance r_{vs} on four representative days, scaled to show behavior on non-wilted days.

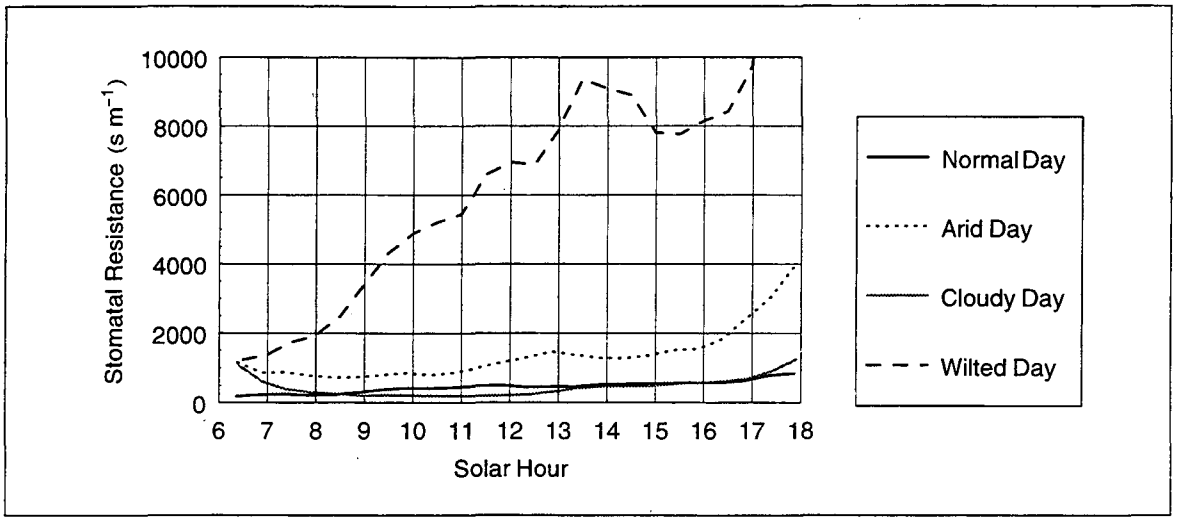

Figure 7-16. Stomatal resistance r_{vs} on four representative days, scaled to show behavior on the wilted day.

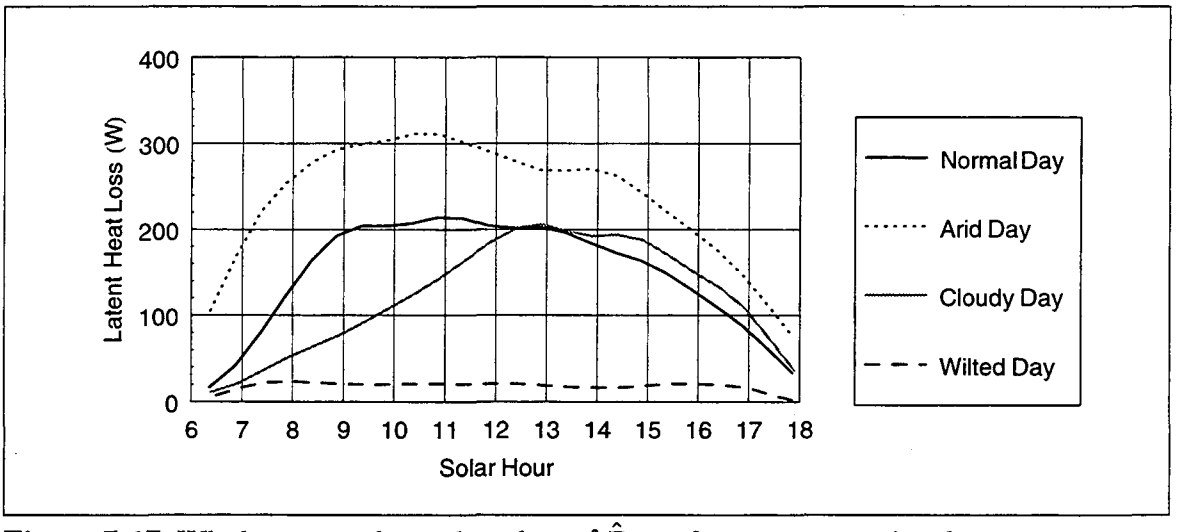

Figure 7-17. Whole-canopy latent heat loss $\lambda\hat{E}_0$ on four representative days.

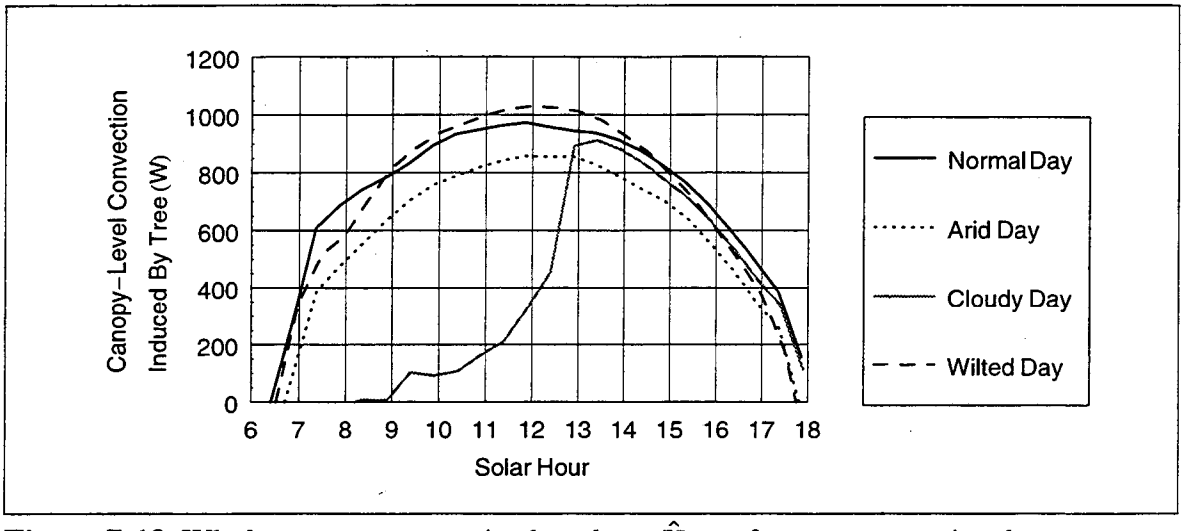

Figure 7-18. Whole-canopy convective heat loss $\hat{H}_0$ on four representative days.

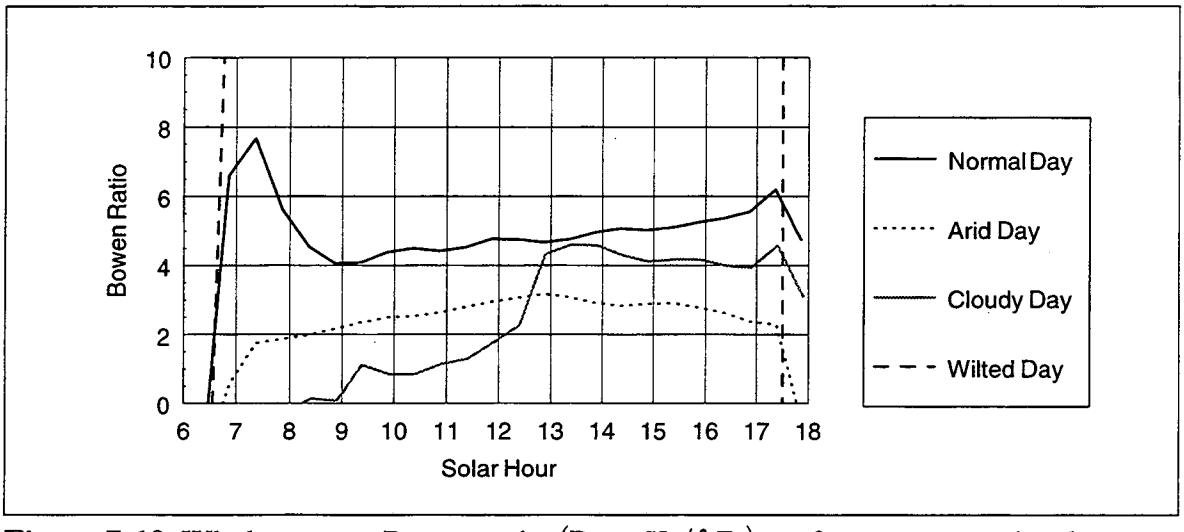

Figure 7-19. Whole-canopy Bowen ratio $\left(\mathrm{Bo} = H_0/\lambda E_0\right)$ on four representative days, scaled to show behavior on non-wilted days.

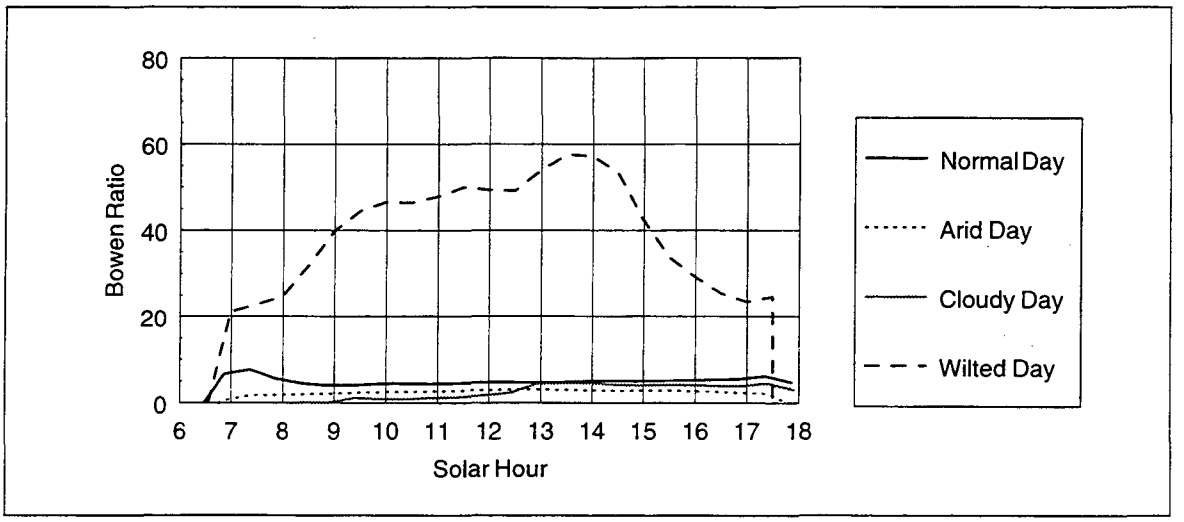

Figure 7-20. Whole-canopy Bowen ratio $\left(\mathrm{Bo} = H_0/\lambda E_0\right)$ on four representative days, scaled to show behavior on the wilted day.

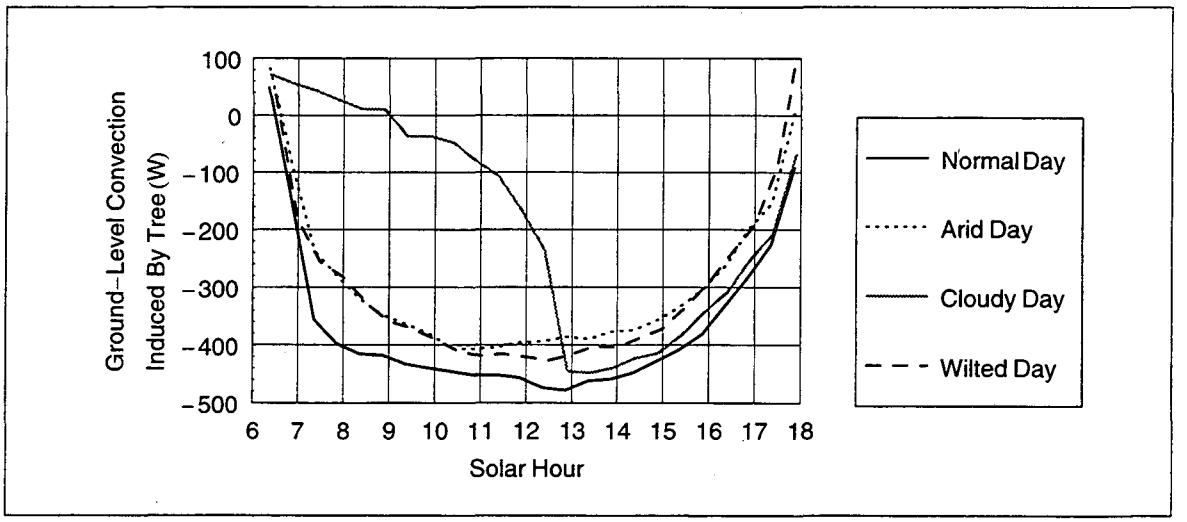

Figure 7-21. Tree-induced change in ground-level convection $\Delta\hat{H}_g$ on four representative days.

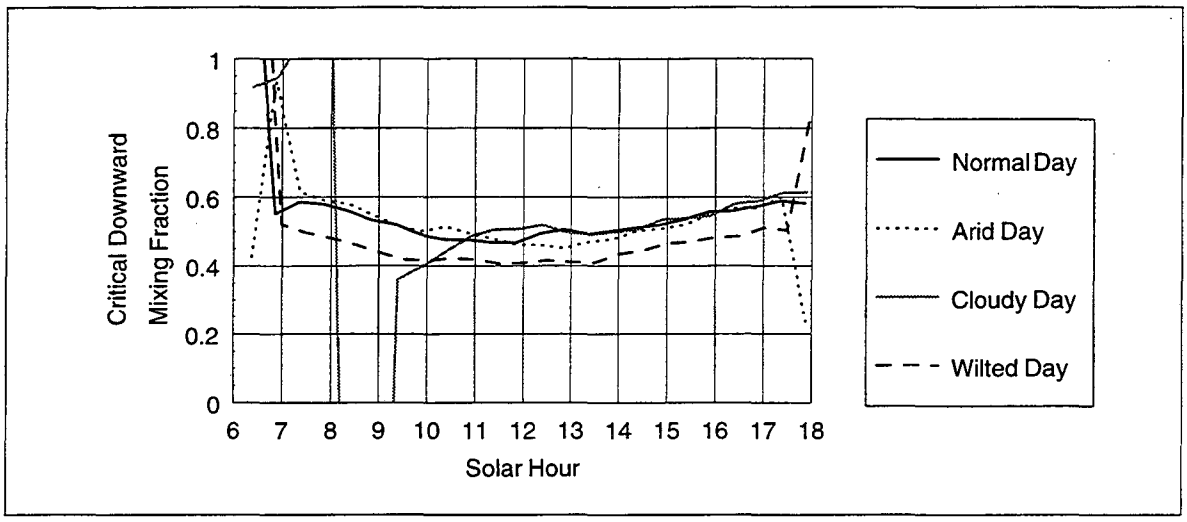

Figure 7-22. Critical downward mixing fraction $f'_{\downarrow}$ on four representative days.

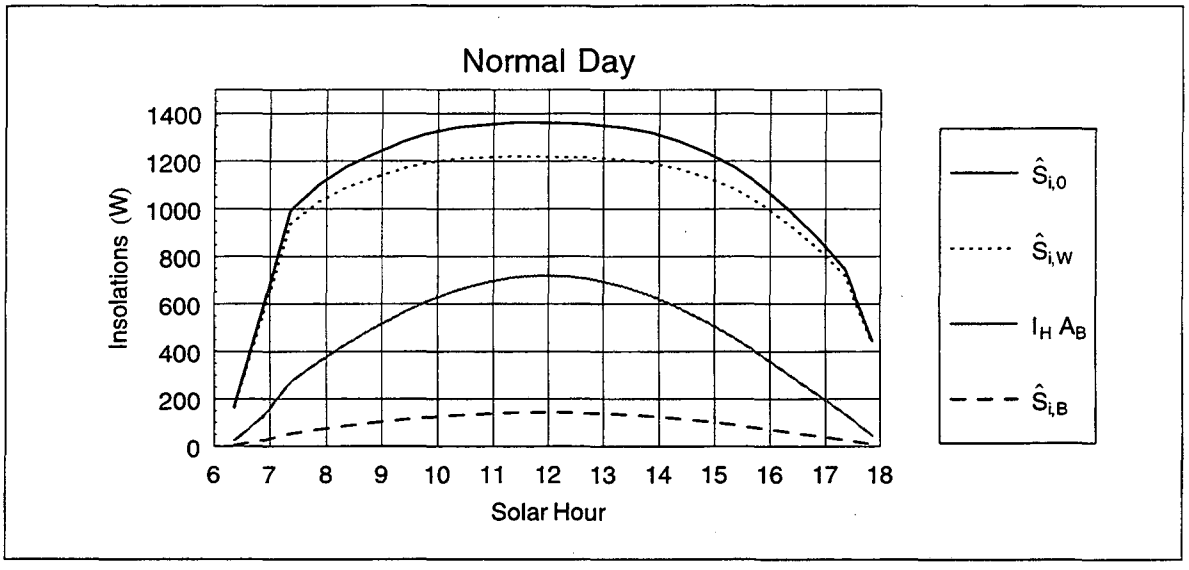

Figure 7-23. Normal-day incident insolations, including whole-canopy incident insolation $\hat{S}_{i,0}$, canopy-wall incident insolation $\hat{S}_{i,W}$, and canopy-base incident insolation $\hat{S}_{i,B}$ on a normal day. Also shown is the insolation incident on a horizontal region of area equal to that of the canopy base, $I_H A_B$.

Chapter 8: Conclusions

Two fundamental questions were posed at the outset of this paper: (a) will raising the albedo of ground surfaces warm or cool near-ground objects, and (b) by how much will the introduction of a tree cool or warm the air near the ground. The short answer is that near-ground objects and air may be either warmed or cooled by increasing albedo and adding trees, and that the magnitudes of these effects tend to be fairly small. This chapter will also discuss the merits of the models introduced herein, and suggest some topics for further exploration.

8.1 Effects of Ground Albedo and Shade Fraction on Near-Ground Objects

8.1.1 Ground Albedo

The calculations performed for a human, a car, and a bungalow suggest that raising the albedo of ground surfaces can reduce the environmental (and thus surface) temperatures of objects that have moderate to high albedos. To be so cooled, a human in a low wind and tall thermal boundary layer requires a surface albedo of only about 0.15, which could readily be achieved with high-albedo clothing. A small building in a moderate wind and a tall thermal boundary layer demands the highest albedo—about 0.7—which would require clean, bright white exterior. The magnitude of the environmental temperature change is not large: a ground albedo increase of 0.25 would alter the temperature of a near-ground object of typical albedo 0.3 by -1 to +2 K.

Convection-critical object albedos are quite high—generally greater than 0.7—suggesting that an increase in ground albedo will almost always raise the amount of heat convected from near-ground objects to the air. However, the convective flux density increase associated with a ground-albedo rise of 0.25 is only about 10 to 60 $W\ m^{-2}$. This is not particularly large when compared to the $200\ W\ m^{-2}$ reduction of ground-to-air convection of that would result from the same rise in ground albedo. Thus, raising the ground albedo will tend to reduce total amount of heat convected into the near-ground air.

8.1.2 Shade Fraction

The shading provided by the canopy of a tree can yield much greater reductions in near-ground-object environmental temperature and convection loss. Increasing the shade fraction from zero to one-half—a modest assumption, since a tree canopy can easily shade the entire surface of human or car-sized objects—will reduce the environmental temperature by 2 to 16 K. The temperature drop is greatest under mild wind conditions. Squat objects exhibit a greater noontime temperature drop than do tall objects. Shading also leads to sizable reductions in object-to-air convection, on the order of $100\ W\ m^{-2}$. This effect varies with wind speed and form factor in the same manner as the temperature drop.

8.2 Air Heating and Cooling Induced by a Tree

8.2.1 Net Ground-Level Effect

The presence of a small tree was found to increase noontime convection from canopy to air by about $1200\ \mathrm{W\ m^{-2}}$, and to reduce the ground-to-air convection by about $550\ \mathrm{W\ m^{-2}}$. These flows are expressed per unit base area of the tree's canopy. The canopy of the experimental specimen was at ground level, and thus induced net ground-level air heating of $650\ \mathrm{W\ m^{-2}}$.

Since the critical downward mixing fraction was 0.45, the net ground-level heating that would have been induced had the canopy been high was $(f_{\downarrow} - 0.45) \times (1200\ \mathrm{W\ m^{-2}})$. A reasonable guess for the downward mixing fraction might be 0.4, at which the net ground-level air cooling induced by the tree is approximately $60\ \mathrm{W\ m^{-2}}$. The actual net cooling or heating will vary strongly with $f_{\downarrow}$, which is a function of the flow around the canopy.

The shape of the conical canopy is captured in the canopy and ground energy balances by its angle of elevation, so the results obtained for this tree should scale to larger trees with a similar angle of elevation (about 75°). It should also extend to collections of well-separated (i.e. non-interfering) trees.

8.2.2 Significance of Evapotranspiration

In general, the canopy's heat gain was dominated by short-wave radiation, and its heat loss was dominated by convection. Evapotranspiration played an important role in the canopy energy balance only on the arid day, when the canopy's latent heat loss was comparable to its convective heat loss. This suggest that evaporation may be neglected in considerations of net ground-level convection on days when the water vapor density saturation deficit is moderate, say less than $5\ \mathrm{g\ m^{-3}}$.

8.3 Merits of Various Models

8.3.1 Near-Ground Object Model

Strengths. The near-ground object model has several attractive features. First, since it focuses solely on the *variation* of environmental temperature and convective loss with ground albedo and shade fraction, it eliminates parameters like the sky and free-stream temperatures. Second, it yields critical values of object albedo that may be calculated explicitly, and to which an object's actual albedo may be compared to determine the sign of the effect of a rise in ground albedo.

Weaknesses. As usual, the price for convenience is accuracy. The near-ground object

model stacks assumption upon assumption, and some hold poorly in certain cases. Notable shortcomings are the application of a conductionless energy balance to the surface of a highly conductive body (e.g. a car), overestimating sensitivities to ground albedo changes; the arbitrary choice of ground convection coefficient, which yields moderate uncertainties in the temperature-critical object albedo; and the arbitrary choice of thermal boundary-layer height, which also yields moderate uncertainties in the temperature-critical object albedo.

8.3.2 Tree and Ground Models

Strengths. The closed form solution for the net ground-level air heating induced by the presence of a tree (Eq. (5-72), with all its attendant substitutions) is explicit, albeit unwieldy. That is, no iteration is required in its evaluation, and there are no concerns about numerical stability. Also, by gauging the tree's effect in terms of a heat flow, rather than by an air temperature change, this model skirts the dicey business of estimating the volume of air into which convected heat will be dispersed. The only flow-related parameter other than free-stream velocity is the downward mixing fraction. The downward mixing fraction is a handy concept because it may be estimated either crudely—from hand-waving considerations of symmetry and buoyancy—or with accuracy, from a study of the flow around a tree.

Weaknesses. The opaque canopy radiation model employed to close the tree's energy balance is cruder than most other models, because it does not account for penetration of sunlight into the canopy. Thus, it is suited only for densely foliated trees. While the canopy energy balance predicts stomatal resistances with approximately correct values and diurnal variations, some of the values are hard to explain from considerations of plant physiologically. This suggest that some aspect of the canopy energy balance is somewhat inaccurate, and the most likely candidate is the relatively crude radiation model.

8.4 Directions for Further Research

Several topics touched upon in this paper may warrant further research:

1. Cooling by other species of trees, which may have solar loads or evapotranspiration rates that differ significantly from those of the specimen studied herein.
2. Cooling by collections of trees. A proper evaluation of the cooling effects of urban forestry must account for the mutual shading and wind screening of a collection of trees.
3. Expression of ground convection coefficient. There does not appear to be a satisfactory formula in the literature for the variation of a smooth ground surface's convection coefficient with wind speed.

Chapter 9: References

Akbari, H. 1990. Heat islands, white surfaces, urban trees: impact on heating and cooling energy use in the urban environment, *Proceedings of the Conference on Enhancing Electricity's Value To Society*, 2:865-882, Canadian Electric Association, October 22-24, Toronto, Canada.

Akbari, H. and Taha, H. 1992. The impact of trees and white surfaces on residential heating and cooling energy use in four Canadian cities, *Energy, the International Journal*, 17(2):141-149. Also Lawrence Berkeley National Laboratory Report LBL-30131, Berkeley, CA.

Akbari, H., Bos, W., Bretz, S., Hanford, J., Rosenfeld, A., Sailor, D., and Taha, H. 1992a. Monitoring peak power and cooling energy savings of shade trees and white surfaces in the Sacramento Municipal Utility District (SMUD) service: project design and preliminary results, Lawrence Berkeley National Laboratory Report LBL-34411, Berkeley, CA.

Akbari, H., Bretz, S., Hanford, J., Fishman, B., and Taha, H. 1993. Monitoring peak power and cooling energy savings of shade trees and white surfaces in the Sacramento Municipal Utility District (SMUD) service: data analysis, simulations, and results, Lawrence Berkeley National Laboratory Report LBL-34411, Berkeley, CA.

Akbari, H., Davis, S., Dosano, S., Huang, J., and Winnett, S. (editors). 1992b. *Cooling Our Communities: A Guidebook on Tree Planting and Light-Colored Surfacing*, Washington, D.C.: United States Environmental Protection Agency, Office of Policy Analysis, Climate Change Division. Also Lawrence Berkeley National Laboratory Report LBL-31587, Berkeley, CA.

Akbari, H., Kurn, D., Taha, H., and Hanford, J. 1995. Peak power and cooling savings of high-albedo roofs, accepted in *Energy and Buildings—Special Issue on Urban Heat Islands*, excepts from Lawrence Berkeley National Laboratory Report LBL-34411.

Akbari, H., Kurn, D., Taha, H., and Hanford, J. 1995. Peak power and cooling savings of shade trees, accepted in *Energy and Buildings—Special Issue on Urban Heat Islands*, excepts from Lawrence Berkeley National Laboratory Report LBL-34411.

Akbari, H., Rosenfeld, A, and Taha, H. 1990. Summer heat islands, urban trees, and white surfaces, *Proceedings of American Society of Heating, Refrigeration, and Air Conditioning Engineers*, Atlanta, GA (February). Also Lawrence Berkeley National Laboratory Report LBL-28308, Berkeley, CA.

Akbari, H., Rosenfeld, A., Taha, H. and Gartland, L. 1996. Mitigation of summer urban heat islands to save electricity and smog, *Proceedings of the 76th Annual American Meteorological Society Meeting*, Atlanta, GA, January 28-February 2. Lawrence Ber-

keley National Laboratory Report LBL-37787, Berkeley, CA.

Akbari, H., Taha, H., Sailor, D., and Bos, W. 1992c. Measured savings in air conditioning from shade trees and white surfaces, Lawrence Berkeley National Laboratory Report LBL-32316.

ASHRAE (American Society of Heating, Refrigerating, and Air-Conditioning Engineers). 1985. *ASHRAE Handbook, 1985 Fundamentals, IP ed.*, American Society of Heating, Refrigerating, and Air-Conditioning Engineers, Atlanta, GA.

Beeson, R.C., Jr. 1992. Restricting overhead irrigation to dawn limits growth in container-grown woody ornamentals, *HortScience*, 27(9):996-999.

Bold, H.C., Alexopoulos, C.J., and Delevoryas, T. 1987. *Morphology of Plants and Fungi: Fifth Edition*, Harper & Row, New York.

Bornstein, R.D. 1989. Nature, limitations, and applications of urban climate models, *Proceedings of the Workshop on Saving Energy and Reducing Atmospheric Pollution by Controlling Summer Heat Islands*, Berkeley, CA, February 23-24, pp.124-149. Lawrence Berkeley National Laboratory Report LBL-27872, Berkeley, CA.

Campbell, G.S. 1977. *An Introduction to Environmental Physics*, Springer-Verlag, New York.

Churchill, S.W. and Bernstein, M. 1977. A correlating equation for forced convection from gases and liquids to a circular cylinder in crossflow, *Journal of Heat Transfer*, 99:300-306.

Cowan, I.R. 1977. Stomatal behavior and environment, *Advances in Botanical Research*, 4:117-228.

De Ridder, K. 1997. Radiative transfer in the IAGL land surface model, *Journal of Applied Meteorology*, 36:12-21.

De Ridder, K. and Schayes, G. 1997. The IAGL land surface model, *Journal of Applied Meteorology*, 36:167-181.

Duffie, J.A. and Beckman, W.A. 1980. *Solar Engineering of Thermal Processes*, Wiley, New York.

Everett, T.H. 1981-82. *The New York Botanical Garden Illustrated Encyclopedia of Horticulture: Volume 6*, Garland, New York.

Fritschen, L.J., Walker, R.B., and Hsia, J. 1980. Energy balances of an isolated Scots pine, *International Journal of Biometeorology*, 24:293-300.

Gabersek, S. and Taha, H. 1995. A preliminary multi-city assessment of the impacts of increased urban albedo and vegetation on regional meteorology and energy use, Lawrence Berkeley National Laboratory Report LBL-37887, Berkeley, CA.

Garratt, J.R. and Hicks, B.B. 1973. Momentum, heat, and vapor transfer to and from natural and artificial surfaces. *Quarterly Journal of the Royal Meteorological Society*, 99:680-687.

Gates, D.M. 1980. *Biophysical Ecology*, Springer, New York.

Geiger, R. 1965. *The Climate Near the Ground*, Harvard University Press, Cambridge, MA.

Gross, G. 1987. A numerical study of the air flow within and around a single tree, *Boundary-Layer Meteorology*, 40:311-327.

Heilman, J.L. and Britin, C.L. 1989. Water use by shrubs as affected by energy exchange with building walls, *Agricultural and Forest Meteorology*, 48:345-357.

Hollinger, D.Y., Kelliher, F.M., Schulze, E.-D., and Köstner, B.M.M. 1994. Coupling of tree transpiration to atmospheric turbulence, *Nature*, 371:60-62.

Honjo, T. and Takakura, T. 1990-91. Simulation of thermal effects of urban green areas on their surroundings areas, *Energy and Buildings*, 15-16:443-446.

Huang, J. Akbari, H., Taha, H., and Rosenfeld, A. 1987. The potential of vegetation in reducing summer cooling load in residential buildings, *Journal of Climate and Applied Meteorology*, 26(9):1103-1116. Also Lawrence Berkeley National Laboratory Report LBL-21291, Berkeley, CA.

Huang, J., Akbari, H., and Taha, H. 1990. The wind-shielding and shading effects of trees on residential heating and cooling requirements, Lawrence Berkeley National Laboratory Report LBL-24131, Berkeley, CA.

Kays, W.M. and Crawford, M.E. 1993. *Convective Heat and Mass Transfer: Third Edition*, McGraw-Hill, New York.

Kobyshev, A.A., Mastyaeva, I.N., Surinov, Yu.A., and Yakovlev, Yu.P. 1976. Study of radiation field created by conical radiators (Russian), *Aviatsionnaya Tekhnika*, 19(3):43-9.

Kozlowski, T.T. (editor). 1981. *Water Deficits and Plant Growth: Volume 6*, Academic, New York.

Kozlowski, T.T. (editor). 1983. *Water Deficits and Plant Growth: Volume 7*, Academic, New York.

Kramer, P.J. 1983. *Water Relations of Plants*, Academic Press, New York.

Kurn, D., Bretz, S., Huang, J., and Akbari, H. The potential for reducing urban air temperatures and energy consumption through vegetative cooling, *Proceedings of the ACEEE 1994 Summer Study on Energy Efficiency in Buildings*, 9:155, Pacific Grove, CA, August. Also Lawrence Berkeley National Laboratory Report LBL-35320, Berkeley, CA.

Lownds, N.K. and Berghahe, R.D. 1991. Relationships between water use of container-grown landscape plants and turf evapotranspiration rates, *Hortscience*, 26(6):131.

Martien, P., Akbari, H., Rosenfeld, A., and Duchesne, J. 1989. Approaches to using models of urban climate in building-energy simulations, *Proceedings of the Workshop on Saving Energy and Reducing Atmospheric Pollution by Controlling Summer Heat Islands*, Berkeley, CA, February 23-24, pp.151-173b. Lawrence Berkeley National Laboratory Report LBL-27872, Berkeley, CA.

Meidner, H. and Mansfield, T.A. 1968. *Physiology of Stomata*, McGraw-Hill, New York.

Monteith, J.L. 1973. *Principles of Environmental Physics*, American Elsevier Publishing, New York.

Oke, T.R. 1978. *Boundary Layer Climates*, Wiley, New York.

Onur, M. 1993. Forced convection heat transfer from a plat-plate model collector on roof of a model house, *Wärme-und Stoffübertragung*, 28:141-145.

Pearman, G.I., Weaver, H.L., and Tanner, C.B. 1972. Boundary layer heat transfer coefficients under field conditions, *Agricultural Meteorology*, 10:83-92.

Penman, H.L. 1948. Natural evaporation from open water, bare soil and grass. *Proc. R. Soc. A*, 194:120.

Pielke, R.A. 1984. *Mesoscale Meteorological Modeling*, Academic Press, Orlando, FL.

Pielke, R.A. 1989. Use of mesoscale meteorological modeling as an assessment of summer urban heat islands, *Proceedings of the Workshop on Saving Energy and Reducing Atmospheric Pollution by Controlling Summer Heat Islands*, Berkeley, CA, February 23-24, pp.177-184. Lawrence Berkeley National Laboratory Report LBL-27872, Berkeley, CA.

Rosenfeld, A., Romm, J., Akbari, H., and Lloyd, A. 1997. Paint the town white—and green, *MIT's Technology Review*, 100(2):52-59.

Rosenfeld, A., Romm, J., Akbari, H., Pomerantz, M., and Taha, H. 1996. Policies to reduce summer heat islands: magnitudes of benefits and incentive to achieve them,

Proceedings of the ACEEE 1996 Summer Study on Energy Efficiency in Buildings, 9:177-186, Pacific Grove, CA, August. Also Lawrence Berkeley National Laboratory Report LBL-38679, Berkeley, CA.

Sailor, D. 1993. The role of surface characteristics in urban meteorology and air quality, Ph.D. Thesis, Lawrence Berkeley National Laboratory Report LBL-34459, Berkeley, CA.

Sailor, D. and Akbari, H. 1992. Meteorological modeling applications in building energy simulations, *Proceedings of the ACEEE 1992 Summer Study on Energy Efficiency in Buildings*, 9:145, Pacific Grove, CA, August. Also Lawrence Berkeley National Laboratory Report LBL-32420, Berkeley, CA.

Salisbury, F.B. and Ross, C.W. 1985. *Plant Physiology: Third Edition*, Wadsworth Publishing, Belmont, CA.

Siegel, R.S. and Howell, J.R. 1992. *Thermal Radiation Heat Transfer: Third Edition*, Hemisphere, Washington, D.C.

Steinberg, S.L., Zajicek, J.M., and McFarland, M.J. 1991. Short-term effect of uniconazole on the water relations and growth of Ligustrum, *Journal of the American Society for Horticultural Science*, 116(3):460-464.

Still, D.W. and Davies, F.T., Jr. 1988. Growth, whole-plant transpiration and water relations of selected woody ornamental species, *HortScience*, 23(3):145.

Still, D.W. and Davies, F.T., Jr. 1993. Water use, water-efficiency and growth analysis of selected woody ornamental species under a non-limiting water regime, *Scientia Horticulturae*, 53:213-223.

Sutton, O.G. 1953. *Micrometeorology: A Study of Physical Processes in the Lowest Layers of the Earth's Atmosphere*, McGraw-Hill, New York.

Taha, H. and Akbari, H. 1995. Urban climates and heat islands: albedo, evapotranspiration, and anthropogenic heat, accepted in *Energy and Buildings—Special Issue on Urban Heat Islands*. Also Lawrence Berkeley National Laboratory Report LBL-29864, Berkeley, CA.

Taha, H., Akbari, H., and Rosenfeld, A. 1991. Heat island and oasis effects of vegetative canopies: micrometeorological field measurements, *Theoretical and Applied Climatology*, 44(2):123-138. Also Lawrence Berkeley National Laboratory Report LBL-36893, Berkeley, CA.

Taha, H., Akbari, H., Rosenfeld, A, and Huang, J. 1988. Residential cooling loads and the urban heat island—the effect of albedo, *Building and Environment*, 23:271-283. Also Lawrence Berkeley National Laboratory Report LBL-24008, Berkeley, CA.

Thorpe, M.R. 1978. Net radiation and transpiration of apple trees in rows, *Agricultural Meteorology*, 19:41-57.

Threlkeld, J.L. 1970. *Thermal Environmental Engineering: Second Edition*, Prentice-Hall, New York.

White, F.M. 1988. *Mass and Heat Transfer,* Addison-Wesley, New York.

Appendix A: Surface Energy Balances

A.1 Overview

This appendix develops the energy balances of a dry surface—e.g. the ground, or a near-ground object—and a wet surface, such as a leaf.

At a dry surface, long and short wave radiation gains are lost by convection and conduction.At a wet, adiabatic[†] surface, the long and short wave gains are dissipated by convection and by the evaporation of water. The rate of evaporation from the wet surface is determined by coupled mass and energy balances.

A.2 Conventions

Unless otherwise indicated, all heat and mass flows are per unit area, units are SI, temperatures are absolute, and fluid properties are evaluated at a standard temperature and pressure (STP) of 20°C and one atmosphere. Area-integrated ("areal") flows are denoted with a hat, e.g. $\hat{Q}$. The abbreviations "LW," "SW," and "AW" may be used to denote long-wave, short-wave, and "all-wave" (long-wave plus short-wave) radiations. Unless otherwise specified, the adjective "radiative" refers to long-wave radiation.

A.3 Linearization of Heat and Mass Flows

A.3.1 Transfer Resistances

It is both traditional and mathematically convenient to linearize the heat flows from a surface by expressing each heat flow as the ratio of a linear temperature difference that drives the flow to a resistance that opposes the flow. Consider a surface at temperature T_0 that convects to air at temperature T_a, conducts to a solid at temperature T_c, and exchanges long-wave radiation with a black-body surface at temperature T_r. Its long-wave (LW) radiative heat gain[‡] L, convective heat loss H, and conductive heat loss K may be written

$$L = C r_r^{-1} (T_r - T_0), \tag{A-1}$$

$$H = C r_h^{-1} (T_0 - T_a), \tag{A-2}$$

---

†. In this paper, adiabatic is taken to mean that no heat is conducted from the surface.

‡. Note that by convention, the LW radiation heat flow is defined as a *gain* to the surface, while the convection and conduction heat flows are written as *losses*. This permits the surface energy balance to be written as AW gain = SW gain + LW gain = convection loss + conduction loss.

and

$$K = C r_c^{-1} (T_0 - T_c). \tag{A-3}$$

Here

$$C \equiv (\rho c_p)_{\text{air}} \tag{A-4}$$

is the volumetric heat capacity of air, and r_r, r_h, and r_c are the radiative, convective, and conductive resistances to heat transfer.

Similarly, vapor diffusion from a wet surface may be expressed as the ratio of a linear difference in vapor density driving the mass flow to a resistance opposing the mass flow. The rate of latent heat loss from a wet surface is

$$\lambda E = \lambda r_v^{-1} (\rho'_{v0} - \rho_{va}), \tag{A-5}$$

where λ is the latent heat of vaporization of water per unit mass, E is the mass loss rate, $\rho'_{v0} \equiv \rho'_v(T_0)$ is the saturation density of water vapor at the surface temperature T_0, ρ_{va} is the density of water vapor in the air, and r_v is the resistance to vapor diffusion. All transfer resistances have been defined to have dimensions of time per length.

The surface may also experience a short-wave (SW) radiative gain S and internal heat generation G. The sum of the short and long wave gains is the "all-wave" (AW) gain

$$Q \equiv L + S. \tag{A-6}$$

A.3.2 Coupling of Vapor Density Difference to Temperature Difference

A common temperature-difference expansion of the vapor density difference in Eq. (A-5) is

$$\rho'_{v0} - \rho_{va} = (\rho'_{v0} - \rho'_{va}) + (\rho'_{va} - \rho_{va}) \approx s(T_0 - T_a) + \rho_{sd}, \tag{A-7}$$

where

$$s \equiv \frac{d\rho'_v(T)}{dT} \tag{A-8}$$

is the slope of the saturation vapor density with respect to temperature. The "saturation deficit"

$$\rho_{sd} \equiv \rho'_{va} - \rho_{va} \tag{A-9}$$

is the additional density of water vapor the air may absorb before reaching saturation, and $\rho'_{va} \equiv \rho'_v(T_a)$ is the saturation vapor density of water at the air temperature. The density of

water vapor in the air may be expressed in terms of the relative humidity, h_r:

$$\rho_{va} = h_r \rho'_{va}. \tag{A-10}$$

Substituting Eq. (A-7) into Eq. (A-5) yields the latent heat loss as a function of the surface temperature:

$$\lambda E \approx \lambda r_v^{-1}\left[s\left(T_0 - T_a\right) + \rho_{sd}\right]. \tag{A-11}$$

A.4 Dry-Surface Energy Balances

A.4.1 Convection and Long-Wave Radiation

The energy balance on dry, adiabatic surface with no heat generation or SW gain $(\lambda E = K = G = S = 0)$ is simply

$$L = H, \tag{A-12}$$

or

$$C r_r^{-1}\left(T_r - T_0\right) = C r_h^{-1}\left(T_0 - T_a\right). \tag{A-13}$$

Radiative Efficiency Parameter. Its solution is

$$\frac{T_0 - T_r}{T_a - T_r} = \eta. \tag{A-14}$$

where the parameter

$$\eta \equiv \frac{r_r}{r_r + r_h}. \tag{A-15}$$

If $r_r \ll r_h$, then $\eta \approx 0$, and $T_0 \approx T_r$; if $r_h \ll r_r$, then $\eta \approx 1$, and $T_0 \approx T_a$. This parameter appears frequently in solutions to more complicated energy balances.

A.4.2 Convection, Long-Wave Radiation, and Short-Wave Radiation

With the addition of SW radiation S to the energy balance,

$$Q = L + S = H, \tag{A-16}$$

or

$$C r_r^{-1}\left(T_r - T_0\right) + S = C r_h^{-1}\left(T_0 - T_a\right). \tag{A-17}$$

The surface temperature will reach

$$T_0 = C^{-1} r_e S + \eta T_a + (1 - \eta) T_r, \tag{A-18}$$

where

$$r_e \equiv \left(r_r^{-1} + r_h^{-1}\right)^{-1} = \frac{r_r r_h}{r_r + r_h} = r_h \eta \,. \tag{A-19}$$

Dry-Surface All-Wave Radiative Gain. Combining Eqs. (A-2), (A-16), and (A-18), the AW radiative gain of this dry surface is

$$Q_{\text{dry}} = Q = L + S = H = C r_h^{-1}\left(T_0 - T_a\right) = \eta\left[C r_r^{-1}\left(T_r - T_a\right) + S\right]. \tag{A-20}$$

The concept of a dry AW gain will prove useful in the solution of wet surface energy balances.

Back-Calculating r_h. The convective resistance r_h may be calculated from an observed surface temperature T_0. Solving Eq. (A-17) for r_h,

$$r_h = \frac{C r_r \left(T_0 - T_a\right)}{C\left(T_r - T_0\right) + r_r S} \,. \tag{A-21}$$

A.4.3 Convection, Radiations, and Constant Conduction

Consider the surface of a body with heat conduction K from surface to core, and surface energy balance

$$Q = L + S = H + K \,. \tag{A-22}$$

If the conduction is constant†—that is, independent of surface temperature—then

$$C r_r^{-1}\left(T_r - T_0\right) + S = C r_h^{-1}\left(T_0 - T_a\right) + K \,. \tag{A-23}$$

If the core temperature is T_c and the surface-to-core conduction resistance is r_c, Eq. (A-3) relates the core temperature to the surface temperature T_0 by

$$K = C r_c^{-1}\left(T_0 - T_c\right), \tag{A-24}$$

or

$$T_0 = T_c + C^{-1} r_c K \,. \tag{A-25}$$

Substituting Eq. (A-25) into Eq. (A-23) and rearranging,

$$C r_e^{-1} T_c = S + C\left(r_r^{-1} T_r + r_h^{-1} T_a\right) - K\left(1 + \frac{r_c}{r_e}\right). \tag{A-26}$$

Environmental Temperature. This solution for the core temperature T_b can be expressed

†. An example of constant core-to-surface conduction would be found in a steady-state body with internal heat generation G that must be conducted to the surface. In that case, $K = -G$.

more neatly by introducing the "environmental temperature"† T_e. If the body were placed in a blackbody enclosure with $T_a = T_r = T_e$ and $S = 0$, the surface energy balance would reduce to

$$L = H + K, \tag{A-27}$$

or

$$C r_r^{-1}(T_e - T_0) = C r_h^{-1}(T_0 - T_e) - K. \tag{A-28}$$

Substituting Eq. (A-25) into Eq. (A-27) and rearranging,

$$C r_e^{-1} T_c = C\left(r_r^{-1} T_e + r_h^{-1} T_e\right) - K\left(1 + \frac{r_c}{r_e}\right). \tag{A-29}$$

Solving Eqs. (A-26) and (A-29) for T_e,

$$T_e = C^{-1} r_e S + \eta T_a + (1 - \eta) T_r. \tag{A-30}$$

Rearranging Eq. (A-28),

$$T_c = T_e - C^{-1}(r_e + r_c) K. \tag{A-31}$$

Substituting Eq. (A-31) into Eq. (A-25),

$$T_0 = T_e - C^{-1} r_e K. \tag{A-32}$$

This analysis holds only for *constant* surface-to-core conduction K. It is most usefully applied to a object with constant internal heat generation G and negligible thermal mass, e.g. a small animal. The core and surface temperatures of such an object will quickly reach steady-state, at which point $K = -G$ will be constant.

A.4.4 Surface Temperature of a Body Not in Steady-State

Adiabatic Surface Temperature. The concept of an environmental temperature may still be applied to an object not in steady state if surface-to-core conduction may be neglected in its surface energy balance. In that case, the object's surface temperature simply equals its environmental temperature:

$$T_0 = T_e. \tag{A-33}$$

This may be obtained formally by setting $K = 0$ in Eq. (A-32), but is really just a restatement of the adiabatic surface temperature solution of Eq. (A-18).

Neglecting Conduction. If $T_0 - T_c$, $T_0 - T_a$, and $T_0 - T_r$ are comparable in magnitude, the ratio of convection to LW radiation to conduction will be

$$H : L : K \approx r_h^{-1} : r_r^{-1} : r_c^{-1}. \tag{A-34}$$

---

†. Also known as the "equivalent blackbody temperature," or "effective temperature."

This ratio of conductances may be used to compare the three heat flows, and thereby determine whether K is negligible.

A.4.5 Utility of Environmental Temperature

Since human, vehicles, and buildings are thermally massive and rarely in steady-state, the constant-conduction expressions for body and surface temperatures, Eqs. (A-31) and (A-32), will rarely apply to near-ground objects of interest. At best, the adiabatic surface temperature solution of Eq. (A-18) will apply. Given this, why introduce the concept of an environmental temperature at all? The answer is threefold. Firstly, for consistency with the literature: environmental physicists commonly describe the climate of animals and humans in terms of environmental temperature (Monteith 1973; Campbell 1977). Secondly, for generality: environmental temperature theory *is* useful for small, steady-state objects, as discussed above, and there may be some interest in the surface and body temperatures of such objects. Thirdly, it is no more difficult to discuss environmental temperature than surface temperature.

A.5 Wet-Surface Energy Balances

A.5.1 Adiabatic Saturation and the Psychrometric Constant

Consider a parcel of air, originally at temperature T_a and water vapor density ρ_{va}, that is adiabatically saturated with water vapor until it reaches "wet bulb" temperature T_w and saturation vapor density $\rho'_{vw} = \rho'_v(T_w)$. With no external source of heat, the latent heat of vaporization must be obtained though sensible cooling of the air, such that

$$\lambda(\rho'_{vw} - \rho_{va}) = \rho c_p (T_a - T_w). \tag{A-35}$$

The ratio of the increase in water vapor density to the accompanying decrease in temperature,

$$\frac{\rho'_{vw} - \rho_{va}}{T_a - T_w} = \frac{\rho c_p}{\lambda}, \tag{A-36}$$

is called the "psychrometric constant"

$$\gamma \equiv \frac{\rho c_p}{\lambda} = \frac{C}{\lambda}. \tag{A-37}$$

This parameter will appear in the solution to the coupled mass and energy balances of wet surfaces.

A.5.2 Convection, Long and Short-Wave Radiations, and Latent Heat Loss

Classic Penman Formulation. Now consider a wet surface with convection, radiation,

and latent heat loss, but no conduction or heat generation. In steady state, the short and long wave radiative gains are dissipated by convection and evaporation of water:

$$Q = L + S = H + \lambda E, \tag{A-38}$$

or

$$Q - \lambda E = H = C r_h^{-1} (T_0 - T_a). \tag{A-39}$$

Combining Eqs. (A-11) and (A-39) to eliminate the temperature difference $(T_0 - T_a)$,

$$\lambda E = \lambda r_v^{-1} \left[s(T_0 - T_a) + \rho_{sd} \right] = \lambda r_v^{-1} \left[s C^{-1} r_h (Q - \lambda E) + \rho_{sd} \right]. \tag{A-40}$$

Solving for λE and rearranging yields the classic Penman expression for latent heat loss from a wet surface (Campbell 1977, p.120):

$$\lambda E = \frac{C^{-1} r_h \rho_{sd} + sQ}{(r_v / r_h)\gamma + s} = \frac{C^{-1} r_h \rho_{sd} + sQ}{\gamma^* + s}. \tag{A-41}$$

where

$$\gamma^* \equiv (r_v / r_h)\gamma. \tag{A-42}$$

Replacing Q by Q_{dry}. The Penman expression above retains an inconvenient dependence on the as-yet-unknown surface temperature because

$$Q = L + S = C r_r^{-1} (T_r - T_0) + S. \tag{A-43}$$

The energy balance in Eq. (A-38) may be manipulated to express Q in terms of Q_{dry} and λE, and this result may be substituted back into Eq. (A-41) to yield λE in terms of Q_{dry}. Writing Eq. (A-38) in the form

$$C r_r^{-1} (T_r - T_0) + S = C r_h^{-1} (T_0 - T_a) + \lambda E \tag{A-44}$$

and solving for $(T_r - T_0)$ yields

$$L = C r_r^{-1} (T_r - T_0) = \frac{C(T_r - T_a) + r_h (\lambda E - S)}{r_r + r_h} \tag{A-45}$$

and thus

$$\begin{aligned} Q = L + S &= \frac{C(T_r - T_a) + r_h (\lambda E - S) + (r_r + r_h) S}{r_r + r_h} \\ &= \frac{C(T_r - T_a) + r_r S}{r_r + r_h} + \frac{r_h}{r_r + r_h} \lambda E \end{aligned} \tag{A-46}$$

Note that

$$\frac{C(T_r - T_a) + r_r S}{r_r + r_h} = \left[\frac{r_r}{r_r + r_h}\right] \times \left[C r_r^{-1}(T_r - T_a) + S\right] = \eta\left[C r_r^{-1}(T_r - T_a) + S\right]. \quad \text{(A-47)}$$

Introducing η and Q_{dry} from Eqs. (A-15) and (A-20),

$$Q = Q_{\text{dry}} + (1-\eta)\lambda E. \quad \text{(A-48)}$$

Substituting Eq. (A-48) into (A-41) and solving the result for λE,

$$\lambda E = \frac{C r_h^{-1} \rho_{sd} + s Q_{\text{dry}}}{\gamma^* + \eta s}. \quad \text{(A-49)}$$

Note that this expression is independent of the surface temperature T_0.

Back-Calculating Convection and Long-Wave Radiation. Eq. (A-48) yields expressions for the convective heat loss

$$H = Q - \lambda E = Q_{\text{dry}} + (1-\eta)\lambda E - \lambda E = Q_{\text{dry}} - \eta \lambda E \quad \text{(A-50)}$$

and the LW heat gain

$$L = Q - S = Q_{\text{dry}} + (1-\eta)\lambda E - S. \quad \text{(A-51)}$$

These formulas are useful when the latent heat loss λE is known.

Aside: Estimating Surface Temperature Without Knowing Diffusion Resistance. A brief digression: Eq. (A-49) can also be used to find the surface temperature T_0 without knowing the precise value of the vapor diffusion resistance r_v. Multiplying its numerator and denominator by

$$(\gamma^*)^{-1} = \left(\gamma \frac{r_v}{r_h}\right)^{-1} = \left(\frac{C}{\lambda}\frac{r_v}{r_h}\right)^{-1} = \frac{\lambda r_h}{C r_v} \quad \text{(A-52)}$$

yields

$$\lambda E = \lambda r_v^{-1}\left\{\frac{\rho_{sd} + s C^{-1} r_h Q_{\text{dry}}}{1 + (\eta s/\gamma^*)}\right\} = \lambda r_v^{-1}\left\{\frac{\rho_{sd} + s\left[(1-\eta)(T_r - T_a) + C^{-1} r_h S\right]}{1 + (\eta s/\gamma^*)}\right\} \quad \text{(A-53)}$$

When $\eta s/\gamma^* \ll 1$, the latent heat loss simplifies to

$$\lim_{\frac{\eta s}{\gamma^*} \to 0} \lambda E = \lambda r_v^{-1}\left\{\rho_{sd} + s\left[(1-\eta)(T_r - T_a) + C^{-1} r_h S\right]\right\}. \quad \text{(A-54)}$$

Subtracting Eq. (A-11) from Eq. (A-54),

$$\lim_{\frac{\eta s}{\gamma^*} \to 0} (T_0 - T_a) = (1-\eta)(T_r - T_a) + C^{-1} r_h S. \quad \text{(A-55)}$$

Thus the exact value of the diffusive resistance r_v is not needed to predict T_0 so long as $\gamma^* = (r_v/r_h)\gamma \gg \eta s$, which is equivalent to $(r_v/r_h) \gg (\eta s/\gamma)$. Since $0 < \eta < 1$ and $(s/\gamma)_{T_a=20°C} \approx 2$, Eq. (A-55) may be used when $(r_v/r_h) \gg 2$. This is very handy for leaves, which typically exhibit $(r_v/r_h) \geq 20$.

Appendix B: Energy-Balance Approximations

This appendix examines the assumptions made in the dry and wet surface energy balances of Appendix A to determine if these assumptions hold for surfaces modeled in this study, i.e. those of the ground, near-ground objects, and tree leaves.

B.1 Neglect of Conduction in Ground Surface Energy Balances

B.1.1 Damping Depth

The dry, adiabatic energy balance of Eq. (A-16) may be applied to a ground surface when the conduction loss to the soil is small compared to the heat carried away by convection and LW radiation. The damping depth† of diurnal surface temperature variations is given by (Campbell 1977, p.16)

$$D = (2\kappa/\omega)^{1/2}, \tag{B-1}$$

where κ is the soil's thermal diffusivity, and $\omega = \frac{2\pi}{1\ \text{day}} = 7.3\times10^{-5}\ \text{s}^{-1}$ is the angular frequency of the diurnal temperature oscillation. The thermal conductivities and diffusivities of soil vary strongly with water content, but a typical moist soil might have conductivity $k \approx 1\ \text{W m}^{-1}\ \text{K}^{-1}$ and diffusivity $\kappa = 5\times10^{-7}\ \text{m}^2\ \text{s}^{-1}$ (Monteith 1973, p.127); this yields $D \approx 0.1\ \text{m}$. Diurnal oscillations will be 95% damped at a depth of $3D = 0.3\ \text{m}$, so the soil temperature T_c at this depth may be assumed equal to the diurnal-average surface temperature.

B.1.2 Soil Resistance

The soil resistance can be estimated from

$$C r_c^{-1} \approx \frac{k}{3D}, \tag{B-2}$$

or

$$r_c \approx \frac{(3D)C}{k} \approx 10^3\ \text{s m}^{-1}. \tag{B-3}$$

B.1.3 Convection vs. Long-Wave Radiation vs. Conduction

To obtain a typical ratio of convection to LW radiation to conduction, assume that at midday the soil and sky are each about 10 K cooler than the near-ground air, and that a black-

†. Also known as "characteristic penetration depth."

top ground surface is approximately 40 K warmer than the air. That is,

$$(T_a - T_c) \approx (T_a - T_s) \approx 10 \text{ K}, \tag{B-4}$$

and

$$(T_0 - T_a) \approx 40 \text{ K}. \tag{B-5}$$

The ground's LW radiative temperature $T_r = T_s$. Since

$$\frac{T_0 - T_r}{T_0 - T_a} = \frac{T_0 - T_s}{T_0 - T_a} = \frac{(T_0 - T_a) + (T_a - T_r)}{T_0 - T_a} = 1 + \frac{T_a - T_r}{T_0 - T_a} \approx 1 + \frac{10}{40} = 1.25, \tag{B-6}$$

the ground-sky temperature difference is close to the ground-air temperature difference. Thus

$$(T_0 - T_c) \approx (T_0 - T_r) \approx (T_0 - T_a), \tag{B-7}$$

and the ratio of convective to LW radiative to conductive heat loss is

$$H : L : K = C r_h^{-1}(T_0 - T_a) : C r_r^{-1}(T_0 - T_s) : C r_c^{-1}(T_0 - T_c) \approx r_h^{-1} : r_r^{-1} : r_c^{-1}. \tag{B-8}$$

Taking $r_h \approx 60$ s m^{-1} $\left(\bar{h} \approx 20 \text{ W m}^{-2} \text{ K}^{-1}\right)$ and $r_r \approx 200$ s m^{-1},

$$H : L : K \approx r_h^{-1} : r_r^{-1} : r_c^{-1} \approx \tfrac{1}{60} : \tfrac{1}{200} : \tfrac{1}{1000} = 50 : 15 : 3. \tag{B-9}$$

Thus, with these rough assumptions, ground conduction may be neglected in the typical summer, midday, dry-surface energy balance.

B.2 Neglect of Conduction in Near-Ground Object Energy Balances

A conductionless energy balance may also be applied to the surface of a near-ground object if its surface-to-core conduction is small compared to its surface-to-environment heat transfer.

B.2.1 Human

For a clothed, 15-cm-radius human in a 3 m s^{-1} wind, $r_r \approx 200$ s m^{-1}, $r_h \approx 50$ s m^{-1}, and $r_c \approx 200$ s m^{-1} (Campbell 1977, p.103). Assuming $T_c = 310$ K, $T_a \approx 300$ K, $T_g = T_a + 25 = 325$ K, $T_s \approx \frac{1}{2}(T_s + T_g) \approx 308$ K, and $T_0 \approx T_a + 15 = 315$ K, then

$$\begin{aligned} H : L : K &= C r_h^{-1}(T_0 - T_a) : C r_r^{-1}(T_0 - T_r) : C r_c^{-1}(T_0 - T_c) \\ &= \tfrac{15}{50} : \tfrac{17}{200} : \tfrac{5}{200} = 60 : 17 : 5 \end{aligned} \tag{B-10}$$

Thus conduction dissipates about 10% of the (dry) human's solar gain, and the conductionless balance holds.

B.2.2 Car

For a 1.5-m-radius, painted[†] metal car in a 3 m s^{-1} wind, $r_r \approx 200$ s m^{-1}, $r_h \approx 150$ s m^{-1}, and, to guess[‡], $r_c \approx 10$ s m^{-1}. Assuming $T_a \approx 300$ K, $T_g = T_a + 25 = 325$ K, $T_s \approx \frac{1}{2}(T_s + T_g) \approx 308$ K, $T_0 \approx T_a + 25 = 325$ K, and $T_c \approx T_a \approx 300$ K,

$$\begin{aligned} H:L:K &= Cr_h^{-1}(T_0 - T_a) : Cr_r^{-1}(T_0 - T_r) : Cr_c^{-1}(T_0 - T_c) \\ &= \tfrac{25}{50} : \tfrac{17}{200} : \tfrac{25}{10} = 100:17:500 \end{aligned} \quad \text{(B-11)}$$

Since conduction dissipates about 80% of the car's solar gain, the conductionless balance fails.

B.2.3 Building

For a 5-m-radius, R-3 building in a 3 m s^{-1} wind, $r_r \approx 200$ s m^{-1}, $r_h \approx 200$ s m^{-1}, and $r_c \approx 600$ s m^{-1}. Using the temperatures assumed for the car,

$$\begin{aligned} H:L:K &= Cr_h^{-1}(T_0 - T_a) : Cr_r^{-1}(T_0 - T_r) : Cr_c^{-1}(T_0 - T_c) \\ &= \tfrac{25}{50} : \tfrac{17}{200} : \tfrac{25}{600} = 75:51:25 \end{aligned} \quad \text{(B-12)}$$

Thus conduction dissipates about 15% of the building's solar gain, and the conductionless balance holds.

B.3 Neglect of Heat Storage in Leaves

B.3.1 Transient Balance With Finite Thermal Mass

When applied to a real surface with finite thickness and thermal mass—e.g. a plant leaf—the wet-surface energy balance in Eq. (A-38) holds only if the surface temperature is no longer changing. The transient energy balance

$$Q = L + S = H + \lambda E + A^{-1} mc\dot{T}_0, \quad \text{(B-13)}$$

includes a heat storage term $A^{-1} mc\dot{T}_0$, where m, c, and A are the mass, specific heat per unit mass, and area of the surface, and $\dot{T}_0 \equiv dT_0/dt$. Applying the usual linearizations,

$$S + Cr_r^{-1}(T_r - T_0) = Cr_h^{-1}(T_0 - T_a) + \lambda r_v^{-1}\left[\rho_{sd} + s(T_0 - T_a)\right] + A^{-1} mc\dot{T}_0. \quad \text{(B-14)}$$

A leaf will exchange LW radiation with some surfaces that are usually cooler than the ambient air, such as the sky, and some that are usually warmer, such as the ground. The

†. A bare-metal car would have low emissivity, and thus a high radiative resistance.

‡. There are typically some plastic components and trapped-air spaces between the metal exterior of a car and the inside of the passenger compartment. These should make the conduction resistance of the car shell about an order of magnitude greater than that of pure metal.

precise LW radiative temperature is not important in the estimation of the characteristic time required for the leaf to reach steady-state, so assume

$$T_r \approx T_a . \tag{B-15}$$

Eq. (B-14) is more compactly written in terms of the homogenous temperature

$$u \equiv T_0 - T_a . \tag{B-16}$$

Substituting Eqs. (B-15) and (B-16) into Eq. (B-14), then rearranging,

$$S - \lambda r_v^{-1} \rho_{sd} = \left(C r_h^{-1} + C r_r^{-1} + \lambda r_v^{-1} s\right) u + A^{-1} m c \dot{u} . \tag{B-17}$$

Dividing through by $A^{-1} mc$ and defining

$$a = \frac{A\left[S - \lambda r_v^{-1} \rho_{sd}\right]}{mc}, \quad b = \frac{A\left(C r_h^{-1} + C r_r^{-1} + \lambda r_v^{-1} s\right)}{mc} \tag{B-18}$$

yields the tidy differential equation

$$\dot{u} = a - bu . \tag{B-19}$$

B.3.2 Characteristic Time of Transient Solution

Solving Eq. (B-19) subject to the initial condition $u(t=0) = u_0$,

$$u(t) = \frac{a}{b} + \left(u_0 - \frac{a}{b}\right) \exp(-bt). \tag{B-20}$$

This solution is the sum of a steady-state term,

$$u_\infty = \lim_{t \to \infty} u(t) = \frac{a}{b}, \tag{B-21}$$

and an exponential term, $\left(u_0 - a/b\right)\exp(-bt)$, that decays with characteristic time

$$t_0 = \frac{1}{b} = \frac{mc}{A\left(C r_h^{-1} + C r_r^{-1} + \lambda r_v^{-1} s\right)} . \tag{B-22}$$

Eq. (B-20) can be rewritten in terms of the steady-state temperature and the characteristic time:

$$u(t) - u_\infty = \left(u_0 - u_\infty\right) \exp\left(-t/t_0\right). \tag{B-23}$$

The extent to which the temperature has changed from its initial value to its steady-state value is gauged by the unit-scale, non-dimensional temperature

$$\theta(t) \equiv \frac{u(t) - u_\infty}{u_0 - u_\infty} = \exp\left(-t/t_0\right), \tag{B-24}$$

which declines from one to zero as t goes from zero to infinity. The non-dimensional tem-

perature falls to within 5% of its steady-state value after $t = 3\,t_0$.

To estimate a typical characteristic time for a leaf, consider a 1 g, 15 cm^2 specimen in a 2 m s^{-1}, 20 °C wind. Assuming $r_h \approx 15\ s\,m^{-1}$, $r_v = 500\ s\ m^{-1}$, $r_r \approx 100\ s\,m^{-1}$, $s \approx 10^{-3}$ kg m^{-3} K^{-1}, and $c \approx 10^3$ J kg^{-1} K^{-1}, Eq. (B-22) yields $t_0 \approx 7$ s. This agrees with other reported leaf time constants of 10 s (Hollinger et al. 1994) and 5 to 15 s (Gates 1980).

Appendix C: Convection and Diffusion

This appendix presents expressions for resistances to heat convection and mass diffusion from ground surfaces, near-ground objects, and leaves, with attention paid the to effects of upstream turbulence and free convection on these resistances. Flat-plate boundary layer theory is found to apply poorly to flow over large ground surfaces, and alternate ways to determine the resistance to convection over a ground surface are discussed.

C.1 Forced Laminar Flow Over a Flat Plate

C.1.1 Nusselt and Sherwood Numbers

A leaf may be modeled as a small, flat plate. Consider a laminar, uniform-velocity free stream striking the leading edge of a flat plate of length d at zero angle-of-attack. The forced convective heat transfer across a laminar boundary layer growing from the plate's leading edge is described by the length-averaged Nusselt number,

$$\overline{\mathrm{Nu}}_d = \frac{\bar{h}\, d}{k} = 0.664\,\mathrm{Re}_d^{1/2}\,\mathrm{Pr}^{1/3} \qquad \left(\mathrm{Pr} > 0.5,\ \mathrm{Re_d} < 5\times 10^5\right). \tag{C-1}$$

If the plate's surface is wet, vapor diffusion across the boundary layer is given by the length-averaged Sherwood number,

$$\overline{\mathrm{Sh}}_d = \frac{\bar{h}_m\, d}{D_{AB}} = 0.664\,\mathrm{Re}_d^{1/2}\,\mathrm{Sc}^{1/3} \qquad \left(\mathrm{Sc} \sim 1,\ \mathrm{Re_d} < 5\times 10^5\right). \tag{C-2}$$

Here

$$\mathrm{Re}_d = U\, d/\nu \tag{C-3}$$

is the Reynolds number, $\mathrm{Pr} \approx 0.71$ is the Prandtl number, $\mathrm{Sc} \approx 0.60$ is the Schmidt number, $\bar{h}$ and $\bar{h}_m$ are the length-averaged convection and diffusion coefficients, k and ν are the thermal conductivity and kinematic viscosity of air, U is the free-stream air speed, and D_{AB} is the diffusivity of water vapor into air. These relations are accurate to $\pm 2\%$ when applied to flat-plate flows under laboratory conditions (White 1988, p.363).

C.1.2 Convection and Diffusion Resistances

The resistances to convection and diffusion across the laminar boundary layer are defined by

$$Cr_{ha,\mathrm{lam}}^{-1} = \bar{h} = \frac{k}{d}\,\overline{\mathrm{Nu}} \tag{C-4}$$

and

$$r_{va,\text{lam}}^{-1} = \bar{h}_m = \frac{D_{AB}}{d}\,\overline{\text{Sh}}\,. \tag{C-5}$$

Evaluating air properties at STP and solving for the resistances,

$$r_{ha,\text{lam}} = 309\,(d/U)^{1/2} \tag{C-6}$$

and

$$r_{va,\text{lam}} = 286\,(d/U)^{1/2}\,. \tag{C-7}$$

If heat or vapor is transferred from both sides of the plate—that is, across *two* boundary layers—the corresponding resistance will be halved.

C.2 Forced Crossflow Past a Circular Cylinder

C.2.1 Nusselt Number

The surface-averaged Nusselt number for laminar or turbulent crossflow past a long circular cylinder of diameter D is

$$\overline{\text{Nu}}_D = 0.3 + \frac{0.62\,\text{Re}_D^{1/2}\,\text{Pr}^{1/2}}{\left[1+(0.4/\text{Pr})^{2/3}\right]^{1/4}}\left[1+\left(\frac{\text{Re}_D}{282{,}000}\right)^{5/8}\right]^{4/5} \qquad (\text{Re}_D\,\text{Pr} \geq 0.2) \tag{C-8}$$

This has an uncertainty of ±30% under laboratory conditions, and may not be accurate for short cylinders (Churchill and Bernstein 1977).

C.2.2 Convective Resistance

The equivalent convective resistance may be calculated from

$$C\,r_{ha,\text{cyl}}^{-1} = \bar{h} = \frac{k}{D}\,\overline{\text{Nu}} \tag{C-9}$$

or

$$r_{ha,\text{cyl}} = \frac{C\,D}{k}\left(\overline{\text{Nu}}\right)^{-1}. \tag{C-10}$$

C.3 Forced Convection Versus Free Convection

C.3.1 Grashof Number

Forced convection will be much stronger than free convection if the Grashof number

$$\text{Gr}_d = a\,g\,d^3\,\Delta T/\nu^2 \tag{C-11}$$

is much less than the square of the Reynold's number, i.e.

$$\mathrm{Gr}_d/\mathrm{Re}_d^2 < 0.1. \tag{C-12}$$

Here $a = 1/273$ is the coefficient of thermal expansion for an ideal gas, $g = 9.81$ m s^{-2} is the acceleration due to gravity, and ΔT is the difference between the surface temperature and the fluid temperature. Evaluating the kinematic viscosity of air at STP,

$$\mathrm{Re}_d^2 = 4.39 \times 10^9 \, U^2 d^2 \tag{C-13}$$

and

$$\mathrm{Gr}_d = 1.58 \times 10^8 \, d^3 \, \Delta T. \tag{C-14}$$

Thus

$$\mathrm{Gr}_d/\mathrm{Re}_d^2 = 0.036 \, d U^{-2} \, \Delta T. \tag{C-15}$$

C.3.2 Leaves

If a 5-cm diameter leaf is 10 K warmer than the air, the ratio

$$\mathrm{Gr}_d/\mathrm{Re}_d^2 = 0.018 \, U^{-2} \tag{C-16}$$

will be less than 0.1 for $U > 0.4$ m s^{-1}. Thus leaf convection will typically be forced rather than free.

C.3.3 Humans

When represented as a cylinder, the diameter of a typical 70 kg person is approximately 30 cm. If the person's skin temperature is 10 K warmer than the air,

$$\mathrm{Gr}_d/\mathrm{Re}_d^2 = 0.108 \, U^{-2} \tag{C-17}$$

will be less than 0.1 for $U > 1.0$ m s^{-1}. Thus convection around people will also usually be forced.

C.3.4 Vehicles and Buildings

A "cylindrical" car may have a diameter of roughly 2 m. Proceeding as for a person, $U > 2.7$ m s^{-1} is required for forced convection to dominate over free convection. A small building with a 10 m diameter would require $U > 6.0$ m s^{-1} to ensure the dominance of forced convection. Thus convection around vehicles and buildings is likely to be a combination of free and forced convection.

C.4 Effect of Upstream Turbulence on Transfer Resistances

The upstream turbulence typical of outdoor flows has been found to decrease the convec-

tive and diffusive resistances of flat-plate boundary-layer flows by a factor n_t, $1 \le n_t \le 2$, such that

$$\frac{r_{\text{turbulent free-stream}}}{r_{\text{laminar free-stream}}} = n_t^{-1} \approx \left(\frac{3}{2}\right)^{-1} = \frac{2}{3}. \qquad \text{(C-18)}$$

(Pearman et al. 1972). Another study showed a similar effect on cylinder crossflow resistance (White 1988, p.347).

C.5 Forced Turbulent Flow Over Large Ground Surfaces

Forced convective heat transfer over a large, flat, smooth, outdoor ground surface such as a parking lot is poorly described by Nusselt number relations for flat-plate flow. Consider a large blacktop surface exposed to

$$S = 1000 \text{ W m}^{-2},\ T_a = 293 \text{ K},\ T_r = 283 \text{ K}, \text{ and } r_r = 200 \text{ s m}^{-1}. \qquad \text{(C-19)}$$

If the surface temperature elevation is $T_0 - T_a = 30$ K, Eq. (A-21) predicts a ground convection coefficient

$$\bar{h} = C r_h^{-1} = 25 \text{ W m}^{-2} \text{ K}^{-1}, \qquad \text{(C-20)}$$

or $r_h = 48 \text{ s m}^{-1}$. If $T_0 - T_a = 50$ K, Eq. (A-21) predicts $r_h = 95 \text{ s m}^{-1}$, or

$$\bar{h} = C r_h^{-1} = 13 \text{ W m}^{-2} \text{ K}^{-1}. \qquad \text{(C-21)}$$

Thus $\bar{h}$ can be expected to be on the order of $20 \text{ W m}^{-2} \text{ K}^{-1}$.

Since a gentle 1 m s^{-1} wind can reach the transition Reynolds number $\text{Re}_d = 5 \times 10^5$ after travelling over just 7.5 m of a flat surface, the flow over the ground can be expected to be quite turbulent. The Nusselt number relation for turbulent flow over a flat plate is (White 1988, p.363)

$$\overline{\text{Nu}}_d = \frac{\bar{h} d}{k} = 0.037 \text{Re}_d^{4/5} \text{Pr}^{1/3} \qquad \left(\text{Pr} > 0.6,\ \text{Re}_d > 5 \times 10^5\right). \qquad \text{(C-22)}$$

Evaluating air properties at 20°C,

$$r_h = 7.35\, d^{1/5} U^{-4/5} \qquad \text{(C-23)}$$

and

$$\bar{h} = C r_h^{-1} = 165\, U^{4/5} d^{-1/5}. \qquad \text{(C-24)}$$

For $U = 1 \text{ m s}^{-1}$ and $d = 25$ m, Eqs. (C-24) and (C-23) predict $\bar{h} = 87 \text{ W m}^{-2} \text{ K}^{-1}$ and $r_h = 14 \text{ s m}^{-1}$. Thus, even in a mild wind, the Nusselt number relation yields an unreasonably high heat transfer coefficients. Given the convective resistance predicted by Eq. (C-23), the aforementioned blacktop surface would achieve a surface temperature elevation of only $T_0 - T_a = 10$ K.

Eq. (C-24) may be rearranged to extract the characteristic length d required to achieve a particular $\bar{h}$:

$$d = \left(\frac{165}{\bar{h}}\right)^5 U^4 . \qquad \text{(C-25)}$$

This formula predicts that a mild wind must travel 38 km over a flat plate to yield $\bar{h} = 20$ W m^{-2} K^{-1}!

C.5.1 Limitations of Flat-Plate Theory

There are at least two reasons why the Eq. (C-22) might not apply to ground surfaces. First, Nusselt-number relations for flat plates assume that the boundary layer begins at the edge of the plate. However, there is no clear leading edge at which a uniform-velocity free stream intersects the ground surface and from which a momentum boundary layer grows. Thus the streamwise length of a boundary layer may not correspond to the size of the surface. Second, frequently and significant fluctuations in the magnitude and direction of the wind can disrupt the boundary layer flow.

C.5.2 Other Empirical Correlations

Solar energy engineering handbooks frequently present dimensional convectional coefficients of the form

$$\bar{h} = 5.7 + 3.8U , \qquad \text{(C-26)}$$

but these are typically based on measurements of heat loss from small $\left(0.5 \text{ m}^2\right)$ solar collector plates, and do not necessarily apply to convection from large ground surfaces (Duffie and Beckman 1980, p.137). Note that Eq. (C-26) gives the right order-of-magnitude solution: $\left(\bar{h}\right)_{U=3 \text{ m s}^{-1}} \approx 17$ W m^{-2} K^{-1}.

C.5.3 Practical Approach

In the absence of other valid correlations, the ground-surface convection resistance may be calculated by supplying ambient conditions and an estimated dark-surface temperature to Eq. (A-21). One drawback is that this expression does not explicitly relate the convection resistance to wind speed. If wind-speed dependence is needed, it may be necessary to resort to the likes of Eq. (C-26), which at least appears to yield values in the correct ballpark.

Appendix D: Radiation

This appendix presents formulas for (a) the resistance to long-wave radiative heat transfer; (b) the view factors between various surfaces; and (c) and the direct and diffuse short-wave radiations incident on various geometries.

D.1 Long-Wave Radiation

D.1.1 Emissivities

Most non-metallic surfaces have emissivities of 0.9 or higher at 20°C (White 1988, p.694) and thus may be approximated as black to LW radiation. Some typical long-wave emissivities are listed in Table D-1.

D.1.2 Exchange From One-Sided Surface to Environment

Linearization. Consider a black, one-sided surface labelled 0 that sees N black exchange surfaces $1...N$ but does not see itself. Its long-wave radiative *loss* is

$$-L = \sum_{n=1}^{N} \sigma_{sb} F_{0\to n} \left(T_0^4 - T_n^4\right) = \sigma_{sb} \sum_{n=1}^{N} F_{0\to n} \left(T_0^4 - T_n^4\right), \tag{D-1}$$

where $\sigma_{sb} = 5.67 \times 10^{-8}$ W m^{-2} K^{-4} is the Stefan-Boltzmann constant and $F_{0\to n}$ is the view factor from surface 0 to surface n.

The difference of fourth powers in Eq. (D-1) may be linearized. Applying the binomial expansion

$$(a+b)^4 = a^4\left(1 + 4c + 6c^2 + 4c^3 + c^4\right), \qquad c \equiv b/a\,. \tag{D-2}$$

The higher-order terms may be dropped from Eq. (D-2) when $c \ll 1$, leaving

$$(a+b)^4 \approx a^4(1+4c)\,. \tag{D-3}$$

This introduces a fractional error of approximately

$$6c^2/4c = 3c/2\,. \tag{D-4}$$

Defining

$$\Delta T \equiv T_0 - T_n\,, \tag{D-5}$$

the fourth-order temperature difference in Eq. (D-1) may be written

$$T_0^4 - T_n^4 = \left(T_n + \Delta T\right)^4 - T_n^4 \approx T_n^4\left[1 + 4\left(\frac{\Delta T}{T_n}\right)\right] - T_n^4 = 4T_n^3\,\Delta T\,. \tag{D-6}$$

Substituting Eq. (D-6) into Eq. (D-1),

$$-L \approx 4\sigma_{sb}\,\bar{T}^3 \sum_{n=1}^{N} F_{0\to n}\left(T_0 - T_n\right) = 4\sigma_{sb}\,\bar{T}^3\left[T_0\left(\sum_{n=1}^{N} F_{0\to n}\right) - \sum_{n=1}^{N} F_{0\to n}\,T_n\right], \qquad \text{(D-7)}$$

where $\bar{T} \approx T_0 \approx T_n$.

Radiative Temperature and Resistance. Since the surface does not see itself,

$$\sum_{n=1}^{N} F_{0\to n} = 1. \qquad \text{(D-8)}$$

Defining the radiative temperature T_r by

$$T_r = \sum_{n=1}^{N} F_{0\to n}\,T_n \qquad \text{(D-9)}$$

and the radiative resistance r_r by

$$C r_r^{-1} = 4\sigma_{sb}\,\bar{T}^3, \qquad \text{(D-10)}$$

Eqs. (D-8) through (D-10) may be substituted into Eq. (D-7) to obtain

$$-L = C r_r^{-1}\left(T_0 - T_r\right). \qquad \text{(D-11)}$$

The LW radiative *gain* may now be written in the form of Eq. (A-1),

$$L = C r_r^{-1}\left(T_r - T_0\right). \qquad \text{(D-12)}$$

D.1.3 Exchange From Two-Sided Surface to Environment

If a surface is flat (so that is does not see itself) and both of its sides exchange radiation with the environment, its LW gain will be

$$L = C r_r^{-1}\left(T_{r1} - T_0\right) + C r_r^{-1}\left(T_{r2} - T_0\right). \qquad \text{(D-13)}$$

where T_{r1} and T_{r2} are the radiative temperatures on each side of the surface as defined by Eq. (D-9). If the radiative resistance and temperature are redefined by

$$C r_r^{-1} = 8\sigma_{sb}\,\bar{T}^3, \qquad \text{(D-14)}$$

and

$$T_r = \tfrac{1}{2}\left(T_{r1} + T_{r2}\right), \qquad \text{(D-15)}$$

the LW radiative gain of this two-sided surface may be written in the one-sided form of Eq. (D-12).

D.1.4 Linearization Errors

Given surface temperatures on the order of 300 K, Eq. (D-6) is accurate to within 10% for

temperature differences up to 20 K, and to within 30% for temperature differences up to 50 K. By comparison, common correlations used to estimate *convective* exchange carry uncertainties of ±30% (White 1988, p.362). Also, the exact value of $\overline{T}$ employed in Eq. (D-10) is not critical because the fractional change of $\overline{T}^3$ with temperature,

$$\frac{d\overline{T}^3/d\overline{T}}{\overline{T}^3} = \frac{3\overline{T}^2}{\overline{T}^3} = \frac{3}{\overline{T}}, \tag{D-16}$$

is only 1% per Kelvin at 300 K.

D.1.5 View Factors

Near-ground radiative exchanges typically involve three surfaces: the ground plane, the sky plane, and the near-ground object, such as a tree, person, vehicle, or building. Here trees will be modeled as cones, while people, vehicles, and buildings will be approximated by cylinders. Let subscripts s, g, and 0 denote the ground, sky, and object. The object is infinitely smaller than the ground and sky planes, so

$$F_{g\to s} = F_{s\to g} \approx 1. \tag{D-17}$$

Also, since the curved surfaces of cones and cylinders are convex and thus do not see themselves,

$$F_{0\to g} + F_{0\to s} = 1. \tag{D-18}$$

By symmetry, the view factors from the curved surface of a cylinder to the ground and sky are equal, so Eq. (D-18) yields

$$F_{\text{cyl}\to g} = F_{\text{cyl}\to s} = \tfrac{1}{2}. \tag{D-19}$$

The view factor from the curved surface of a vertical, upward-pointing, right-circular cone of radius R_0 and height H_0 to the sky is

$$F_{\text{cone}\to s} = \tfrac{1}{2}(1+\cos\alpha), \tag{D-20}$$

where α is the cone's angle of elevation given by

$$\tan\alpha = H_0/R_0. \tag{D-21}$$

This view factor was not found in the literature, and has been derived in Section E.2.1.

D.1.6 Sky Emissivity and Sky Temperature

The sky emissivity ε_s relates the LW radiative sky temperature T_s to the near-ground air temperature T_a by

$$\sigma_{\text{sb}} T_s^4 = \varepsilon_s \sigma_{\text{sb}} T_a^4 \tag{D-22}$$

or

$$T_s = \varepsilon_s^{1/4} T_a . \tag{D-23}$$

One of many empirical correlations for the sky emissivity† is (Campbell 1977, p.57)

$$\varepsilon_s = 1.56 \rho_{va}^{1/7} . \tag{D-24}$$

D.2 SHORT-WAVE RADIATION

D.2.1 Areal Direct Radiation

Incident Radiation. The areal (area-integrated) direct solar radiation $\hat{S}_i$ received by some sunlit surface A is

$$\hat{S}_i = \iint_A \mathbf{I} \cdot \mathbf{n} \, dA , \tag{D-25}$$

where $\mathbf{n}$ is the inward-facing surface normal and $\mathbf{I}$ is the insolation vector that points from the sun to the Earth.

Solar Flux Density. The intensity of insolation normal to the sun's rays $I_N = |\mathbf{I}|$ may be computed from the measured horizontal-surface insolation I_H via

$$I_N \sin\beta = (1-\delta) I_H , \tag{D-26}$$

where $\delta \sim 0.2$ is the fraction of I_H that is diffuse in origin (White 1988, p.508). The solar altitude β is given by

$$\cos\beta = \sin l \sin d + \cos l \cos d \cos h , \tag{D-27}$$

where l is the latitude angle, d is the solar declination angle, and h is the solar hour angle (ASHRAE 1985, p.30.3).

Absorbed Radiation. The areal SW radiation actually absorbed by the surface is

$$\hat{S} = (1-\alpha_0) \hat{S}_i , \tag{D-28}$$

where α_0 is the surface's albedo. Some typical albedos are presented in Table D-1.

D.2.2 Direct Flux Incident on a Cone

The areal direct solar flux incident upon a vertical, upward-pointing, right-circular cone of

†. Campbell's expression has been converted from centimeter-gram-second units to SI.

radius R_0 and height H_0 is

$$\hat{S}_i = \begin{cases} (1-\delta) I_H \pi R_0^2 & \beta > \alpha \\ (1-\delta) I_H R_0^2 \left[(\pi - \phi_0) + \tan\phi_0 \right] & \beta < \alpha \end{cases}, \tag{D-29}$$

where

$$\cos\phi_0 = \tan\beta / \tan\alpha \tag{D-30}$$

and

$$\alpha = \arctan\left(H_0 / R_0\right). \tag{D-31}$$

The sunlit area is

$$A_{\text{sun}} = \begin{cases} \pi R_0^2 \left(1 + \tan^2\alpha\right)^{1/2} & \beta > \alpha \\ (\pi - \phi_0) R_0^2 \left(1 + \tan^2\alpha\right)^{1/2} & \beta < \alpha \end{cases}. \tag{D-32}$$

The derivations of $\hat{S}_i$ and A_{sun} are presented in Section E.1.1.

D.2.3 Direct Flux Incident on a Cylinder

The areal direct solar flux incident on a vertical, right-circular cylinder of radius R_0 and height H_0 is

$$\hat{S}_i = (1-\delta) I_H \left[\pi R_0^2 + 2 H_0 R_0 \cot\beta \right]. \tag{D-33}$$

The first term of the sum is the area of the cylinder top, and the second is the area of the shadow cast by the cylinder's side wall. This derivation may be found in Section E.1.2.

D.2.4 Areal Diffuse Flux

The areal diffuse solar flux from the sky plane s to an surface 0 is simply

$$\hat{S}_i = \delta I_H A_s F_{s\to 0} = \delta I_H A_0 F_{0\to s}, \tag{D-34}$$

where $F_{s\to 0}$ and $F_{0\to s}$ are the view factors from sky to surface and from surface to sky, related by the reciprocity rule

$$A_1 F_{1\to 2} = A_2 F_{2\to 1}. \tag{D-35}$$

As before, the absorbed radiation

$$\hat{S} = (1-\alpha_0)\hat{S}_i. \tag{D-36}$$

Surface	Albedo	Emissivity
Leaves	0.28-0.34	0.94-0.99
Forests, deciduous	0.15-0.20	0.97-0.98
Forests, coniferous	0.05-0.15	0.97-0.99
Grasses	0.16-0.26	0.90-0.95
Soils	0.05-0.40	0.90-0.98
Asphalt	0.05-0.20	0.95
Concrete	0.10-0.35	0.71-0.90
Brick	0.20-0.40	0.90-0.92
Paint, white	0.50-0.90	0.85-0.95
Paint, red, brown, green	0.20-0.35	0.85-0.95
Paint, black	0.02-0.15	0.90-0.98
Human skin, white	0.35	0.98
Human skin, black	0.18	0.98

Table D-1. Typical albedos and long-wave emissivities of common surfaces (Oke 1978 and Monteith 1973).

Appendix E: Geometric Aspects of Radiation

This appendix presents lengthy derivations of expressions for (a) the direct solar flux incident on various surfaces, and (b) the view factors between various surfaces.

E.1 Direct Short-Wave Radiation Flux Incident on Various Shapes

E.1.1 Right Circular Cone

Surface Equation. The equation of an upward-pointing right circular cone of height H_0 and radius R_0 is

$$z = H_0(1 - r/R_0), \tag{E-1}$$

or, expressed in the form $G(r,z) = \text{constant}$,

$$G(r,z) = H_0 = z + \frac{H_0}{R_0} r = z + r \tan\alpha, \tag{E-2}$$

where $\alpha = \arctan(H_0/R_0)$ is the cone's angle of elevation. The inward surface normal vector

$$\mathbf{n} = -\frac{\nabla G}{|\nabla G|} = \frac{\mathbf{e}_r \tan\alpha + \mathbf{e}_z}{(1+\tan^2\alpha)^{1/2}}. \tag{E-3}$$

Insolation Vector. Let β be the solar altitude angle. Since the cone is axially symmetric, the insolation vector $\mathbf{I}$ may arbitrarily be oriented parallel to the x-z plane:

$$\mathbf{I} = I_N\left(-\mathbf{e}_x \cos\beta - \mathbf{e}_z \sin\beta\right) \tag{E-4}$$

The coordinate transform

$$\mathbf{e}_x = \mathbf{e}_r \cos\theta - \mathbf{e}_\theta \sin\theta \tag{E-5}$$

yields

$$\mathbf{I} = I_N\left(\mathbf{e}_\theta \sin\theta\cos\beta - \mathbf{e}_r \cos\theta\cos\beta - \mathbf{e}_z \sin\beta\right). \tag{E-6}$$

Flux. The flux is the dot product of the insolation and surface-normal vectors,

$$\mathbf{I}\cdot\mathbf{n} = I_N \frac{\tan\alpha\cos\beta\cos\theta + \sin\beta}{(1+\tan^2\alpha)^{1/2}}, \tag{E-7}$$

and the areal direct radiation incident on the cone is

$$\hat{S}_i = \iint_A \mathbf{I} \cdot \mathbf{n}\, d\sigma, \tag{E-8}$$

where A is the base area below the illuminated fraction of the cone, and $d\sigma$ is the curved surface area differential

$$d\sigma = \frac{|\nabla G|}{|\nabla G \cdot \mathbf{e}_z|}\, dA = (1 + \tan^2 \alpha)^{1/2}\, r\, dr\, d\theta. \tag{E-9}$$

The illuminated curved surface area is

$$\sigma = \iint_A d\sigma. \tag{E-10}$$

Range of Polar Angles Illuminated. The flux integrand

$$\mathbf{I} \cdot \mathbf{n}\, d\sigma = I_N\, (\tan\alpha \cos\beta \cos\theta + \sin\beta)\, r\, dr\, d\theta \tag{E-11}$$

vanishes at some angle $\theta = \theta_0$ where $\tan\alpha \cos\beta \cos\theta_0 + \sin\beta = 0$, or

$$\cos\theta_0 = -\tan\beta/\tan\alpha. \tag{E-12}$$

$\cos\theta_0$ must be greater or equal to -1, and since α and β are each between 0 and $\pi/2$, $-\tan\beta/\tan\alpha$ will be less than or equal to 0. Thus $-1 \le \cos\theta_0 \le 0$, $\pi/2 \le \theta_0 \le \pi$, and the maximum solar altitude β for which there exists some θ_0 at which the flux vanishes is given by

$$\tan\beta/\tan\alpha = -\cos\theta_0 = 1 \tag{E-13}$$

or

$$\beta = \alpha \tag{E-14}$$

Thus, if $\beta > \alpha$, the flux never vanishes, but if $\beta < \alpha$, there exists some angle θ_0 satisfying Eq. (E-12). Since $\cos(-\theta_0) = \cos(\theta_0)$, the flux will also vanish at $-\theta_0$, and thus the cone is illuminated only for polar angles $-\theta_0 < \theta < \theta_0$.

Effect of Solar Altitude on Areal Flux and Illuminated Area. Integrating $\hat{S}_i$ and σ yields

$$\hat{S}_{i,\beta>\alpha} = I_N\, \pi\, R_0^2 \sin\beta \tag{E-15}$$

$$\sigma_{\beta>\alpha} = \pi R_0^2\, (1 + \tan^2 \alpha)^{1/2} \tag{E-16}$$

for $\beta > \alpha$, and

$$\hat{S}_{i,\beta<\alpha} = I_N\, R_0^2\, [\, \theta_0 \sin\beta + \sin\theta_0\, \tan\alpha \cos\beta\,] \tag{E-17}$$

$$\sigma_{\beta<\alpha} = \theta_0 R_0^2 (1+\tan^2\alpha)^{1/2} \tag{E-18}$$

for $\beta < \alpha$.

Horizontal Surface Insolation. This quantity can be more compactly expressed in terms of I_H, the flux incident on a horizontal surface. If some fraction $(1-\delta)$ of I_H is direct, the cosine law gives

$$(1-\delta)I_H = I_N \sin\beta . \tag{E-19}$$

Substituting Eq. (E-19) into Eqs. (E-15) and (E-17),

$$\hat{S}_i = \begin{cases} (1-\delta)\, I_H \pi R_0^2 & \beta > \alpha \\ (1-\delta)\, I_H R_0^2 \left[\theta_0 + \sin\theta_0 \tan\alpha \cot\beta\right] & \beta < \alpha \end{cases} \tag{E-20}$$

Trigonometric Simplifications. Substituting

$$\sin\theta_0 \tan\alpha \cot\beta = \sin\theta_0 (\tan\beta/\tan\alpha)^{-1} = -\sin\theta_0/\cos\theta_0 = -\tan\theta_0 \tag{E-21}$$

into Eq. (E-20),

$$\hat{S}_i = \begin{cases} (1-\delta)\, I_H \pi R_0^2 & \beta > \alpha \\ (1-\delta)\, I_H R_0^2 \left[\theta_0 - \tan\theta_0\right] & \beta < \alpha \end{cases} . \tag{E-22}$$

Since θ_0 has the awkward range $\pi/2 \le \theta_0 \le \pi$, define

$$\phi_0 = \pi - \theta_0 \tag{E-23}$$

which has the range $0 \le \phi_0 \le \pi/2$. Then

$$\cos\phi_0 = \cos(\pi - \theta_0) = -\cos\theta_0 = \tan\beta/\tan\alpha \tag{E-24}$$

and

$$\sigma_{\beta>\alpha} = (\pi - \phi_0) R_0^2 (1+\tan^2\alpha)^{1/2} . \tag{E-25}$$

Substituting

$$\tan\theta_0 = \tan(\pi - \phi_0) = -\tan\phi_0 \tag{E-26}$$

and

$$\theta_0 = \pi - \phi_0 \tag{E-27}$$

into Eqs. (E-22), the total direction insolation on the cone is

$$\hat{S}_i = \begin{cases} (1-\delta) I_H \pi R_0^2 & \beta > \alpha \\ (1-\delta) I_H R_0^2 \left[(\pi - \phi_0) + \tan\phi_0\right] & \beta < \alpha \end{cases} . \tag{E-28}$$

The sunlit area is

$$\sigma = \begin{cases} (\pi - \phi_0) R_0^2 \left(1 + \tan^2 \alpha\right)^{1/2} & \beta > \alpha \\ \pi R_0^2 \left(1 + \tan^2 \alpha\right)^{1/2} & \beta < \alpha \end{cases} . \tag{E-29}$$

E.1.2 Right Circular Cylinder

Consider a vertical, right-circular cylinder of height H_0 and radius R_0. All of its top wall, half of its side wall, and none of its bottom wall will be directly sunlit. The area-integrated insolation on the top is simply

$$\hat{S}_{i,\text{top}} = \pi R_0^2 I_N \sin\beta . \tag{E-30}$$

On its side wall, the inward-facing surface normal is

$$\mathbf{n} = -\mathbf{e}_r , \tag{E-31}$$

which combined with Eq. (E-6) yields the flux integrand

$$\mathbf{I} \cdot \mathbf{n} = I_N \cos\beta \cos\theta . \tag{E-32}$$

Integrating Eq. (E-32) over the sunlit half of the side wall,

$$\hat{S}_{i,\text{wall}} = \int_{z=0}^{H_0} \int_{\theta=-\pi/2}^{\pi/2} I_N \cos\beta \cos\theta \, R_0 \, d\theta \, dz = 2 H_0 R_0 I_N \cos\beta . \tag{E-33}$$

Summing the contributions to the top and side,

$$\hat{S}_i = \hat{S}_{i,\text{top}} + \hat{S}_{i,\text{wall}} = I_N \sin\beta \left[\pi R_0^2 + 2 H_0 R_0 \cot\beta\right] . \tag{E-34}$$

Applying the cosine law substitution from Eq. (E-19),

$$\hat{S}_i = (1 - \delta) I_H \left[\pi R_0^2 + 2 H_0 R_0 \cot\beta\right] . \tag{E-35}$$

E.2 GEOMETRIC VIEW FACTORS

E.2.1 View Factor From a Cone to The Sky

Mapping of Disk to Plane. Consider a right circular cone of radius R_0 and height H_0 that rests on ground plane g. Place in plane g a disk d of radius R_1 concentric with the base of the cone. As the disk radius $R_1 \to \infty$, the disk becomes the ground plane. The view factor† from the cone's curved surface c to the ground g is

$$F_{c \to g} = \lim_{R_1 \to \infty} F_{c \to d} , \tag{E-36}$$

†. The view factor from surface A to surface B is the fraction of radiant energy leaving surface A that reaches surface B.

and the view factor from the cone's curved surface to the sky plane, above the cone and parallel to g, is

$$F_{c\to s} = 1 - F_{c\to g}. \tag{E-37}$$

View Factor From Disk To Cone. An earlier paper† (Kobyshev et al. 1976) has calculated

$$F_{d\to c} = \frac{2}{\pi(r^2-1)}\left[\begin{array}{l}\dfrac{\pi}{2}\left(1-k^{-1}\right)\dfrac{r^2-1}{2} - r^2 \arctan\sqrt{\dfrac{r-1}{r+1}} \\ +\dfrac{k_2^2}{2k}\arctan\dfrac{\sqrt{r^2-1}}{k}\end{array}\right] \tag{E-38}$$

where

$$r = R_1/R_0 \tag{E-39}$$

$$h = H_0/R_0 \tag{E-40}$$

$$k = \sqrt{1+h^2} \tag{E-41}$$

and

$$k_2 = \sqrt{r^2+h^2}\,. \tag{E-42}$$

Behavior as Disk Radius Grows Infinite. Note that as the disk radius $R_1 \to \infty$, $r \to \infty$, but h and k remain finite and positive. The view factor reciprocity rule

$$A_d\, F_{d\to c} = A_c\, F_{c\to d} \tag{E-43}$$

yields the view factor from the cone to the disk,

$$F_{c\to d} = \frac{A_d}{A_c} F_{d\to c} = \frac{\pi R_1^2}{\pi R_0^2\, k} F_{d\to c} = k^{-1}\, r^2\, F_{d\to c}. \tag{E-44}$$

Thus

$$F_{c\to g} = \lim_{r\to\infty} k^{-1}\, r^2\, F_{d\to c}\,, \tag{E-45}$$

and the view factor from the cone to the sky is

$$F_{c\to s} = 1 - F_{c\to g} = 1 - \lim_{r\to\infty} r^2\, F_{d\to c}. \tag{E-46}$$

---

†. In Russian!

Substituting Eq. (E-42) into Eq. (E-38) and rearranging,

$$F_{d\to c}=(\pi k)^{-1}\left[\begin{array}{l}\dfrac{\pi}{2}(k-1)-\dfrac{2kr^2}{r^2-1}\arctan\left(\dfrac{r-1}{r+1}\right)^{1/2}+\\ \dfrac{r^2+h^2}{r^2-1}\arctan\dfrac{\left(r^2-1\right)^{1/2}}{k}\end{array}\right]. \tag{E-47}$$

Defining

$$a(r)=\left(\frac{r-1}{r+1}\right)^{1/2} \tag{E-48}$$

and

$$b(r)=k^{-1}\left(r^2-1\right)^{1/2}, \tag{E-49}$$

Eq. (E-47) can be rewritten

$$F_{d\to c}=(\pi\,k)^{-1}\left[k\left(\frac{\pi}{2}-\frac{2\,r^2}{r^2-1}\arctan a\right)+\frac{r^2+h^2}{r^2-1}\arctan b-\frac{\pi}{2}\right]. \tag{E-50}$$

Rearranging,

$$F_{d\to c}=\pi^{-1}\left\{2\left[\frac{\pi}{4}-\frac{1}{\left(1-r^{-2}\right)}\arctan a\right]+k^{-1}\left[\frac{\left(1+h^2/r^2\right)}{\left(1-r^{-2}\right)}\arctan b-\frac{\pi}{2}\right]\right\}. \tag{E-51}$$

Substituting (E-51) into (E-44) and rearranging,

$$F_{c\to d}=(\pi k)^{-1}\left\{\begin{array}{l}r^2\left[2\left(\dfrac{\pi}{4}-\dfrac{\arctan a}{1-r^{-2}}\right)+k^{-1}\left(\dfrac{\arctan b}{1-r^{-2}}-\dfrac{\pi}{2}\right)\right]+\\ k^{-1}\left[\dfrac{h^2\arctan b}{1-r^{-2}}\right]\end{array}\right\}. \tag{E-52}$$

Define

$$f_1=2\left[\frac{\pi}{4}-\frac{\arctan a}{\left(1-r^{-2}\right)}\right]+k^{-1}\left[\frac{\arctan b}{\left(1-r^{-2}\right)}-\frac{\pi}{2}\right], \tag{E-53}$$

$$f_2=k^{-1}\left[\frac{h^2\arctan b}{\left(1-r^{-2}\right)}\right], \tag{E-54}$$

and

$$g=r^{-2}, \tag{E-55}$$

such that

$$F_{c\to d}=(\pi\,k)^{-1}\left[\frac{f_1}{g}+f_2\right]. \tag{E-56}$$

As $r \to \infty$,

$$\lim_{r\to\infty} f_2 = \lim_{r\to\infty} k^{-1}\left[\frac{h^2 \arctan b}{\left(1-r^{-2}\right)}\right] = k^{-1}\, h^2\left(\frac{\pi}{2}\right) = \frac{\pi h^2}{2k}, \tag{E-57}$$

but

$$\lim_{r\to\infty} \frac{f_1}{g} = \frac{0}{0}. \tag{E-58}$$

Applying L'Hôpital's rule and a great deal of algebra,

$$\lim_{r\to\infty} \frac{f_1}{g} = \lim_{r\to\infty} \frac{df_1/dr}{dg/dr} = \frac{\pi}{2}\left(\frac{1-k}{k}\right). \tag{E-59}$$

Substituting Eqs. (E-59) and (E-57) into Eq. (E-56) and then into Eq. (E-45),

$$F_{c\to g} = \lim_{r\to\infty} \phi_{c\to d} = (\pi k)^{-1}\left[\frac{\pi}{2}\left(\frac{1-k}{k}\right) + \frac{\pi}{2}\left(\frac{h^2}{k}\right)\right] = \frac{1-k+h^2}{2k^2}. \tag{E-60}$$

As defined in Eq. (E-41), $h^2 = k^2 - 1$, so

$$F_{c\to d} = \frac{1-k+k^2-1}{2\,k^2} = \frac{k-1}{2k} \tag{E-61}$$

and

$$F_{c\to s} = 1 - F_{c\to g} = \tfrac{1}{2}\left(1+k^{-1}\right). \tag{E-62}$$

Since $h = H_0/R_0$ is the tangent of the cone's angle of elevation α,

$$k = \sqrt{1+h^2} = \sqrt{1+\tan^2\alpha} = 1/\cos\alpha \tag{E-63}$$

Thus the view factor from the cone's curved surface to the sky is simply

$$F_{c\to s} = \tfrac{1}{2}(1+\cos\alpha) \tag{E-64}$$

Limiting Cases. Checking this result in two limiting cases, Eq. (E-64) predicts

$$\lim_{\alpha\to 0} F_{c\to s} = \tfrac{1}{2}\left[1+\cos(0)\right] = 1 \tag{E-65}$$

as the cone's surface becomes horizontal and

$$\lim_{\alpha\to\infty} F_{c\to s} = \tfrac{1}{2}\left[1+\cos(1)\right] = \tfrac{1}{2} \tag{E-66}$$

as the cone's surface becomes vertical.

E.2.2 View Factor From A Conical or Cylindrical Wedge To The Sky

The view factor to the sky plane from a vertical wedge of an axially-symmetric, vertical object such as a cone or cylinder can be shown to equal the view factor of entire object to

the sky plane. Let subscripts 0, w, and s denote the object, wedge, and sky. By symmetry,

$$F_{s\to w} = \frac{A_w}{A_0} F_{s\to 0}, \tag{E-67}$$

and by reciprocity,

$$A_s F_{s\to w} = A_w F_{w\to s} \tag{E-68}$$

and

$$A_s F_{s\to 0} = A_0 F_{0\to s}. \tag{E-69}$$

Combining Eqs. (E-67) through (E-69), the view factor from the wedge to the sky

$$F_{w\to s} = \frac{A_s}{A_w} F_{s\to w} = \frac{A_s}{A_w}\left(\frac{A_w}{A_0} F_{s\to 0}\right) = \frac{A_s}{A_0} F_{s\to 0} = \frac{A_s}{A_0}\left(\frac{A_0}{A_s} F_{0\to s}\right) = F_{0\to s} \tag{E-70}$$

equals the view factor from the object to the sky.

Appendix F: Thermal Boundary Layers

F.1 Thermal Law of the Wall

Van Driest's thermal law of the wall indicates that turbulent eddy diffusion of heat in a thermal boundary layer over the ground is negligible within a very thin sublayer next to the ground. Above that thin sublayer, the air's turbulent eddy diffusivity is large compared to its molecular thermal diffusivity, growing linearly with distance from the ground (White, p.317). Therefore, to vertically transport a steady flow of heat away from the ground, the air must exhibit a large temperature gradient in the low-diffusivity sublayer near the ground, and a much smaller, linearly-decreasing temperature gradient in the region away from the ground. This linear decrease in temperature gradient is the basis of the logarithmic profile usually assumed for the variation of air temperature with height above ground.

F.2 Ambiguity in Thermal Boundary Layer Height

There is some ambiguity in the definition of a near-ground thermal boundary layer. While, for example, the air temperature gradient is much smaller at a height of 1 m than it is within the first centimeter or so above the ground, there is no obvious height at which the thermal free stream begins. It will be assumed here that there is some height above the ground at which horizontal mixing of the air renders the air temperature insensitive to changes in the ground temperature that are restricted to a finite ground region. Thus, the air temperature will equal the ground temperature at the ground surface, will drop rapidly within a short sublayer above the ground, and will decline gradually above that sublayer, eventually reaching the free-stream temperature at the top of the boundary layer.

F.3 One-Seventh Power Law Approximation

A common formula for the temperature profile above a wall is the one-seventh power law (Kays & Crawford 1993, p.280):

$$\theta \equiv \frac{T_0 - T_a(z)}{T_\infty - T_0} = (\bar{z})^{1/7} \qquad (\bar{z} < 1). \tag{F-1}$$

(Figure F-1). Here T_0 is the wall (ground) surface temperature, T_∞ is the free-stream air temperature, Δ is the boundary layer thickness, $\bar{z} \equiv z/\Delta$ is the normalized distance from the ground, and θ is the normalized temperature. Note that $\theta(\bar{z} = 0) = 0$ corresponds to the ground temperature, and $\theta(\bar{z} = 1) = 1$ corresponds to the free-stream air temperature. The dimensional air temperature at height $\bar{h} = \bar{H}_0/\Delta$ is

$$T_a = T_\infty + [T_0 - T_\infty]\left[1 - \theta(\bar{h})\right]. \tag{F-2}$$

The one-seventh-power profile is a convenient engineering approximation to the law of the wall. It has a large gradient at the ground,

$$d\theta/d\bar{z}\big|_{\bar{z}=0} = \infty, \tag{F-3}$$

and a small gradient at the free-stream interface, "far" from the ground:

$$d\theta/d\bar{z}\big|_{\bar{z}=1} = \tfrac{1}{7} \tag{F-4}$$

(Figure F-2).

F.4 Damping of Effect of Ground Temperature Change

The combination of a large temperature gradient near the ground and a free-stream temperature that is insensitive to changes in ground temperature makes the air temperature increasingly insensitive to changes in ground temperature as the height above ground increases. Using the arbitrary but popular temperature profile of Eq. (F-1), $1-\theta_{\bar{z}=0.2} = 0.21$. Considering the definition of dimensional air temperature in Eq. (F-2), this result indicates that the change in air temperature at a height one-fifth that of the boundary layer will be only 21% of the change at the ground surface.

Integrating Eq. (F-1), the mean normalized air temperature averaged between the wall and some normalized height $\bar{h}$ is

$$\tilde{\theta}(\bar{h}) \equiv \frac{1}{\bar{h}}\int_{\bar{z}=0}^{\bar{h}} \theta(\bar{z})\, d\bar{z} = \begin{cases} \dfrac{7}{8}(\bar{h})^{1/7} & \bar{h} < 1 \\ 1 - \dfrac{1}{8\bar{h}} & \bar{h} > 1 \end{cases}. \tag{F-5}$$

(Figure F-2). Dimensionally,

$$\tilde{T}_a = T_\infty + [T_0 - T_\infty]\left[1 - \tilde{\theta}(\bar{h})\right]. \tag{F-6}$$

The height-averaged air temperature is only slightly more sensitive than the air temperature to changes in ground temperature. From Eq. (F-5), $1-\tilde{\theta}_{\bar{z}=0.2} \approx 0.31$. This means that the change in air temperature averaged between the ground and one-fifth of the boundary layer height will be only 31% of the change at the ground surface.

F.5 Sensitivity to Boundary Layer Height

Physical intuition is required in the choice of Δ. However, the magnitude of the height-averaged air temperature change induced by a given change in ground temperature is weakly sensitive to assumptions of boundary layer thickness. Consider a 1.7-m human in a 10-m-high boundary layer $(\bar{z} = 0.17)$. An 10 K decrease in the ground temperature will lower the human's average ambient air temperature by $\left(1-\tilde{\theta}_{\bar{z}=0,17}\right)\times 10\text{ K} = 3.2\text{ K}$. If the boundary layer height is increased to 100 m, so that $\bar{z} = 0.017$, the 10 K decrease in

ground temperature will lower the human's average ambient air temperature by $\left(1-\tilde{\theta}_{\tilde{z}=0,017}\right)\times 10\ \mathrm{K} = 5.1\ \mathrm{K}$. Thus a tenfold increase in the boundary layer height increases the change in the human's average air temperature by a factor of just 1.6.

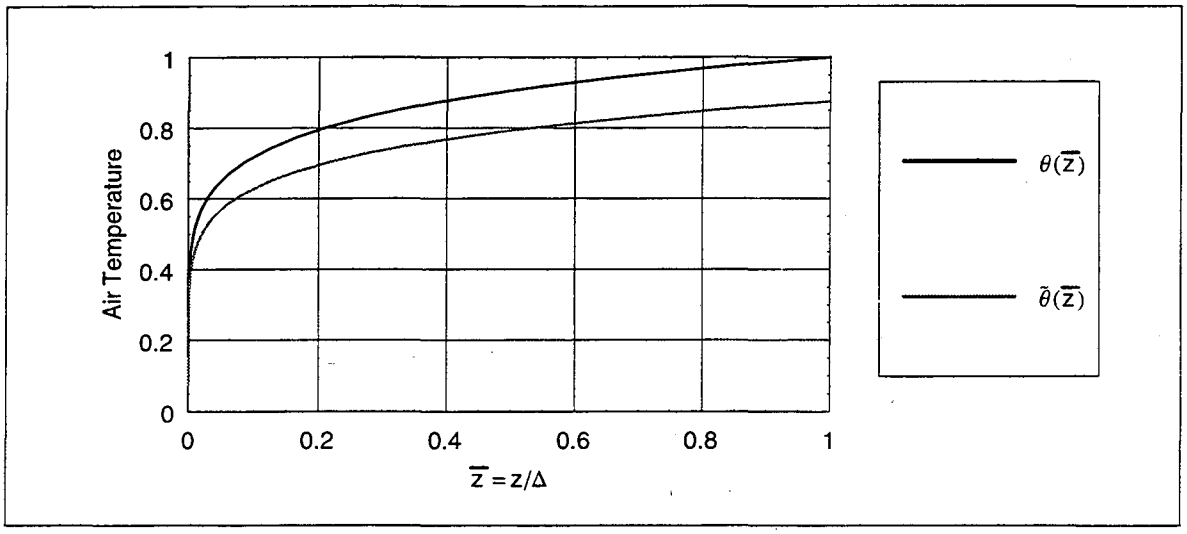

Figure F-1. One-seventh-power temperature profiles used to approximate the thermal boundary layer air temperature [Eq. (F-1)]. $\theta(\bar{z})$ is the normalized air temperature at height $\bar{z} = z/\Delta$, while $\tilde{\theta}(\bar{z})$ is the normalized air temperature averaged between the ground plane and height $\bar{z}$.

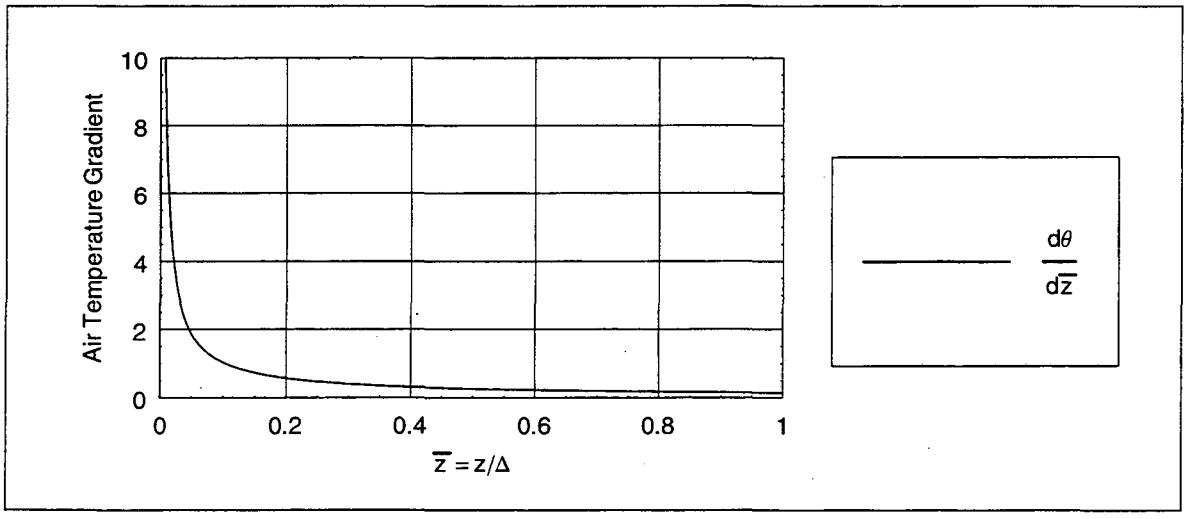

Figure F-2. Gradient of the one-seventh-power normalized air temperature profile, $d\theta/d\bar{z}$ [(Eq. (F-3)]. Note that the derivative is very large near the ground, but falls rapidly with height above ground.

Appendix G: Properties of Air and Water

G.1 Constant Properties

At standard temperature and pressure, the volumetric heat capacity of air, latent heat of vaporization of water, and the psychrometric constant are

$$C \equiv \left(\rho c_p\right)_{\text{air}} = 1210 \text{ J m}^{-3} \text{ K}^{-1}, \tag{G-1}$$

$$\lambda = 2454 \times 10^3 \text{ J kg}^{-1} \text{ K}^{-1}, \tag{G-2}$$

and

$$\gamma \equiv C/\lambda = 4.931 \times 10^{-4} \text{ kg m}^{-3} \text{ K}^{-1}. \tag{G-3}$$

C and λ vary negligibly near 20°C (0.3% and 0.1% per degree Kelvin, respectively), so C, λ, and γ may be treated as constants.

G.2 Variable Properties

Water's saturation vapor pressure is approximately (Campbell 1977, p.22)

$$p_v'(T) \approx 10^3 \exp(a - b/T - c \ln T), \tag{G-4}$$

where

$$a = 52.75633, b = 6790.4985, c = 5.02808, \tag{G-5}$$

and its saturation vapor density is

$$\rho_v'(T) = \frac{p_v'(T)}{R\,T} = e\,p_v'(T)/T, \quad e = 1/461.8. \tag{G-6}$$

The slope of the saturation vapor density curve is

$$s(T) \equiv \frac{d\rho_v'(T)}{dT} \approx e\,T^{-3}[b - (c+1)\,T]\,p_v'(T). \tag{G-7}$$

The saturation density curve is not linear, but may be treated as such for small changes in water temperature:

$$\Delta\rho_v' \equiv \rho_v'(T_1) - \rho_v'(T_0) \approx s(T_0) \times (T_1 - T_0). \tag{G-8}$$

At 20°C, the linearized density increase on the right side of Eq. (G-8) is about 12% low for a 5°C temperature rise and about 23% low for a rise of 10°C. It is best to evaluate the slope s at the mean temperature $\frac{1}{2}(T_0 + T_1)$, but often only one temperature (usually the air temperature) is known a priori. In that case, it is convenient to use

$$s_a \equiv s(T_a). \tag{G-9}$$

in Eq. (G-8).

Appendix H: Water Relations of Plants

H.1 Overview

Water evaporating inside a leaf diffuses through surface pores (stomata) and into the air. This process is termed evapotranspiration, and nearly all of the water consumed by plants is lost to stomatal evapotranspiration. Thus, the water relations of a tree are strongly controlled by the dynamics of (a) the opening and closing of stomata, and (b) the availability of water to the leaves.

H.2 Evapotranspiration, Photosynthesis, and Plant Survival

From the perspective of plant survival, evapotranspirative water losses are simply an unfortunate side effect of stomatal behavior patterns that are optimized to maximize photosynthesis. That is, when plants open their stomatal pores in sunlight to admit carbon dioxide for photosynthesis, the pore openings permit water vapor to escape from the leaf interior. Only a small fraction of water intake is employed in plant growth; the remainder, about 95%, is lost to evapotranspiration. Evaporative cooling of the leaves surfaces is beneficial, but not crucial to plant survival (Kramer 1983, pp.292-293).

Photosynthesis consumes only 2-3% of the total radiation incident on a leaf, and thus may be neglected in the leaf energy balance (Kramer 1983, p.297).

H.3 Stomata and Vapor Diffusion

H.3.1 Stomatal Mechanics

Opening. A low concentration of carbon dioxide within the leaf, or exposure of the leaf to sunlight, triggers a chemical process† that lowers the water potential‡ of the leaf's epidermal guard cells. This causes the cells to take up water, swell, and thereby deform in a fashion that opens the intercellular voids known as stomatal pores. Whether it is sunlight or a low carbon-dioxide level that triggers the opening of stomata is a long-debated and still open topic of plant physiology. However, very little insolation is needed; stomata begin to open in $1/1000$ to $1/30$ of full sunlight (Salisbury and Ross 1985, pp.58-63).

Closing. Stomata close when the water potential of the guard cells is higher than that of the rest of the plant, driving water out of the leaf toward regions of lower potential. This

†. Potassium ions $\left(K^{+}\right)$ move from surrounding cells into the guard cells, increasing the guard cells' solute concentration and lowering their osmotic potential. The biochemical mechanism that drives the ion motion is complex (Salisbury and Ross 1985, pp. 60-63).

‡. The water potential is the chemical potential of water $\left(\mathrm{J\ mol^{-1}}\right)$ divided by its partial molar volume $\left(\mathrm{m^3\ mol^{-1}}\right)$. It has units of pressure.

causes the guard cells to dry out, lose turgor, and collapse the walls that provided the inter-cell void. Dry-out may be triggered chemically—that is, when high levels of CO_2 in the leaf or the absence of light increases the guard cell water potential—or mechanically, when the rest of the plant dries out and achieves a water potential lower than that of the guard cells.

H.3.2 Effect of Negative Water Potential on Vapor Pressure

The negative water potentials associated with stomatal opening have little effect on leaf water vapor pressure. Transpiring leaves with typical water potentials of -1.0 to -5.0 MPa will exhibit vapor pressure reductions of only 1-3% (Kramer 1983, p.299).

H.3.3 Dominance of Stomatal Resistance

The resistance to vapor diffusion from the interior of a leaf to the air is the sum of the stomatal pore resistance, r_{vs}, and the boundary-layer resistance, r_{va}:

$$r_v = r_{vs} + r_{va}. \tag{8-1}$$

The stomatal resistance is low when the stomatal pores are open and high when they are closed, varying from about $100 - 4{,}000$ s m^{-1}. Typical boundary layer resistances range from about $10 - 40$ s m^{-1}, increasing with leaf size and decreasing with wind speed (Cowan 1977, p.216). Thus the vapor diffusion from the leaf to the air is usually controlled by the stomatal resistance.

H.4 Coupling of Water Availability to Leaf Evapotranspiration

H.4.1 Role of Water Availability in Steady-State Analysis

As leaves evapotranspire water, the leaf moisture lost to the air must be resupplied from the stem system, and the stem, in turn, must draw moisture from the soil via the roots. If the soil, roots, stem, and finally leaves dry out, evapotranspiration will cease. Most plants have evolved a negative-feedback mechanism to prevent leaf dryout: when the stem water potential falls below that of the leaves, the leaves' epidermal guard cells deflate and collapse, closing the stomata and thereby reducing the rate of evapotranspiration. While the steady-state wet-surface analysis in Section A.5 does not account explicitly for the availability of water to the leaf, the steady-state rate of latent heat loss does depend on the stomatal resistance to vapor diffusion, which in turn depends on the water availability.

H.4.2 Diurnal Patterns of Stomatal Resistance

Wet Soil. Consider a tree with unlimited soil moisture. At night, when stomata are closed by darkness and little heat is available to evaporate water, leaf evapotranspiration is low to non-existent. This allows the roots, stem, and leaves to fully charge themselves with soil

water overnight. As the sun rises, the stomata open for photosynthesis, and the leaves begin to lose water to the air. As the transpiring leaves draw from the stem, the stem draws water from the roots, and the roots draw water from the soil. The rate of evapotranspiration increases as the ambient air temperature rises and the sun climbs higher in the sky. If a leaf evapotranspires water faster than it can be replenished from the soil-root-stem system, the leaf will begin to wilt and its stomata will begin to close. This type of stomatal closure is commonly observed in the late morning (Salisbury and Ross 1985, p.61).

Once the stomata close and the evapotranspiration rate falls, the rate of water supply from the soil-root-stem system may exceed the rate of leaf water loss to the air. If so, the leaf will regain its turgor and reopen its stomata in what is known as a mid-day recovery. If not, the stomata will remain closed all afternoon. When the sun sets, the cycle will begin again.

In the typical night-day cycle outlined above, stomatal resistance will be very high at night, low in the early morning, and increase sharply by late morning. If the plant recovers its leaf turgor, the stomatal resistance will fall again by mid-day. If not, resistance will remain elevated all afternoon. As the sun sets, the resistance will return to its nighttime high.

Dry Soil. If soil moisture is somewhat limited, the roots, stem, and leaves may be unable to fully charge themselves with water overnight. Thus, the leaves may wilt early in the day and remain wilted until nighttime, yielding high daytime stomatal resistances. Long periods of extremely limited soil moisture will kill most plants.

Appendix I: Measurement and Data Analysis Techniques

I.1 Overview

Useful techniques acquired in the course of the lysimeter experiment include (a) the calculation of evapotranspiration rates from a noisy mass signal; (b) the estimation of canopy leaf area; and (c) the mutual calibration of air temperature sensors.

I.2 Calculating the Rate of Evapotranspiration

I.2.1 Wind Noise in First Derivative

The simplest way to calculate the rate of evapotranspiration E is to take the finite-difference approximation to the first derivative of the mass signal, $\dot{m}$:

$$-E = \dot{m} \approx \frac{\Delta m}{\Delta t} = \frac{m_t - m_{t-\Delta t}}{\Delta t} \tag{I-1}$$

Lift forces generated by wind flowing around the tree introduce high-frequency random noise of some magnitude n in its measured mass, suggesting that the time interval Δt should be chosen to make $\Delta m \gg n$. This can require large values of Δt that make the calculated evapotranspiration time series quite crude. If, for example, the tree loses approximately 200 g of water per hour, and the magnitude of the wind noise is 20 g, the time interval Δt required to obtain the signal-to-noise ratio $\Delta m/n = 5$ would be one half-hour. This represents a great loss of information when the mass signal was measured once per second.

I.2.2 Moving Average Equivalent to Long-Period Finite Difference

Another option would be to take a moving average of the short-interval finite-differences derivative, but this turns out to be equivalent to a finite-difference derivative calculated using the end points of the moving average interval. The moving average of $\dot{m}$ over the long interval $(2N+1)(\Delta t)$ centered at t_i is

$$\left(\overline{\dot{m}}\right)_i = \frac{1}{(2N+1)} \sum_{j=i-N}^{i+N} \dot{m}_j , \tag{I-2}$$

where the finite-difference derivative over the short interval Δt is

$$\dot{m}_i = \left(m_i - m_{i-1}\right)/\Delta t . \tag{I-3}$$

Since all but the end terms in the expanded summation of Eq. (I-2) cancel, i.e.

$$\begin{aligned}\sum_{j=i-N}^{i+N}\dot{m}_j &= \left[\left(m_{i-N}-m_{i-N-1}\right)+\cdots+\left(m_{i+N}-m_{i+N-1}\right)\right]/(\Delta t)\\ &= \left(m_{i+N}-m_{i-N-1}\right)/(\Delta t),\end{aligned} \tag{I-4}$$

the moving average reduces to

$$\left(\overline{\dot{m}}\right)_i = \frac{m_{i+N}-m_{i-N-1}}{(2N+1)(\Delta t)}. \tag{I-5}$$

This is simply the finite-difference derivative calculated over the interval $(2N+1)(\Delta t)$ centered at t_i.

I.2.3 Sampling Frequency Too Low For Fourier Transforms

It would be better to remove the random noise from the mass signal, then take the finite-difference approximation with a small time interval. Several types of Fourier-transform-based filters explored for this purpose gave unsatisfactory results, possibly because the original mass sampling rate of 1 Hz was less than twice the highest frequency of the wind noise. However, the next algorithm, designed to remove noise in a time series' first derivative by reducing the value of its second derivative, was found to work very well.

I.2.4 Iterative Linear Filter: "Maximum Smoothness"

Random noise in a time series $y_n = y(t_n)$ can lead to wild fluctuations in the finite difference approximation of the time series' first derivative,

$$\dot{y}_n \approx \frac{y_n - y_{n-1}}{t_n - t_{n-1}}. \tag{I-6}$$

The "maximum smoothness" algorithm is a linear filter that generates a less-noisy time series z_n that approximates y_n but has a smaller second derivative, and thus a more slowly-varying first derivative. This algorithm is computationally inexpensive and may be iterated many times to yield a very smooth time series.

Consider a time series y_n, $n = 1 \ldots N$, with constant time step $h = t_n - t_{n-1}$. The finite difference approximation to the second derivative of the time series is

$$\ddot{y}_n = \frac{y_{n+1} + y_{n-1} - 2y_n}{h^2}. \tag{I-7}$$

Writing y_n in terms of its neighbors y_{n-1} and y_{n+1} and its second derivative $\ddot{y}_n$,

$$y_n = \frac{y_{n+1} + y_{n-1}}{2} - \frac{h^2}{2}\ddot{y}_n \tag{I-8}$$

Let ε be a small positive fraction such that $\varepsilon \ll 1$. Define a new time series

$$z_n = \frac{y_{n+1} + y_{n-1}}{2} - \frac{h^2}{2}(1-\varepsilon)\,\ddot{y}_n, \quad n = 2 \ldots N-1 \tag{I-9}$$

that approximates y_n but has a smaller second derivative. Substituting Eq. (I-7) into Eq. (I-9),

$$z_n = (1-\varepsilon)\,y_n + \varepsilon\left(\frac{y_{n+1} + y_{n-1}}{2}\right), \quad n = 2 \ldots N-1. \tag{I-10}$$

The new time series value z_n is the weighted average of y_n and the value at time t_n that would be linearly interpolated from neighboring values y_{n-1} and y_{n+1}. For completeness, define

$$z_1 = y_1 \tag{I-11}$$

and

$$z_N = y_N. \tag{I-12}$$

Iteration. This process may be repeated. Defining

$$z_n^0 = y_n, \tag{I-13}$$

the time series generated by the i^{th} iteration

$$z_n^i = (1-\varepsilon)\,z_n^{i-1} + \varepsilon\left(\frac{z_{n+1}^{i-1} + z_{n-1}^{i-1}}{2}\right). \tag{I-14}$$

Each series is calculated from the values of its immediate predecessor.

I.3 Estimation of Canopy Leaf Area

I.3.1 Procedure

The canopy's complex geometry and the wide variation of leaf sizes precluded estimation of total leaf area by the sampling of a small section of the canopy, so the tree was defoliated at the end of the experiment to obtain its total leaf area†. The leaf area was estimated as follows:

1. All leaves were stripped from the tree, placed in airtight plastic bags, and weighed.
2. A randomly-chosen subset of 100 leaves was weighed.
3. Each member of the subset was placed on a flatbed computer scanner and scanned in black-and-white at a resolution of 50 dots per inch. Leaves registered as black pixels.
4. The number of black pixels in each leaf image was divided by 2,500 to obtain the leaf's area in square inches.

†. And the leaves grew back the following spring, despite that fact that the tree was an evergreen.

5. The area of the entire canopy was estimated as

$$A_{\text{canopy}} = \frac{m_{\text{canopy}}}{m_{\text{subset}}} A_{\text{subset}} . \qquad \text{(I-15)}$$

The scans also yielded the distribution of areas in the random subset of leaves.

I.3.2 Results

The canopy leaf statistics are given in Table I-1, and the leaf area distribution is shown in Figure I-1.

I.4 Mutual Calibration of Air Temperature Sensors

I.4.1 Procedure

Four shielded, aspirated thermocouples were mutually calibrated by connecting the inlet of each sensor to a pipe assembly that joined all sensors to the same air source. Identical 0.5 m lengths of white PVC piping ran from each sensors to the air source, and the piping was shaded to minimize solar heating of the air as it flowed through the pipe. Each sensor (Figure 6-4) was oriented vertically to expose all four sensors to similar insolation. Air temperature readings were recording day and night for one week.

I.4.2 Results

At night, the spread in sensor readings was less than 0.3 K, but daytime differences ran from 0.5 to 2 K. The difference between the temperatures recorded by each pair of sensors showed rapid random noise of magnitude 0.2 - 1.0 K superimposed on a slow, repeating diurnal signal that slowly varied from approximately 0.2 K to 1.5 K. The diurnal temperature difference profiles were quite sensitive to the orientation of the sensors. That is, if a sensor was skewed from vertical, its pattern of solar heating would change.

I.4.3 Calibration by Fog†

When nighttime fog settled on the experimental site, all thermocouples —those in the air temperature sensors, and those attached to the undersides of canopy leaves—would register the same temperature to within 0.3 K. This suggests that the uniform temperatures induced by the high thermal diffusivity of fogs provides an easy way to mutually calibrate thermocouples, at least within the small range of temperatures provided by fog (at this site, fog temperatures fell in the range of 283 to 288 K.)

---

†. Or, "Berkeley by Night."

I.4.4 Conclusions

The susceptibility of the shielded, aspirated thermocouples to orientation-dependent solar heating made it difficult to mutually calibrate their daytime readings to accuracies better than ±1 K. Experiments that report outdoor temperature difference measurements of 1 K or less should be regarded with caution unless the sensors' insensitivity to solar heating has been demonstrated.

Total-canopy leaf mass	3.6 kg
Total-canopy leaf area	6.9 m^2
Number of leaves in canopy	4,800
Average leaf mass	0.76 g
Average leaf area	14.4 cm^2

Table I-1. Canopy leaf statistics.

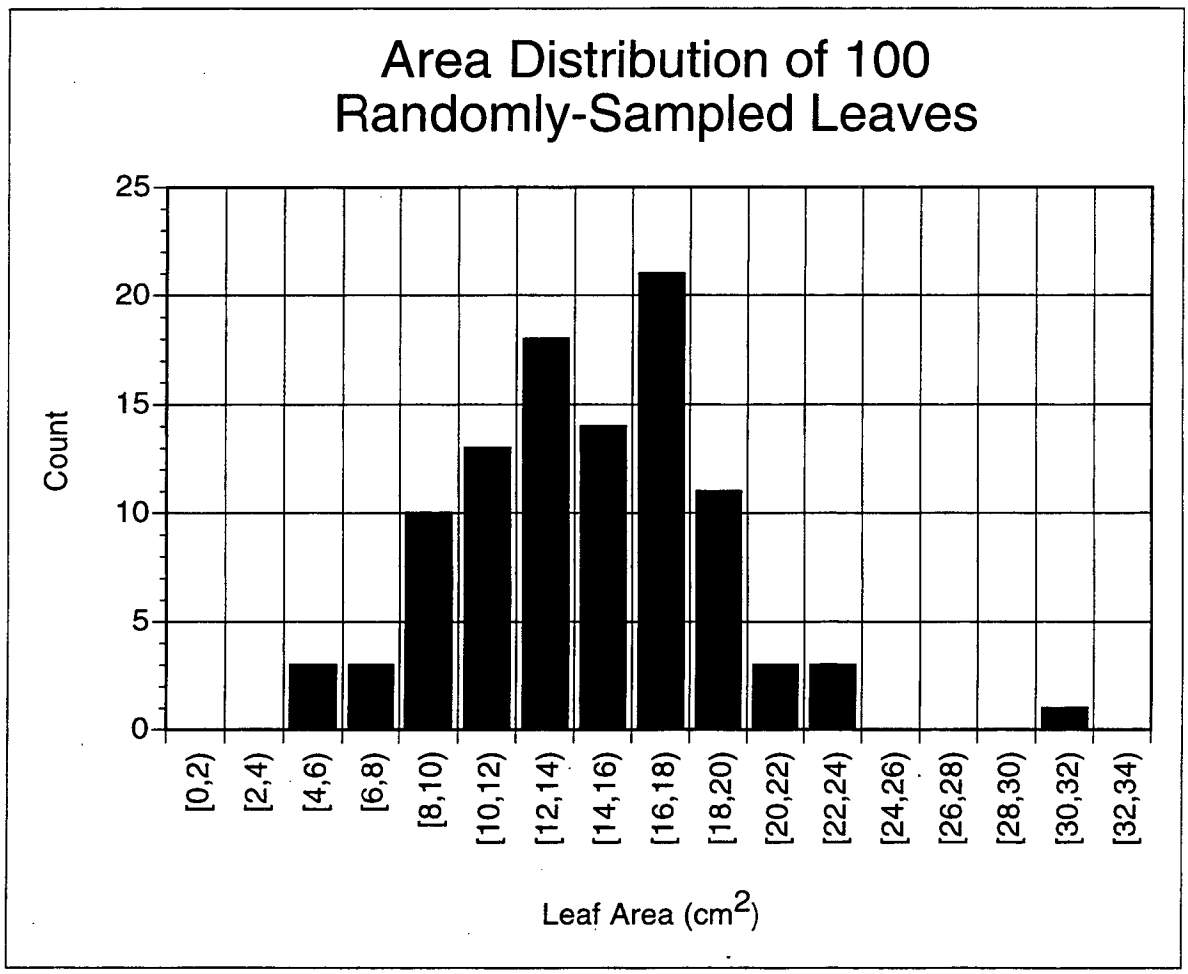

Figure I-1. Area distribution of 100 leaves randomly chosen from the tree's canopy.

Appendix J: Computer Code

The following *Mathematica 3.0* code computes the heat flows of a near-ground object and of a tree.

Near-Ground-Object Sensitivity Computation Engine

```
Clear[compute];
compute[vars_, evaluateGroundResistance_: True] :=
 Block[
  {C, ν, k, Pr, σsb, D0, ReD, U , Nu, rh, nt, rr, η, re, AW, H0, AT, IN,
   T̄, fW, fT, rr,g, rh,g, h̄g, re,g, α0, IH, Δ, β, δ,
   ∂Te/∂αg, ∂Te/∂σ, ∂Ĥ/∂αg, ∂Ĥ/∂σ, ∂H/∂σ, ∂H/∂αg, α0', α0'', Si,↓*, θ, θ̃, θ̄, extraRules},

  (* Constants. Air properties are evaluated at 20 °C and 1 atm. *)

  C = 1210;
  ν = 1.508 × 10^-5;
  k = 2.563 × 10^-2;
  Pr = 0.712;
  σsb = 5.67 × 10^-8;

  (* IN is the beam-normal magnitude of the solar flux density. *)

  IH = IN Sin[β] / (1 - δ);

  (* Cylinder properties, unsubscripted. *)

  D0 = 2 R0;
  ReD = U D0 / ν;
  NuD = 0.3 + (0.62 ReD^1/2 Pr^1/2) / (1 + (0.4/Pr)^2/3)^1/4 (1 + (ReD/282000)^5/8)^4/5;
  rh = nt^-1 * C D0 / k NuD^-1;
  rr = C / (4 σsb T̄^3);
  η = rr / (rr + rh);
  re = rh η;
  AW = 2 π R0 H0;
  AT = π R0^2;
  fW = 2 H0 / (R0 + 2 H0);
  fT = 1 - fW;

  (* Ground properties, denoted with subscript g. *)

  rr,g = rr;
  h̄g = 5.7 + 3.8 U ;
```

```
If[evaluateGroundResistance, r_{h,g} = C/h̄_g];

η_g = r_{r,g} / (r_{r,g} + r_{h,g});
r_{e,g} = r_{h,g} η_g;

(* Sensitivities. *)

∂T_e/∂α_g = f_W r_e I_H / (2 C) (α_0' - α_0);
∂T_e/∂σ = -C^-1 (1 - α_0) r_e S*_{i,↓};

∂H/∂α_g = 1/2 f_W η I_H (α_0'' - α_0);
∂Ĥ/∂α_g = (A_T + A_W) ∂H/∂α_g;
∂H/∂σ = -(1 - α_0) η S*_{i,↓};
∂Ĥ/∂σ = (A_T + A_W) ∂H/∂σ;

α_0' = 1 - ((1 - η) + 2 η f_W^-1 θ̄) r_{e,g}/r_e;
α_0'' = 1 - (1 - 2 f_W^-1 θ̄) r_{e,g}/r_r;

S*_{i,↓} = I_H (f_T + f_W ((1 - δ)/π Cot[β] + δ/2));

θ[H_0] = (H_0/Δ)^1/7;
θ̃[H_0] = 7/8 (H_0/Δ)^1/7;
θ̄ = 1 - (f_T θ[H_0] + f_W θ̃[H_0]);

(* Return values. *)

Evaluate[vars]
]

depVars = {α_0', α_0'', ∂T_e/∂α_g, ∂T_e/∂σ, ∂H/∂α_g, ∂H/∂σ};

indepVars = {α_0, Δ, r_{h,g}};
```

```
sensitivities[depVar_Symbol, indepVars_] :=
 Module[
  {y},
  y = compute[depVar, False];
  Return[compute[(∂# y&) /@ indepVars]];
 ]

sensitivities[depVars_List, indepVars_] :=
 sensitivities[#, indepVars]& /@ depVars
```

```
calculate[expr_, rec_] :=
 Block[
  {σsb, C, λ, γ, zeroC, gramPerHour, δ, nt, αg, α0, dleaf,
      R0, H0, A, f, Tr, t, Ta, hr, IB, U , λÊ, Tsunny, m, β, tsol, hsol,
      ρva′, ρva, ρsd, sa, εs, Ts, rha, rh, rva, T̄, rr, η, re, rr,g, h̄g,
      rh,g, Tg, ηg, regions, α, FW→s, FW→g, T, ϕ0, Ŝi, Ŝ, S, Q̂, Q̂dry, Q,
      ω, Ĥ, H, λE, L̂, L, rvs, ΔĤg, ΔŜg, ΔĤind, ΔĤ0, f↓, f↓′, ΔĤ, Bo},

  (* Constant physical properties. *)

  σsb = 5.67 × 10^-8;
  C = 1210;
  λ = 2454 × 10^3;
  γ = 4.931 × 10^-4;

  (* Conversion factors to SI. *)

  zeroC = 273.15;
  gramPerHour = (3600 * 1000)^-1;

  (* Assumed values. *)

  δ = 0.2;
  nt = 1.5;
  αg = 0.2;
  α0 = 0.2;

  (* Constant measured values. *)

  dleaf = 4.3 × 10^-2;
  H0 = 1.7;
  R0 = 0.5;
  A[0] = 6.9;

  (* Time-varying measured values. *)

  {t, Ta, hr, IB, U , λÊ[0], Tsunny, m} = subs[{time, airTemp + zeroC, hr100/100,
        sun, speed, λ × evap × gramPerHour, sunny + zeroC, mass}, rec];


  (* Solar properties. *)

  tsol = tsol,calc[t];
  hsol = FractionalPart[tsol] × 24;
  β = βcalc[t];
  If[β < 0, β = 0];

  (* Air properties. *)
```

$\rho_{va}' = \rho_v'[T_a];$
$\rho_{va} = h_r\, \rho_{va}';$
$\rho_{sd} = \rho_{va}' - \rho_{va};$
$s_a = s[T_a];$

(* Sky properties. *)

$\epsilon_s = 1.56\, \rho_{va}^{1/7};$
$T_s = \epsilon_s^{1/4}\, T_a;$

(* Ground properties. *)

$\bar{T} = T_a;$

$$r_{r,g} = \frac{C}{4\, \sigma_{sb}\, \bar{T}^3};$$

$\bar{h}_g = 5.7 + 3.8\, U;$

$$r_{h,g} = \frac{C}{\bar{h}_g};$$

$$\eta_g = \frac{r_{r,g}}{r_{r,g} + r_{h,g}};$$

$r_{e,g} = r_{h,g}\, \eta_g;$
$T_g = C^{-1}\, r_{e,g}\, (1 - \alpha_g)\, I_R + \eta_g\, T_a + (1 - \eta_g)\, T_s;$

(* Leaf properties. *)

$$r_{ha} = n_t^{-1} \times 309 \left(\frac{d_{leaf}}{U}\right)^{1/2};$$

$$r_h = \frac{1}{2}\, r_{ha};$$

$$r_{va} = n_t^{-1} \times 286 \left(\frac{d_{leaf}}{U}\right)^{1/2};$$

$$r_r = \frac{1}{2}\, r_{r,g};$$

$$\eta = \frac{r_r}{r_r + r_h};$$

$r_e = r_h\, \eta;$

(* Tree properties. *)

regions = {$\mathcal{B}$, $\mathcal{W}$, $\mathcal{I}$};

$$\alpha = \text{ArcTan}\left[\frac{H_0}{R_0}\right];$$

$$F_{W \to s} = \frac{1}{2}\, (1 + \text{Cos}[\alpha]);$$

$F_{W \to g} = 1 - F_{W \to s};$

$A[\mathcal{B}] = \pi\, R_0^2;$

$A[\mathcal{W}] = \pi\, R_0 \sqrt{R_0^2 + H_0^2};$

```
A[ℐ] = A[0] - (A[𝒲] + A[ℬ]);

Function[n, f[n] = A[n]/A[0]] /@ zones;

T_r[ℐ] = T_a;
T_r[𝒲] = 1/2 ((1 + ε_s^(1/4) F_W→s) T_a + (1 - F_W→s) T_g);
T_r[ℬ] = 1/2 (T_a + T_g);

ϕ_0 = ArcCos[Tan[β]/Tan[α]];
Ŝ_i[ℐ] = 0;
Ŝ_i[ℬ] = A[ℬ] α_g I_H;
Ŝ_i[𝒲] =
 Which[
  β == 0, 0,
  β > α, A[ℬ] I_H ((1 - δ) + (1 + Tan[α]^2)^(1/2) (δ F_W→s + α_g (1 - F_W→s))),
  β ≤ α, A[ℬ] I_H (
        (1 - δ) π^-1 ((π - ϕ_0) + Tan[ϕ_0]) + (1 + Tan[α]^2)^(1/2) (δ F_W→s + α_g (1 - F_W→s)))
 ];

Function[n, Ŝ[n] = (1 - α_0) Ŝ_i[n]] /@ regions;
Ŝ[0] = Plus @@ (Function[n, Ŝ[n]] /@ regions);

Function[n, Q̂_dry[n] = η (A[n] C r_r^-1 (T_r[n] - T_a) + Ŝ[n])] /@ regions;
Q̂_dry[0] = Plus @@ (Function[n, Q̂_dry[n]] /@ regions);

Function[n, ω[n] = (A[n] C r_h^-1 ρ_sd + s_a Q̂_dry[n])/(A[0] C r_h^-1 ρ_sd + s_a Q̂_dry[0])] /@ regions;

Function[n, λÊ[n] = ω[n] λÊ[0]] /@ regions;

Function[n, Ĥ[n] = Q̂_dry[n] - η λÊ[n]] /@ regions;

Ĥ[0] = Q̂_dry[𝒲] + Q̂_dry[ℬ] - (η (1 - ω[ℐ]) + ω[ℐ]) λÊ[0];

Function[n, L̂[n] = Ĥ[n] + λÊ[n] - Ŝ[n]] /@ Append[regions, 0];
Function[n, Q̂[n] = Ŝ[n] + L̂[n]] /@ Append[regions, 0];

Function[n, λE[n] = λÊ[n]/A[n]] /@ Append[regions, 0];
Function[n, H[n] = Ĥ[n]/A[n]] /@ Append[regions, 0];
```

```
Function[n, S[n] = Ŝ[n] / A[n]] /@ Append[regions, 0];

Function[n, L[n] = L̂[n] / A[n]] /@ Append[regions, 0];

Function[n, Q[n] = Q̂[n] / A[n]] /@ Append[regions, 0];


Function[n, T[n] = Ta + (A[n] C)^-1 rh (Q̂dry[n] - η λÊ[n])] /@
    DeleteCases[regions, I];


(* Stomatal resistance. *)

rvs = rh/γ (A[0] C rh^-1 ρsd + sa Q̂dry[0] / λÊ[0] - η sa) - rva;

(* Bowen Ratio *)

Bo = Ĥ[0] / λÊ[0];

(* Tree-induced changes in
        heat flow to canopy air and near-ground air. *)

ΔŜg = -(1 - αg) (1 - FW→g α0) Ŝi[W];
ΔĤg = ηg (C rr,g^-1 (A[B] (T[B] - Ts) + A[W] FW→s (T[W] - Ts)) + ΔŜg);
ΔĤ0 = Ĥ[0];

f↓ = 0.5;

ΔĤind = f↓ ΔĤ0;

f↓' = -ΔĤg / ΔĤ0;

ΔĤ = ΔĤg + ΔĤind;

(* Return value of submitted expression. *)

Return[expr]
]
```

Miscellaneous Physical Functions

■ Solar Properties

```
EqnOfTime =
 Interpolation[
  {
   {218, -5.8}, {223, -5.1},
      {228, -4.3}, {233, -3.1}, {238, -1.8}, {244, 0.0},
   {249, 1.6}, {254, 3.3}, {259, 5.0}, {264, 6.8}, {269, 8.6}, {274, 10.2},
   {279, 11.8}, {284, 13.1}, {289, 14.3}, {294, 15.3}
  }
 ];


(*
 The solar time and declination angle are computed for Berkeley, CA
  in summer (latitude 37 °52'N, longitude 122 °20'W, P.D.T.). Times
  are in the form (calendar day + day fraction).  For example,
 222.5 would be August 10 at noon.  The input to the
  declination angle function is P.D.T., not solar time.
*)

t_sol,calc = Compile[
  {t},
   t - 1/24 + (EqnOfTime[t] - 9.33)/(24 * 60)
];

β_calc = Compile[t,
  Module[
   {ℓ = π/180 (37 + 52/60), d, h, day, t_sol},

   day = Floor[t];
   t_sol = t_sol,calc[t];
   h = 2 π (t_sol - Floor[t_sol] - 1/2);
   d = π/180 23.45 Sin[2/365 π (284 + day)];

   ArcSin[Sin[ℓ] Sin[d] + Cos[ℓ] Cos[d] Cos[h]] // N
  ]
 ];
```

■ Saturated Water Properties

```
(* Properies of saturated water vapor at 1 atm. *)

With[
 {a = 52.57633, b = 6790.4985, c = 5.02808, d = 1/461.8},
 p = Compile[T, 10^3 Exp[a - b/T - c Log[T]]];
 ρv' = Compile[T, d p[T]/T];
 s = Compile[T, d (b - (c + 1) T) p[T]/T^3];
];
```

Ernest Orlando Lawrence Berkeley National Laboratory
One Cyclotron Road ⁞ Berkeley, California 94720

Prepared for the U.S. Department of Energy under Contract No. DE-AC03-76SF00098